REPUBLIC OF TÜRKİYE

YILDIZ TECHNICAL UNIVERSITY

GRADUATE SCHOOL OF SCIENCE AND ENGINEERING

DEVELOPMENT OF AQUEOUS-CORROSION RESISTANT ALKALINE BOROSILICATE GLASS COATING FOR USE IN HOT WATER STORAGE SYSTEMS

Ömer Furkan ÖTKEN

MASTER OF SCIENCE THESIS

Department of Metallurgical and Materials Engineering

Material Program

Supervisor

Assoc. Prof. Dr. Buğra ÇİÇEK

July, 2024

REPUBLIC OF TÜRKİYE

YILDIZ TECHNICAL UNIVERSITY

GRADUATE SCHOOL OF SCIENCE AND ENGINEERING

DEVELOPMENT OF AQUEOUS-CORROSION RESISTANT ALKALINE BOROSILICATE GLASS COATING FOR USE IN HOT WATER STORAGE SYSTEMS

A thesis submitted by Ömer Furkan ÖTKEN in partial fulfillment of the requirements for the degree of **MASTER OF SCIENCE** is approved by the committee on 22.07.2024 in Department of Metallurgical and Materials Engineering, Material Program.

Assoc. Prof. Dr. Buğra ÇİÇEK
Yıldız Technical University
Supervisor

Approved By the Examining Committee

Assoc. Prof. Dr. Buğra ÇİÇEK, Supervisor

Yildiz Technical University _____

Assoc. Prof. Dr. Metin GENÇTEN

Yildiz Technical University _____

Prof. Dr. Suat YILMAZ

Istanbul University _____

I hereby declare that I have obtained the required legal permissions during data collection and exploitation procedures, that I have made the in-text citations and cited the references properly, that I haven't falsified and/or fabricated research data and results of the study and that I have abided by the principles of the scientific research and ethics during my Thesis Study under the title of Development of Hot Aqueous-Corrosion Resistance Alkaline Borosilicate Glass Coating for Use In hot Water Storage Systems supervised by my supervisor, Assoc. Prof. Dr. Buğra ÇİÇEK. In the case of a discovery of false statement, I am to acknowledge any legal consequence.

Ömer Furkan ÖTKEN

Dedicated to my family

and my best friends

ACKNOWLEDGEMENTS

I am immensely grateful and wish to express my deepest appreciation to my esteemed advisor, Assoc. Prof. Dr. Buğra ÇİÇEK, whose unwavering support and encouragement played a pivotal role in revitalizing my commitment to my profession when I had contemplated giving up. His guidance and assistance throughout the entire project have been invaluable.

Special thanks are due to the esteemed members of the Akcoat Advanced Chemical Coating Materials Co.'s Enamel Solutions Research & Developments Department for generously sharing their unique knowledge and experiences, which greatly contributed to the success of this research.

I want to acknowledge and express my gratitude to all my colleagues in the Advanced Ceramic Research Group, under the guidance of Dr. Oğuz KARAAHMET, for their collaboration and shared commitment to excellence.

My deepest gratitude goes to my beloved family and cherished friends, who have been an unwavering source of love and support throughout this journey. Their encouragement has been a constant motivation, and I am truly fortunate to have them by my side.

I would like to extend my heartfelt thanks to my dear wife Cemre Cansu ÖTKEN, whose support and love have been a source of strength. Her insightful support is genuinely appreciated.

Ömer Furkan ÖTKEN

TABLE OF CONTENTS

ACKNOWLEDGEMENTS iv
TABLE OF CONTENTS v
LIST OF SYMBOLS viii
LIST OF ABBREVIATIONS ix
LIST OF FIGURES x
LIST OF TABLES xii
ABSTRACT xiii
ÖZET xv
1 INTRODUCTION 1
1.1 Literature Reviev 1
1.2 Objectives of Thesis 4
1.3 Hypothesis 4
2 GLASS-CERAMIC 6
2.1 Glass 6
2.2 Glass-Ceramic Definition 7
2.3 Glass-Ceramic Properties 10
2.4 Glass-Ceramic Applications 12
2.4.1 Technical Application 12
2.4.2 Opticical Application 14
2.4.3 Medical and Dental Glass-Ceramics 14
2.4.4 Electrical and Electronic Applications 15
2.4.5 Architectural Applications 16
2.4.6 Glass-Ceramics for Energy Application 16
3 GLASS-CERAMIC COATING (ENAMEL) 18
3.1 Chemical Components of Glass-Ceramic Coatings and Their Purposes 19
3.1.1 Fluxes 23
3.1.2 Refractories 23
3.1.3 Adhesion Agent 23
3.1.4 Opacifiers 24
3.1.5 Colour Agents 24
3.2 Types of Enamels 24
3.2.1 Ground Coat 24

3.2.2 Cover Coat 25
3.3 Adhesion Mechanism Between Glass-Ceramic and Metallic Substrate 26
3.3.1 Diffusion Theory 26
3.3.2 Chemical Theory 26
3.4 Properties of Glass-Ceramic Coatings 29
3.4.1 Thermal Properties 29
3.4.2 Physical and Mechanical Properties 35
3.4.3 Chemical Properties 36
3.5 The Area of Utilization of Glass-Ceramic Coatings 38
3.6 Application Processes 38
3.6.1 Coating Process By Wet Method 38
3.6.2 Spraying Method 39
3.6.3 Thermal Spray Method 41
3.6.4 Powder Electrostatic Application 42
3.7 Toxicological Properties of Enamel Coating 43
4 GLASS/GLASS-CERAMIC CORROSION 45
4.1 Glass Corrosion Mechanism 45
4.2 Effect of Glass Chemical Composition on Glass Alteration 50
4.3 Environmental Factor: Aqeous Solution Parameters for Glass Alteration 53
4.4 Glass-Ceramic Corrosion 60
4.5 Boiler and Hot Water Storage Tank 62
5 EXPERIMENTAL PROCEDURE 64
5.1 Production of Precursor Glass, i.e., Frit 64
5.2 Hot Water Corrosion Test 66
6 CHARACTERIZATION PROCEDURE 68
6.1 Preparation of Glass-Ceramic Coatings 68
6.2 Chemical Analysis 69
6.3 Crystal Phase Analysis 69
6.4 Raman Spectrometer 69
6.5 Thermal Analysis 69
6.6 Hot Water Resistance Test 70
6.7 Inductively Coupled Plasma Mass Spectrometry (ICP-MS) 70
6.8 Scanning Electron Microscope (SEM) 70
6.9 Surface Profilometer 70
6.10 Gloss Determination 71

7 RESULT AND DISCUSSION **72**
7.1 Analysis of Frits and Bulk Glass/Glass-Ceramics 74
7.1.1 Thermal Analysis 74
7.1.2 Crystallographic Analysis 75
7.1.3 Raman Spectrometer Analysis 78
7.2 Enamel Coating Analysis 82
7.2.1 Hot Water Corrosion Test 82
7.2.2 Element Migration Analysis 84
7.2.3 Macro and 3D Surface Topography Image Analysis 92
7.2.4 Gloss Measurement Analysis 96
7.2.5 SEM Analysis 97
8 CONCLUSION **101**
REFERENCES **104**
PUBLICATIONS FROM THE THESIS **114**

LIST OF SYMBOLS

Ra	Average Roughness
°C	Celcius Degree
Cm	Centimeter
E	Elastic Modulus
Tg	Glass Trantion Temperature
GPa	Giga Pascal
GU	Gloss
G	Gram
C	Heat Capacity
MPa	Mega Pascal
µm	Micrometer
mL	Mililiter
nm	Nanometer
N	Newton
Sec	Second
Δt	Temperature Difference
P	Tensile Strenght
Λ	Thermal Conductivity
B	Volumetric Thermal Expension
W	Watt
W	Weight
wt%	Weight Percent

LIST OF ABBREVIATIONS

ATR-IR	Attenuated Total Reflectance
BEI	Back-scattered Electron Images
BSE	Blackscatter Electron
BO	Bridging Oxygen Atom
CAD	Computer-Aided Design
CAM	Computer-Aided Manufacturing techniques
DIN	Deutsche Institut für Normung
DTA	Differential Thermal Analysis
IRFT-ATR	Fourier-transform Infrared Spectroscopy Sample Technic
GC	Glass-Ceramic
ICP-MS	Inductively Coupled Plasma Atomic Emission Spectroscopy
LCD	Liquid Crystal Displays
NBO	Non-Bridging Oxygen Atom
OSHA	Occupational Safety and Health Administration
PCT	Product Consistency Test
SEM	Scanning Electron Microscopy
SPFT	Single Pass Flow Test
3D	Three-dimensional
2D	Two-dimensional
UV	Ultraviolet Light
XRD	X-Ray Diffraction
XRF	X-Ray Fluorescence
XRR	X-Ray Reflectometry

LIST OF FIGURES

Figure 2.1 The precursor glass is transformed into a glass-ceramic structure by a sequence of events that (a) begin with nuclei production, (b) continue with crystal growth on these nuclei, and (c) end with the final development of the glass-ceramic material 9

Figure 2.2 Glass-ceramic formation time-temperature transition diagram..... 10

Figure 3.1 The illustration of Elligram Diagrams..... 28

Figure 3.2 Viscosity-Temperature curve for a theoretical glass 34

Figure 3.3 The Electrophoresis Method: Electrophoresis and Deposition Procedure 41

Figure 4.1 Schematic demonstration of ion transfer of between glass and aqueous solution..... 45

Figure 4.2 Graphic shows corrosion mechanism rates depending on time stages from l to lll 47

Figure 4.3 Cross-section of glass corrosion layers schematically demonstrated.. 49

Figure 4.4 Image of domestic hot water boiler 63

Figure 5.5 Schematic illustration of DIN 4753-3 hot water corrosion test procedure 67

Figure 6.1 Chart of the characterization procedure conducted in the study 68

Figure 7.1 DTA analysis of frits; F-Ca, F-Sr, and F-Ba 75

Figure 7.2 XRD patterns of the studied a) frits F-Ca, F-Sr, and F-Ba b) after crystallization of bulk glass BG-Ca, BG-Sr and bulk glass-ceramic BGC-Ba..... 77

Figure 7.3 Raman spectrum curves of a) frits and b) after crystallization heat treatment of frits, resulting bulk glasses and bulk glass-ceramics..... 80

Figure 7.4 According to DIN 4753-3 corrosion testing the glass/glass-ceramic coatings were exposed to hot water (95 °C) after 21 days and after 42 days weight loss values..... 83

Figure 7.5 ICP-MS analysis results (Figure out of black lines for the first 21 days, red lines for the second 21 days) for determining elements released from coating to water a) Silicon, b) Boron, c) Sodium, d) Cobalt, and e) Iron. The determined Iron element could be released from the steel substrate into water 89

Figure 7.6 ICP-MS analysis results (Figure out of black lines for the first 21 days, red lines for the second 21 days) for determining elements released from coating to water a) Silicon, b) Boron, c) Sodium, d) Cobalt, and e) Iron. The determined Iron element could be released from the steel substrate into water 90

Figure 7.7 Macro images of coatings pre- and post-hot aqueous corrosion 93

Figure 7.8 3D surface topography and 2D surface plot for three different glass/glass-ceramic coatings; a) GC-Ca pre-corrosion, b) GC-Ca post-corrosion, c) GC-Sr pre-corrosion d) GC-Sr post corrosion e) GC-Ba pre-corrosion f) GCC-Ba post-corrosion. 95

Figure 7.9 3D surface topography and 2D surface plot for three different glass/glass-ceramic coatings; a) GC-Ca pre-corrosion, b) GC-Ca post-corrosion, c) GC-Sr pre-corrosion d) GC-Sr post corrosion e) GC-Ba pre-corrosion f) GCC-Ba post-corrosion 97

Figure 7.10 SEM analysis surface images with 150x magnification in SEI mode of a) GC-Ca pre-corrosion, b) GC-Ca post-corrosion, c) GC-Sr pre-corrosion, d) GC-Sr post-corrosion e) GC-Ba pre-corrosion f) GCC-Ba post-corrosion 98

Figure 7.11 SEM analysis cross-section images with 250x magnification in HD BSD mode for pre-corrosion and 500x magnification in SEI mode of a) GC-Ca pre-corrosion, b) GC-Ca post-corrosion, c) GC-Sr pre-corrosion, d) GC-Sr post-corrosion e) GC-Ba pre-corrosion f) GCC-Ba post-corrosion 100

LIST OF TABLES

Table 2.1 The main crystalline phases, properties, and application areas of some glass-ceramic systems 11

Table 3.1 The purposes of the oxides and minerals utilized in glass-ceramic coatings 20

Table 3.2 The division of oxides into groups according to their functions inside the glass structure..... 222

Table 3.3 The coefficients of cubical thermal expansion that several glass-ceramic coatings and some metals exhibit. 31

Table 5.1 Chemical composition of frits (molar%) 65

Table 5.2 Batch (mill) recipe of the samples. 65

Table 7.1 Roughness values of three different glass/glass-ceramic coatings pre- and post-corrosion. 95

ABSTRACT

Development of Aqueous-Corrosion Resistant Alkaline Borosilicate Glass Coating For Use In Hot Water Storage Systems

Ömer Furkan ÖTKEN

Department of Metallurgical and Materials Engineering

Master of Science Thesis

Supervisor: Assoc. Prof. Dr. Buğra ÇİÇEK

Glass and glass-ceramic materials have extensive applications in various fields; including bio-glas s, nuclear waste containment, simple international glass, enamel-coated boiler systems, and water storage and dispersion systems. These materials are designed to withstand constant exposure to aqueous solutions throughout their lifespan. One notable characteristic of glass and glass-ceramic materials is their exceptional chemical resistance to aqueous solutions, rendering them well-suited for water contact applications. However, it is crucial to consider the potential leaching of heavy metal ions from these materials into water, as it may result in their accumulation in the environment or living organisms. Such accumulation can reach levels that pose toxicological risks to human health and water sources. The purpose of the investigation is to the effect of alkaline-earth oxides on the alteration of enamel coatings on steel under hot-water exposure conditions. Enamel coatings based on glass/glass-ceramic coating obtained from frit, i.e., precursor glass, produces via melting-quenching of glass formers, fluxes, and modifiers and coating of powdered frits onto substrate. We conducted experiments involving the

incorporation of various 2A alkaline-earth oxides, including CaO, SrO, and BaO, into sodium-borosilicate glass systems denoted as F-Ca, F-Sr and F-Ba. Comprehensive characterization of frits was carried out, encompassing chemical compositions, phase transitions, and thermal behaviour, utilizing techniques such as, x-ray diffractometry (XRD), and differential thermal analysis (DTA). Coated samples were sinter-crystallized at 860 °C and exposed according to DIN 4753-3 to hot aqueous corrosion at 95 °C, which determined weight loss after 42 days. Pre- and post-hot water exposure samples, surface, cross-section, roughness, and gloss were examined by SEM, a 2D and 3D surface profilometer, and a gloss meter. Hot aqueous solutions that were exposed to the coatings were analyzed by ICP-MS to determine the leaching and migration of elements from the enamel coating. A hot water corrosion resistance test showed that glass-ceramic coatings provide more resistance (weight loss value for GCC-Ba=25,77 g/dm^2 and migration of elements Si=309788, B=40765, which are glass formers) to hot water corrosion than glass coatings.

Keywords: Water corrosion, inductively coupled plasma, surface profilometer, chemical resistance, element release.

ÖZET

Sıcak Su Depolama Sistemlerinde Kullanılmak Üzere Sulu Korozyona Dayanıklı Alkali Borosilikat Cam Kaplamanın Geliştirilmesi

Ömer Furkan ÖTKEN

Metalurji ve Malzeme Mühendisliği Departmanı

Yüksek Lisans Tezi

Danışman: Doç. Dr. Buğra ÇİÇEK

Cam ve cam-seramik malzemelerin çeşitli alanlarda geniş uygulamaları vardır; biyo-cam, nükleer atık muhafazası, basit uluslararası cam, emaye kaplı kazan sistemleri ve su depolama ve dağıtma sistemleri dahil. Bu malzemeler, ömürleri boyunca sulu çözeltilere sürekli maruz kalmaya dayanacak şekilde tasarlanmıştır. Cam ve cam-seramik malzemelerin dikkate değer bir özelliği, sulu çözeltilere karşı olağanüstü kimyasal dirençleridir, bu da onları suyla temas uygulamaları için çok uygun kılar. Ancak, ağır metal iyonlarının bu malzemelerden suya sızma potansiyelinin dikkate alınması çok önemlidir çünkü bu, bunların çevrede veya canlı organizmalarda birikmesine neden olabilir. Bu tür birikimler insan sağlığına ve su kaynaklarına toksikolojik risk oluşturacak düzeylere ulaşabilmektedir. Araştırmanın amacı, alkali toprak oksitlerin, sıcak suya maruz kalma koşulları altında çelik üzerindeki emaye kaplamaların değişimi üzerindeki etkisini araştırmaktır. Fritten, yani öncü camdan elde edilen cam/cam-seramik kaplamaya dayalı emaye kaplamalar, cam oluşturucuların, eritkenlerin ve değiştiricilerin

eritilmesi-söndürülmesi ve toz haline getirilmiş fritlerin alt tabaka üzerine kaplanması yoluyla üretilir. CaO, SrO ve BaO dahil olmak üzere çeşitli 2A alkalin toprak oksitlerin F-Ca, F-Sr ve F-Ba olarak adlandırılan sodyum-borosilikat cam sistemlerine dahil edilmesini içeren deneyler gerçekleştirdik. X-ışını difraktometrisi (XRD) ve diferansiyel termal analiz (DTA) gibi teknikler kullanılarak kimyasal bileşimleri, faz geçişlerini ve termal davranışı kapsayan cam hamurunun kapsamlı karakterizasyonu gerçekleştirildi. Kaplanmış numuneler 860 °C'de sinter kristalize edildi ve DIN 4753-3'e göre 95 °C'de sıcak sulu korozyona maruz bırakıldı; bu, 42 gün sonra ağırlık kaybını belirledi. Sıcak suya maruz kalma öncesi ve sonrası numuneler, yüzey, kesit, pürüzlülük ve parlaklık, SEM, bir 2D ve 3D yüzey profilometresi ve bir parlaklık ölçer ile incelendi. Kaplamalara maruz kalan sıcak sulu çözeltiler, emaye kaplamadan elementlerin sızmasını ve migrasyonunu belirlemek için ICP-MS ile analiz edildi. Sıcak su korozyon direnci testi, cam-seramik kaplamaların sıcak suya karşı cam kaplamalara göre daha fazla direnç sağladığını (GCC-Ba için ağırlık kaybı değeri=25.77 g/dm^2 ve cam oluşturucu olan Si=309788, B=40765 elementlerinin geçişi) sağladığını göstermiştir.

Anahtar Kelimeler: Su korozyonu, endüktif eşleşmiş plazma kütle spektrometresi, yüzey profilometresi, kimyasal direnç, element salınımı.

1
INTRODUCTION

1.1 Literature Reviev

The intricate global challenge of corrosion, an annual cause for the loss of both lives and property, underscores the imperative for a comprehensive understanding and mitigation of this pervasive phenomenon to foster sustainability. In the vast realm of solid-form materials, encompassing ceramics, metals, polymers, and composites, corrosion manifests as a common adversary, rendering materials either functionally obsolete or diminishing their overall performance. The nuanced susceptibility of each material to corrosion is contingent upon the specificities of its usage and the intricate interplay of environmental factors. Notably, even seemingly inert substances like glass, often hailed for their chemical inertness, succumb to rapid corrosion when encountering Hydrogen Fluoride (HF). In stark contrast, polyethylene bottles can robustly contain this corrosive acid for prolonged durations, epitomizing the relative nature of material corrosion resistance depending on the prevailing environmental and usage conditions [1], [2].

Further complexity emerges in the perennial confrontation of materials with one of the most formidable and relentless corrosive environments nature. Over protracted timelines, natural elements such as water, wind, and sunlight orchestrate erosions and corrosions, shaping landscapes in the process. Particularly noteworthy is the behavior of non-oxide metals like steel, which, when subjected to water and heat, commence a transformative journey back to stable oxidic structures. This phenomenon is not merely an aesthetic concern; it fundamentally compromises the mechanical integrity of these materials, emphasizing the paramount need for protective measures [1].

In this context, the application of various coatings stands out as a strategic response to safeguard materials against the corrosive impacts of nature. Among these, glass-ceramic coatings emerge as exemplars of resilience, adeptly withstanding the triad of challenges posed by heat, water, and mechanical abrasion. This unique characteristic ensures the preservation of the mechanical robustness of steel,

thereby fostering extended durability within corrosive environments, contributing significantly to the overarching discourse on material sustainability.

As this thesis embarks on a nuanced exploration of the multifaceted realm of glass ceramics, it is pivotal to underscore the ubiquitous presence of enamel coatings, a predominant manifestation of glass ceramics prevalent in households. The intricate interplay between glass and aqua solutions catalyzes a complex process of corrosion, the subject of hundreds of scholarly articles, with research efforts intensifying over the last few decades. Inextricably linked to the broader societal context, the thesis recognizes the fundamental importance of securing access to safe water for human health and well-being, amplifying the urgency to shield pristine water sources from anthropogenic contaminants.

Amid the diverse array of choices for water storage units ranging from large industrial reservoirs to compact domestic containers materials such as tanks and pipes, invariably in contact with water during storage or distribution, stand as sentinels in the perpetual quest for securing access to safe water. The preference for boilers coated with glass or glass ceramics in drinkable or hot water storage tanks attests to the trust placed in these materials. Additionally, glass garners recommendations even for the storage of nuclear waste, underscoring its exceptional properties in diverse applications[3-6].

Yet, even as these materials fulfill their intended roles, they undergo a transformative process of corrosion when interfacing with water during usage. The intricate interaction between glass, glass-ceramic coatings, or glass, and water unfolds through a kaleidoscope of reaction mechanisms, including ion exchange, hydrolysis, dissolution, diffusion, and adsorption. This rich tapestry of interactions has spurred a prolific body of literature, delving into nuanced aspects such as the chemical composition of glass, aqueous solution parameters encompassing pH and temperature, and the influence of externally introduced elements. This comprehensive review will navigate the complex terrain of glass and glass-ceramic corrosion mechanisms, shedding light on the role of alkaline and earth-alkaline oxides and unraveling the intricate interplay of solution parameters, including varied pH values, chemical content, and temperature, in shaping the corrosion dynamics of glass [1], [7-9].

The aqueous corrosion resistance of alumina-silicate glass with various CaO contents at temperatures up to 300 °C was investigated by Galuskova [10]. Corrosion experiments with model calcium aluminosilicate glass revealed that increased concentrations of calcium in glass have only a negligible influence on the initial dissolution rates of the CaO-Al_2O_3-SiO_2 (CAS) glass in deionized water at 290 °C. Sodium aluminum silicates precipitated from the NaCl solution and calcium aluminum silicates from deionized water reach their solubility limits as a result of increased calcium concentration in the corrosion solution, resulting in the precipitation of crystalline phases adhering to the material surface and impeding the glass dissolution process.

Bergeron's [11] study consists of the influence of the effects of Ti, Zr, and Hf elements on the chemical durability of the soda-lime-borosilicate glass system. The roles of Ti, Zr, and Hf elements are different during the initial dissolution rate and residual rate regimes, as shown by the increase in the residual rate when increasing the Zr content of the glass. The formation of the sodic-silicate and magadiite second crystalline phase is caused by a 1 mol% Ti addition in glass that increases the residual dissolution rate. Also highlight the synergy between the gel components (Si, Ca, and Na) and the Ti, Zr, and Hf elements on the surface, which play a major role in the alteration of glass.

Gin [12] investigated the short- and long-term dissolution rates of ten borosilicate glass ranging in complexity from three to thirty oxides. Al, Ca, Zr, and Ce elements were chosen as key elements. They were added to borosilicate glass that was leached in pure water at 90 °C and monitored for up to 14 years. Gin [12] evidenced a qualitative inverse correlation between the initial and residual rates. Between Ca and hardener elements such as Al and Zr, they have the lowest residual rates compared with glass, which has a few elements. Also, during his study, long-term experiments will help understand how glass behaves once the solution is saturated with the main glass formers.

With an emphasis on the mechanism of hot water corrosion in glass/glass-ceramic coatings, the thesis attempts to investigate the impact of earth-alkaline oxides, especially CaO, SrO, and BaO, on the corrosion resistance of enamel surfaces. The goal of the study is to close a gap in the literature by investigating the hot water

corrosion resistance over a 42-day period and to shed light on how these oxides affect the structure of sodium-borosilicate glass.

To investigate the impact of earth-alkaline oxides on glass structure, basic sodium borosilicate compositions were modified to include them. It is expected that corrosion behavior studies on these materials would shed light on their structural influence in the absence of any prior corrosion, leading to a more thorough comprehension of their connection.

1.2 Objectives of Thesis

The primary objective of this thesis is to explore the influence of earth-alkaline oxides on the corrosion resistance of an enamel surface, particularly focusing on the mechanism of hot water corrosion in glass/glass-ceramic coatings. Addressing a gap in the existing literature, the study aims to investigate the impact of alkaline earth oxides on the hot water corrosion of enamel coatings. To examine the specific effects of earth-alkaline oxides, namely CaO, SrO, and BaO, MgO was intentionally omitted due to its comparatively low thermal expansion coefficient when contrasted with other earth-alkaline oxides. For assessing the hot water corrosion resistance of the coatings, standard test equipment was employed, subjecting the coatings to a 42-day exposure to hot water to simulate realistic conditions. Another objective of the thesis is to gain insights into how earth-alkaline oxides influence the structure of sodium-borosilicate glass. To achieve this, concurrent morphological analyses and examinations will be conducted alongside the corrosion studies.

1.3 Hypothesis

Despite existing studies on the resistance of earth-alkaline oxides in formulations to corrosive environments in coatings, no such application or research has been encountered within the context of enamel coating endeavors. Earth-alkaline oxides, namely CaO, SrO, and BaO, are recognized as fluxes in glass science and are known to diminish the corrosion resistance of the glass structure within enamel coatings.

However, comprehending how the presence of distinct types of earth-alkaline oxides in resistance to hot water corrosion impacts changes in the enamel structure

will enhance our understanding of corrosion resistance in this specific type of coating. This study aims to compare the crystallization behavior of earth-alkaline oxides with identical molar values added to the sodium borosilicate glass structure and subsequently examine their response to hot water attacks. By doing so, the reasons for improvements or deteriorations in corrosion resistance can be comparatively analyzed.

Furthermore, earth-alkaline oxides were incorporated into simple sodium borosilicate compositions because of the understanding of the earth's alkaline oxide effect on glass structure. It is anticipated that these materials, when subjected to corrosion behavior investigations, will provide insights into their structural impact without any pre-existing corrosion, thus contributing to a more comprehensive understanding of their relationship.

2
GLASS-CERAMIC

2.1 Glass

Glass is a versatile inorganic material characterized by its non-crystalline, amorphous structure, which distinguishes it from crystalline solids. The primary component of glass is silica, often in the form of silicon dioxide or quartz, accompanied by additional materials such as soda and lime. The manufacturing process involves melting these raw materials and then carefully cooling them to achieve a rigid condition without crystallization, resulting in the transparent and brittle substance known as glass [13].

One of the defining properties of glass is its optical transparency. This quality allows glass to transmit light, making it invaluable for applications such as windows, lenses, and optical devices. The brittleness of glass is another notable characteristic, indicating its tendency to fracture or shatter rather than undergo plastic deformation under stress. Although glass is brittle, modifications and treatments, such as tempering, can enhance its strength and durability [14].

Glass exhibits chemical inertness, resisting reactions with most substances, which renders it suitable for storage containers for various chemicals and liquids. The durability of glass is underscored by its resistance to environmental factors such as moisture, air, and sunlight. This durability contributes to the long-lasting nature of glass products. Furthermore, glass possesses thermal insulation properties, though not as pronounced as some other materials. Its recyclability is a notable environmental advantage, as glass can be melted down and reused, promoting sustainability [15].

The malleability of glass at high temperatures is exploited in glassblowing and forming processes, allowing it to be molded into intricate shapes and designs. This property is fundamental to the artistry and craftsmanship associated with glasswork. Additionally, glass is an exceptional electrical insulator, finding applications in the electronics industry [13].

In terms of hardness, glass is classified as a hard material, albeit susceptible to scratching or damage. Its diverse range of appearances, from transparent to opaque,

and the ability to introduce various colors during the production process make glass highly adaptable for different aesthetic and functional purposes.

In conclusion, the unique combination of properties in glass, including transparency, brittleness, chemical inertness, durability, and recyclability, makes it an indispensable material with diverse applications across industries, from everyday items to specialized fields such as optics and electronics. These qualities position glass as a subject of academic interest, offering a rich area for research and exploration within the realm of materials science [13-15].

2.2 Glass-Ceramic Definition

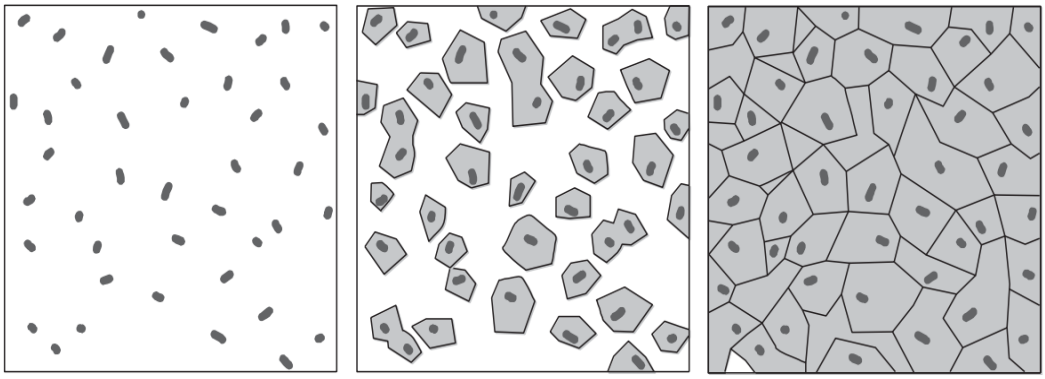
The important discovery and subsequent definition of glass-ceramics were made in the 1950s by famous glass scientist Dr. S.D. Stookey. According to Dr. Stookey, the creation of glass-ceramics is a two-step process that begins with the melting and shaping of specially prepared glasses that contain nucleating agents and ends with controlled crystallization [16]. It should be emphasized that although while this definition was developed during this time, it does not disprove the presence of materials with a comparable structure from earlier years. In reality, glass crystallization techniques were used by scientists to make solid ceramic materials as early as the 1700s.

Dr. Stookey first became interested in glass-ceramics when he ran into an odd occurrence while experimenting with silver precipitation on lithium silicate glass for use in making permanent photographic images in his lab. Since lithium silicate glass has improved chemical stability, it was chosen. Stookey accidentally heated the glass to 450 °C during a study on precipitation, which led to an overnight increase in furnace temperature of 850 °C. Unexpectedly, the glass did not melt as he had expected and stayed intact. Additionally, the glass did not shatter when it unintentionally dropped to the ground while being removed from the furnace; instead, it behaved more metallically. Stookey was intrigued by this occurrence and continued to research the substance after realizing the importance of crystals with low expansion coefficients thanks to earlier research on -spodumene's nearly zero thermal expansion [17].

As part of his ongoing investigation, Stookey looked at other crystals including titania and zinc sulphide. Notably, via his study with titania, he discovered the durability of titania-doped aluminosilicate glass-ceramics and successfully marketed this substance under the name Corning Ware®, which was used even in rocket nose cones.

Glass-ceramics have seen improvements throughout time, as well as broader uses. The merging of glass-ceramic materials with glass-crystal composites is the result of the confluence of several areas, including ceramics, glass, metals, and nanomaterials. According to Deubener et al., "Glass-ceramics are inorganic, non-metallic materials prepared by controlled crystallization of glasses via various processing methods." These materials have at least one functioning crystalline phase and a residual glass phase. The amount of crystallization might be as little as ppm or as high as about 100%. By carefully controlling the nucleation and crystallization of glasses, polycrystalline materials known as glass-ceramics are created.

The glass matrix is combined with nucleating chemicals that serve as sites for nucleation, such as titanium dioxide (TiO_2), chromium (III) oxide (Cr_2O_3), zirconium dioxide (ZrO_2), and phosphorus pentoxide (P_2O_5) oxides and fluorides. These nuclei develop and form crystals under regulated heat, taking on different forms including rods, sheets, and spheres. The resultant crystals, which are generally less than 1 μm in size, give glass-ceramic structures qualities like remarkable toughness, impact resistance, and wear resistance [18-20]. The process of glass-ceramic production is shown in Figure 2.1.



(a) (b) (c)

Figure 2.1 The precursor glass is transformed into a glass-ceramic structure by a sequence of events that (a) begin with nuclei production, (b) continue with crystal growth on these nuclei, and (c) end with the final development of the glass-ceramic material [18].

The complex transformation mechanisms present in glass-ceramics are made clear by time-temperature transformation (TTT) diagrams. When using the melt-quenching method, Figure 2.2 offers helpful insights into the creation and behavior of glass-ceramics. Glass must be subjected to cooling rates that are higher than the critical thresholds (q > qc) in order to be produced successfully. This circumstance demonstrates a clear association between the commencement of crystallization and the crystalline fraction reaching a tiny percentage of one part per million ($X = 10^{-6}$), as predicted by Uhlmann's classical theorem. The essential modifications shown in the graphical depiction (Figure 2.2) are seen and analyzed by following these predetermined ratios.

In the graphic;

q: indicates the cooling rate of the glass,

q_c: gives the critical cooling rate, q_c: $(T_L - T_N)/ \delta_t$ T_g: Glass transition temperature,

T_L: Liquidus temperature,

T_N and δ_t: The nose coordinates that can change according to nucleation mechanism.

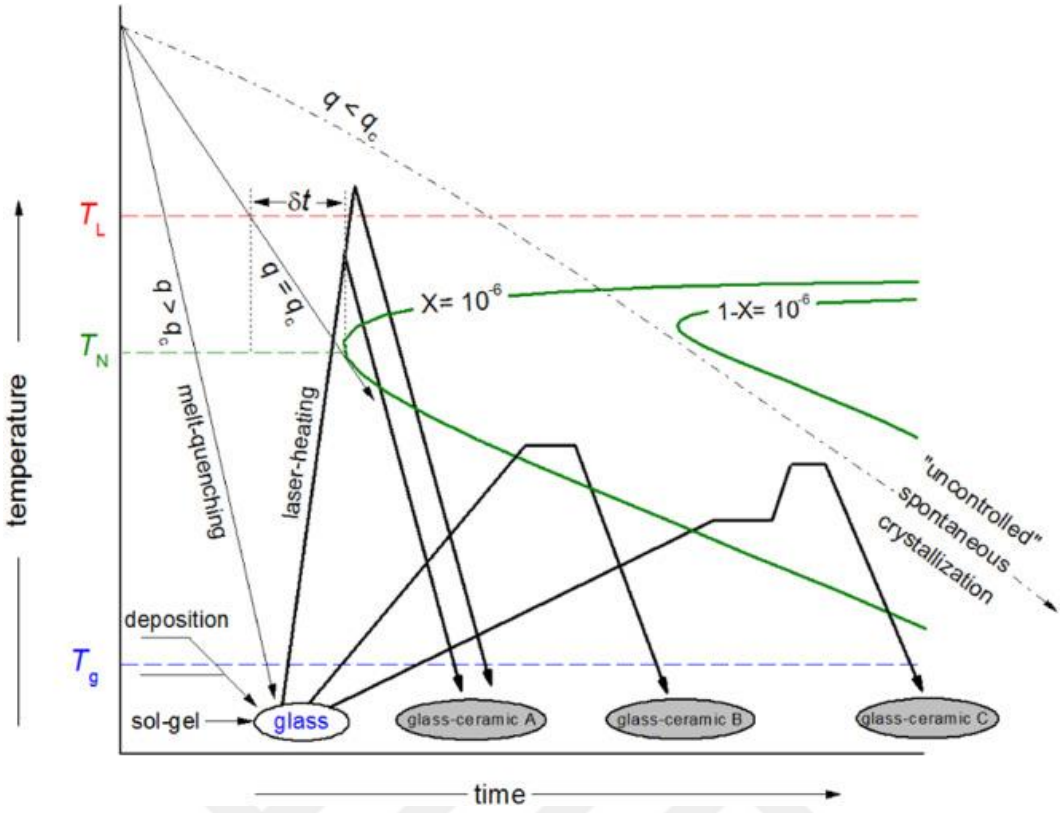


Figure 2.2 Glass-ceramic formation time-temperature transition diagram.

2.3 Glass-Ceramic Properties

The remarkable thermal characteristics of glass-ceramic materials contribute to their particular feature of zero shrinking during manufacture. They are ideally suited for a wide range of industrial and technological applications because to their intrinsic quality, notably in the field of cookery. Glass-ceramics' glassy phase and nonporous structure make it easier to precisely regulate the crystals and microstructure to achieve desired transparency and opacity levels. Additionally, a variety of hues may be realized in glass-ceramic applications because to their optical characteristics.

Glass-ceramics have outstanding chemical qualities when it comes to chemical aspects because of their crystal structure, glass structure, and intrinsic chemical resilience. These parameters control how chemicals interact with glass-ceramics, leading to increased chemical resistance. Mechanically speaking, glass-ceramics have excellent flexural strengths of up to 500 MPa, and development advances have led to toughness values above 3 $MPam^{1/2}$ [18], [21-23].

Table 2.1 The main crystalline phases, properties, and application areas of some glass-ceramic systems [20], [24].

System	Main Crystalline	Property	Application Area
$Li_2O.Al_2O_3.SiO_2$ (ZrO_2, TiO_2)	β-quartz β-spodumene β- eucryptite	Low thermal expansion High temperature resistance	Kitchenware Telescope Mirrors Oven Tops
$Li_2O.Al_2O_3.SiO_2$ (P_2O_5)	$Li_2O.Al_2O_3.SiO_2$	Dielectric properties Chemical resistance	Electronic Insulation Optical Coding Magnetic Recording Head Electric Sleeve
$MgO.Al_2O_3.SiO_2$ (P_2O_5, TiO_2)	Cordierite ($Mg_2Al_4Si_5O_{18}$)	Radar permeable Low thermal expansion High strength	Missile Cap Radar Dome
$PbO.ZnO.B_2O_3.SiO_2$ (F)	Rankinite ($3CaO.SiO_2$)	Heat & Vacuum insulation	Electrotechnology Microelectronic Circuits Capacitor
$BaO.Al_2O_3.SiO_2$ (TiO_2)	Celsian ($BaAl_2Si_2O_8$) Barium Titanate ($BaTiO_3$)	High strength Thermal shock resistance	Kitchenware Cookware
$SiO_2.Al_2O_3.MgO.K_2O$	Phlogopite [$KMg_3AlSi_3O_{10}(F,OH)_2$]	Turning ability Dielectric properties	Electrotechnology Insulator Hermetic Seals

Table 2.2 The main crystalline phases, properties, and application areas of some glass-ceramic systems (Continue) [20], [24].

SiO_2.CaO.Na_2O (P_2O_5)	Apatite $Ca_5(PO_4)_3(F,Cl,OH)$	Biocompatibility Chemical resistance	Dentistry Prothesis
SiO_2.Al_2O_3.MgO (TiO_2)	Mg-Al Titanate $Mg_xAl_{2(1-x)}Ti_{(1+x)}O$	High hardness Resistance	Construction
SiO_2.Al_2O_3.CaO (ZnO)	Wollastonite ($CaSiO_3$)	High hardness Resistance	Architectural Materials
SiO_2.Al_2O_3.MgO. CaO (Sulphide, fluoride)	Wollastonite ($CaSiO_3$) Anorthite ($CaAl_2Si_2O_8$) Diopside ($MgCaSi_2O_6$) Pyroxene [(Na,Ca)(Mg,Fe, Al)$(Al,Si)_2O_6$]	High hardness Abrasion resistance Chemical resistance	Floor Tile Exterior Architectural Materials Pump Pipe

2.4 Glass-Ceramic Applications

2.4.1 Technical Application

The first generation of readily available glass-ceramic products are radomes. They provide the crucial function of protecting radar antennas by serving as structural, weather-resistant casings. Given their innate sensitivity to radio waves, these radome glass-ceramics are designed particularly to reduce electromagnetic signal interference experienced during signal transmission or reception by the antenna. Notably, these materials have critical properties that are necessary for their successful application in this field, such as low dielectric loss, low dielectric

constant, little coefficient of thermal expansion, increased strength, and exceptional resistance to abrasion [25].

With their small sizes and great sensitivity, photosensitive and etched patterned materials have several uses in the fields of electronics, chemistry, acoustics, optics, mechanics, and biology. One popular method for creating these glass-ceramics is the SiO_2-Li_2O system. Ce^{3+} and Ag^+ ions make up the majority of the parent glass's ions. Photoelectrons cause the oxidation of Ce^{3+} to Ce^{4+} and Ag^+ to Ag^0 within the compositions when exposed to ultraviolet (UV) light. Crystal phases are precipitated during heat treatment as a result of controlled crystallization at 600 °C [26].

Lithium metasilicate crystals are etched with diluted hydrofluoric acid to get the finished product. Corning Glass uses the name Fotoform® to sell these upscale glassy bodies. The market also offers a slightly modified version of the non-etched construction called Fotoceram®. Due to their distinctive photosensitivity and etchability characteristics, both product versions are extremely useful across a range of sectors.

Machinable glass-ceramics (GCs) are defined as glass-ceramics that contain fluoromic acid. The fluorphlogopite phase of MACOR® ($KMg_3AlSi_3O_{10}F_2$) is one of the most well-known properties of such machinable GCs. Spacecraft boundary retainers, electrical insulators, suction feedthroughs, microwave-type component screens, field-ion microscope components, seismograph coils, and gamma-ray lens frames are just a few examples of the numerous uses for MACOR® [27].

Several glass-ceramic materials, such as canasite, lithium disilicate, spinel-enstatite, and spinel, are often used in the field of magnetic memory discs. Young's modulus and nanostructured fracture toughness are essential for these applications. For instance, a solid solution of the spinel or gahnite crystal types, $MgAl_2O_4$ or $ZnAl_2O_4$, alone or in combination, should have crystallite sizes less than 0.1 m. The Young's modulus for spinel-enstatite materials varies from 100 to 165 GPa, which is a noticeably high number when compared to other GC materials. Enstatite fracture toughness must also surpass 1 $MPa.m^{1/2}$. Because of this property, spinel-enstatite is the best material to use for magnetic memory applications [18].

In order to create substrates for Liquid Crystal Displays (LCD) in personal laptop computers, the SiO_2-Al_2O_3-Li_2O system is frequently used. Transparency in these glass-ceramics is attained when the wavelength of visible light is greater than the size of the crystallite, and the crystals have approximately equal refractive indices to the parent glass. These glass-ceramics may be used effectively as LCD substrates thanks to their special characteristic, enabling the display of high-quality pictures and graphics.

2.4.2 Opticical Application

To properly survive temperature changes, telescope mirror materials need to have a very low coefficient of thermal expansion. Glass ceramics (GCs) made of -quartz solid solution are used to satisfy this criterion. In a different application, the Integrated Lens Array uses glass-ceramics made of lithium metasilicate and lithium disilicate with a thickness of around 20 micrometers [28].

Because they use less energy and have less data loss, luminescent glass-ceramics are becoming more and more popular. Chromium (Cr^{4+})-Doped Forsterite, -Willemite, and other Orthosilicates for broad wavelength amplification, Ni^{2+}-Doped Gallate Spinel for amplification and broadband infrared source are a few examples of luminescent GCs. These materials are used in solar concentrators [18].

It is also possible to create optical components using a variety of crystal-based glass-ceramics, including Fiber Bragg Grating Athermalization, Laser-Induced Crystallization for optical gratings and waveguides, Ferrule for optical connectors, Transparent ZnO Glass-Ceramics with Controlled Infrared Absorbance, and Microwave Susceptibility. These glass-ceramic materials possess unique qualities that make them useful in a variety of optical applications [29].

2.4.3 Medical and Dental Glass-Ceramics

With implantology (for medical prostheses) and restorative dentistry (for dental prostheses), this term encompasses the use of dental prosthetic materials in two separate biomedical applications [30]. Dental implants, head and neck surgery, orthopedics, and root fillers are just a few of the medical prostheses that may be made through the process of implantology and are all meant to be inserted into human bodies. In contrast, restorative dentistry materials, which include dental

inlays, crowns, bridges, and veneers among other uses, are used to rebuild natural teeth outside of the body.

The materials utilized in these two groupings appear to be identical, yet they really differ greatly. In order to bind with bones and even soft organs, it is essential to utilize biocompatible and bioactive materials that can promote the growth of a physiologically active hydroxycarbonate apatite layer. Implant materials may also be subject to mechanical forces, which calls for strength characteristics including compression, tensile, shear, toughness, and Young's modulus. Visual qualities of implant materials are frequently of less importance. In contrast, materials used in restorative dentistry must be aesthetically pleasing and resemble natural teeth while yet being corrosion and abrasion-resistant. Additionally, they shouldn't interact with any substances that are commonly present in drinks and meals. Both kinds of materials demand exacting care during manufacture, with micrometer-level dimensional precision and surface characteristics adjusted to obtain the required level of roughness or smoothness. Depending on their particular uses and needs, these materials may be produced utilizing a variety of procedures, including sintering, molding, or machining using computer-aided design (CAD)/computer-aided manufacturing (CAM) techniques.

2.4.4 Electrical and Electronic Applications

Mica-type Glass-Ceramics (GCs), noted for their high dielectric constants, are used to create insulator materials. Sintered ceramics are combined with SiO_2-TiO_2-Nd_2O_5 and SiO_2-Al_2O_3-PbO GC systems to create composite materials with high dielectric constants. The procedure entails mixing inorganics with a plasticizer (dibutyl phthalate), a solvent (toluene), and a binder resin (butyl methacrylate) before employing the Doctor Blade Technique on a flat, smooth surface to obtain a thickness of between 0.1 and 0.3 mm. The organics are then burned out at a temperature of 400 °C, and the material is subsequently sintered at a temperature of 900 °C to create a dense and mechanically durable material. The surface is then printed with circuit designs [31].

The use of GC systems in electronic packaging is also useful. Advanced ceramics like ZrO_2 are mixed with SiO_2-Al_2O_3-MgO and SiO_2-Al_2O_3-ZnO systems to form

composite materials. This packaging technology for multilayer chip carriers is used in IBM's specialist computers.

Specific GC formulations are required for Dielectric Glass-Ceramics made for GHz Electronics. Dielectric oxide ceramics, which are used to make resonator and antenna components for products like mobile phones and GPS systems, have transformed the field of microwave wireless communication. However, these ceramics have several disadvantages that are unrelated to their electrical characteristics, such as porosity that causes metallization problems and inhomogeneity that reduces performance. Glass-ceramics with the SiO_2-B_2O_3-TiO_2-ZrO_2-La_2O_3-RE_2O_3 system have been developed to address these issues and offer exceptional homogeneity and porosity-free properties. To satisfy the needs of current ceramics while improving performance characteristics, these glass compositions are designed to precipitate either $La_2Ti_2SiO_9$ or $La_4Ti_9O_{24}$, or a mix of both.

2.4.5 Architectural Applications

Under the brand name NeopariésTM, Nippon Electric Glass has created a very important glass-ceramic material specifically designed for architectural applications [32]. Granular glass particles are used during the production process as the building block. Through a completely automated tunnel furnace process at temperatures as high as 1100°C, these granular glass particles are formed into flat or curved panels. Sintering of the granular glass takes place at 850°C during the subsequent heat treatment, and wollastonite crystallizes at temperatures beyond 950°C.

These glass-ceramic materials are designed to demonstrate crucial characteristics necessary for applications in the building industry. Significant characteristics include outstanding resistance to weathering, absence of water absorption, reduced weight compared to construction materials made of natural stone, and increased hardness exceeding that of natural stone. Fire-resistant windows are also included in this category; they improve the security and dependability of building structures.

2.4.6 Glass-Ceramics for Energy Application

Glass-ceramics are essential in many applications that attempt to improve the effectiveness of energy management and production. Glass-ceramics are used in

three crucial energy generating areas: (i) solar energy efficiency, (ii) battery components, and (iii) solid oxide fuel cells [33].

Glass-ceramics have the potential to replace all three of the cathode, anode, and electrolyte components in batteries, which normally have three primary parts. For instance, after melting in a reducing atmosphere, the parent glass with the chemical formula Li_2O-Fe_2O_3-P_2O_5-Nb_2O_5 can be heated to start the crystallization process. As a result, a continuous phase of $LiFePO_4$ develops inside the glass-ceramic material. Compared to when it is created by a solid-state reaction, $LiFePO_4$ in the glass-ceramic state demonstrates extraordinary chemical resistance to charge-discharge intercalation cycles and has a greater thermal conductivity. In contrast to conventional $LiFePO_4$ ceramic batteries, glass-ceramic batteries display reduced internal resistance and higher high-rate discharge performance. These characteristics help the battery system function and operate efficiently overall.

3
GLASS-CERAMIC COATING (ENAMEL)

Glass-ceramic coatings, sometimes referred to as vitreous enamel coatings, provide a very efficient way to safeguard metal substrates and increase the useful life of metal objects [34], [35]. Precursor glass, also known as frit, together with other additives, such as colours and floaters, are used to create glass-ceramic coatings [36-38]. The primary element of the glass-ceramic coatings is the precursor glass, which has a totally amorphous structure. It is made by rapidly cooling after melting a variety of inorganic oxides at temperatures between 1000°C and 1500°C [39], [40]. Specific features, such as application characteristics, ornamental elements, and technical needs, are enhanced by the use of various additives.

To get the required particle size, which is decided based on the application technique, the mixture of precursor glass and additives is milled prior to application. A screening technique is used to assure the right particle sizes for the application [36].

The glass-ceramic coating wet application methods include flow coating, spraying, dipping, and electrophoretic deposition. The water is mixed with the powdered frit and the other components are ground to make a suspension. When glass-ceramic coatings are applied to metal substrates using thermal spray coating or electrostatic powder spraying after the crystallization process, on the other hand, powdered frits are utilized [37], [39], [40].

The devitrification phase, which starts when the frit powder is applied to the substrate, is when the devitrification or crystallization qualities are affected by the coating formulation and metallic substrates. Glass-ceramic coatings, for instance, are heated between 780°C and 850°C for steel substrates and between 500°C and 570°C for aluminum substrates [37], [40].

3.1 Chemical Components of Glass-Ceramic Coatings and Their Purposes

Glass-ceramic coatings are made of "frit," which are amorphous structures that act as semicrystalline glassy coating materials. These coatings are made using oxides such SiO_2, B_2O_3, Al_2O_3, Na_2O, NiO, CuO, P_2O_5, and Fe_2O_3 that adhere to the Seger formulation by vitrification and subsequent recrystallization [41]. The manufacturing process can be broken down into four main stages: i) high-temperature fusing-quenching to obtain frit; ii) frit milling with or without milling additives; iii) application of the milled frit to the metal substrate; and iv) the stage of crystallization, which takes place at relatively high temperatures (720-850 °C) [18]. Due to the crystal and amorphous structure that is created at the end of the process, this extensive process leads to the formation of an aesthetically beautiful coating material that demonstrates resistance to mechanical, chemical, and thermal damages [36].

The oxides in Table 3.1 are divided into groups according to how they act in the glass-ceramic structure. Silica (SiO_2) has the singular capacity to spontaneously create glass at sufficiently high temperatures, exceeding 1700 °C, without requiring any extra components, especially in glass-ceramic systems. Comparatively to other ingredients, SiO_2 is used the most frequently in diverse glass-ceramic compositions. Glass-ceramic coatings, like vitreous coatings, are made of a network of silica tetrahedra to which additional substances are added as modifiers.

Table 3.3 The purposes of the oxides and minerals utilized in glass-ceramic coatings [42], [43].

Component	Minerals	Functions
SiO_2	Quartz Feldspar	Glass-forming oxide, a component of the refractory, enhances chemical resistance, increases the glass-transition temperature of the vitreous system, and increases viscosity.
B_2O_3	Borates	The flux that decreases viscosity, raises surface hardness, and creates the vitreous matrix.
Na_2O K_2O Li_2O	Albite Feldspar Microcline Spodumene Petalite Lepidolite	Alkaline substances make glass less elastic, brighter, and decrease the temperature at which it softens.
Al_2O_3	Feldspar Corundum	Decreases the expansion coefficient, promotes an opaque finish, and increases viscosity as well as mechanical, chemical, and thermal resistance.
ZrO_2	Zirconia	Enhances tolerance to shocks, knocks, and acids and serves as an opacifier.
ZnO	Zincite Blende Wurtzite	Superior flux, which reduces the expansion coefficient and enhances surface quality and brightness.

Table 3.1 The purposes of the oxides and minerals utilized in glass-ceramic coatings (Continue) [42], [43].

CoO	Cobaltite	It is an extremely potent adhesion agent that creates a structure full of tiny, evenly spaced bubbles.
NiO	Niccolite	It is a second adherence agent that results in a structure with few large bubbles.
CuO	Copper Oxide	At lower temperatures, it initiates the adhesion reaction when coupled with primary bonds.
MnO_2	Manganese Dioxide	Produces frits with a brown color, enhances dark colors, and functions as a weak bonding agent and oxidant.
Sb_2O_3	Antimonite	Increases resistance to acids and produces a high degree of opacity.
TiO_2	Rutile Anatase	Opacifiers: they improve a material's whiteness, brightness, and heat and acid resistance.
BaO CaO MgO	Baryte Witherite Calcite Dolomite Limestone Periclase	Alkaline-earthy components with integrated glass-ceramic covering that resist acidity and increase viscosity, resistance, and CaO smelting capacity.
P_2O_5	Apatite	Decreases chemical resistance, enhances color stability, and modifies the finish's opacity.
CaF_2	Fluorite	Softens glass and influences the opacity

Low melting point materials, which melt at 1050 °C or below, are included by using one or two parts of SiO_2 for everyone or more additional materials. On the other hand, materials that melt at greater temperatures of 1250 °C or above usually include three to five parts of SiO_2. Despite being a common constituent in coatings, SiO_2 has a substantial disadvantage because of its exceptionally high melting temperature, which exceeds 1700 °C [44].

Table 3.2 The division of oxides into groups according to their functions inside the glass structure [45-48].

Glass Former	Glass Modifier	Glass Modifier	Glass Former (RO_2, R_2O_3)	Adhesion Promoter
SiO_2	Li_2O	MgO	TiO_2	CaF_2
B_2O_3	Na_2O	CaO	ZrO_2	MnO_2
	K_2O	SrO	SnO_2	CoO
		BaO	Fe_2O_3	NiO
		ZnO	Al_2O_3	

Numerous oxides are used in the chemical makeup of glass-ceramic coatings; these oxides may be categorized into five groups according to their purposes as follows:

Fluxes: These oxides are essential for decreasing the glass-ceramic mixture's melting point and enabling the fusing of the parts during the heat treatment procedure.

Refractories: These oxides increase the glass-ceramic coatings' high-temperature stability, making them durable and resistant to thermal shocks.

Adhesion agents: These elements are in charge of fostering good bonding and adhesion qualities between the glass-ceramic covering and the metal substrate.

The glass-ceramic coatings are given opacity by the oxides in this category, making them perfect for applications where opacity or translucency is sought.

3.1.1 Fluxes

Lowering the melting point of silicon dioxide, which is the main glass-forming oxide in enamel formulations, is the main purpose of the oxides classified as fluxes. These flux oxides are important in improving the enamel's homogeneity, which results in better surface quality. Additionally, they help to make the link between the metal substrate and the enamel stronger, ensuring a solid and long-lasting connection. These fundamental oxides assist in the production of the glass structure when combined with acidic refractories.

This group includes a number of raw materials, such as zinc oxide (ZnO), borax, soda ash, soda nitrate ($NaNO_3$), fluorspar (CaF_2), cryolite (Na_3AlF_6), litharge (lead (II) oxide), red lead (lead (II, IV) oxide, and barium carbonate ($BaCO_3$) [41].

Glass-ceramic coatings may be tailored to achieve desired melting temperatures, surface characteristics, and overall structural integrity for a variety of industrial and architectural applications by deftly combining these flux oxides into the enamel composition.

3.1.2 Refractories

These substances are very important in the formation of the glass structure and in supporting the acidic component of the glass melt. Quartz, feldspar, and clay are three of the components in this category that are of particular significance. Particularly quartz plays a crucial role in the glass-ceramic formulation, helping to produce a glassy matrix and giving the finished product crucial mechanical and chemical qualities [49]. Feldspar and clay also contribute to the overall composition of glass-ceramic, strengthening its structural integrity and offering certain qualities that affect the material's ultimate attributes and performance.

3.1.3 Adhesion Agent

The interaction between glass-ceramic coatings and the metallic substrate's adhesion properties is of utmost relevance. During the melting process, specific oxides, such as CoO (cobalt oxide), NiO (nickel oxide), and CuO (copper oxide), are added in order to create high adhesion. CoO (cobalt oxide) stands out among them as the most important adhesion agent, offering both powerful adhesion and a blue colorant for aesthetic purposes [49].

3.1.4 Opacifiers

The principal function of the oxides in this group is to provide glass-ceramic coatings their opaque properties. These opacifying oxides include Sb_2O_3, $NabO_3$, TiO_2, $ZrSiO_4$, and ZrO_2, as well as sodium antimonate, titanium dioxide, and zirconium oxide. The particular refractory qualities of these oxides contribute to the opacifying effect. To further improve the melt's fluidity throughout the process, other additives such Na_3AlF_6 (cryolite) and CaF_2 (fluorspar) are used in addition to these basic opacifiers [49].

Glass-ceramic coatings with these opacifying oxides added have an opaque look, making them perfect for applications where opacity or translucency is sought. In addition to providing aesthetic appeal and visual opacity to improve the overall design and performance of the coated materials, these coatings are used in a number of architectural and ornamental applications.

3.1.5 Colour Agents

Glass-ceramic coatings stand out for their extraordinary fusion of technical and aesthetic excellence, making them a popular option in a variety of applications. This coatings' attractiveness is further increased by the wide variety of hues and tints they give. The most often used oxides in this category are CoO (cobalt oxide), CuO (copper oxide), FeO (iron oxide), and NiO (nickel oxide).

These oxides act as effective colorants that can give the glass-ceramic coatings vivid colours. Without the addition of any additional chemicals, they can be used as colorants on their own. As an alternative, frits may contain pigments to act as colorants while being coated [49].

3.2 Types of Enamels

Enamel coatings can differ depending on how they are applied and where they are used, which is why terminology like "ground coat" and "cover coat" were created to express these differences.

3.2.1 Ground Coat

The best possible adherence between the metal substrate and the enamel layer is the main goal of the ground coat enamel coating. It is essential to guarantee excellent

impact resistance since enamel coatings are exposed to possible impacts when being applied. As a result, the ground coat is made to have sufficient strength so that it may attach to the metal surface firmly, protecting the enamel coating's general integrity and increasing its endurance.

A number of pre-processes are routinely carried out before to applying enamel coatings to metal surfaces, including degreasing, acid bath treatment, hot water rinsing, cold water rinsing, and drying. These procedures guarantee a complete cleaning of the metal surface, eliminating any dirt, grease, or scale that can impair the coating's quality [49].

The criteria for applying the cover coat as well as the requirement to provide good adherence to the metal substrate are taken into account while creating the ground coat enamel composition. Careful consideration is made to minimize the influence on the overall quality of the enamel coating in order to handle the possible concerns caused by variations in thermal expansion coefficients between the ground coat and the tile lining in the higher layer. Unwanted cracking or shrinkage during cooling might result from thermal expansion during heating. The creation of new-generation enamels, however, as a result of developments in enamel technology makes it possible to achieve the appropriate technical and aesthetic aspects merely by the application of a base coat in some circumstances [49].

Enamel coatings may be applied with improved adhesion, structural integrity, and aesthetic appeal thanks to the adoption of suitable pre-treatment procedures and the optimization of the ground coat enamel composition, leading to high-quality, long-lasting, and aesthetically pleasing finished products.

3.2.2 Cover Coat

Usually, cover coat enamel treatments are done to provide the enamel coating the appropriate technical qualities. It might be difficult to achieve other features like acid resistance, alkali resistance, boiling water resistance, simple cleaning, abrasion resistance, and color because the main goal of ground coat coatings is to ensure adhesion. In order to impart these particular qualities, cover coat treatments are essential [49].

The thermal expansion coefficient must be taken into account in cover coat applications to guarantee compatibility with the ground coat. The thermal

expansion coefficients of the ground coat and cover coat enamel compositions must be almost identical. After the coating is applied, a considerable difference in these coefficients might cause cracking or other flaws. The topic of color is also important, particularly in white cover coat enamel coatings where it shouldn't be possible to see the ground coat's color. Therefore, cover coat coatings must have a rather high level of concealment [49].

When one cover coat is insufficient in some circumstances, the "three coatings" procedure is used, which involves applying a second cover coat. The middle coat acts as the intermediary layer in these situations. However, due to the increased crystallization during fire, it is necessary to carefully examine the thermal expansion coefficient in three-coat applications. As ceramic crystals expand in the glass-ceramic structure during the firing process, the coating's amorphous structure decreases. Additionally, hydrogen may try to escape from the surface due to an increase in hydrogen solubility inside the metal substrate during burning, which has been seen most often in steel sheets. This tendency greatly increases the likelihood of cracking and other enamel surface flaws, particularly re-boiling [49].

For effective enamel applications with optimal technical qualities and to guarantee the lasting durability of the completed goods, it is crucial to take these parameters into account and adhere to accurate thermal expansion coefficient matching.

3.3 Adhesion Mechanism Between Glass-Ceramic and Metallic Substrate

3.3.1 Diffusion Theory

Diffusion occurs at the interfaces between the glass-ceramic coating and the metallic substrate, where silicon from the glass-ceramic material diffuses into the substrate material and iron from the metallic substrate diffuses into the glass-ceramic material. The bonding process between the glass-ceramic covering and the metallic substrate is thought to be significantly influenced by this diffusion phenomena [50].

3.3.2 Chemical Theory

According to this idea, when the glass contacts the metal substrate's existing oxide layer during the sintering of the glass-ceramic coating, a driving force is created

that causes the metal to oxidize, resulting in the creation of iron oxide (FeO) molecules [51].

The oxidation of the metal, in which iron present in the substrate combines with oxygen from the glass-ceramic to generate iron oxide (FeO), is one of the reactions that take place in the substrate material during the fire of the glass-ceramic covering. A robust and well-adhered contact between the glass-ceramic coating and the metallic substrate is made possible by the fact that silicon from the glass-ceramic may seep into the substrate material. This diffusion-driven process aids in the two materials' adhesion mechanism [50].

$$Fe_3O_4 \rightarrow Fe^{2+} + 2Fe^{3+} + 4O_2 \quad (1)$$

$$2Fe^{3+} + Fe \rightarrow 3Fe^{2+} \quad (2)$$

In a glass-ceramic coating composition, Fe reduces the molecules of cobalt oxide (CoO) and nickel oxide (NiO) to produce metallic cobalt and nickel;

$$Fe + CoO \rightarrow FeO + Co \quad (3)$$

$$Fe + NiO \rightarrow FeO + Ni \quad (4)$$

The compound's affinity for oxygen grows at the bottom of the Ellingham diagram. Iron demonstrates a stronger oxygen affinity than nickel and cobalt in the glass-ceramic heating scenario at the particular temperature range, as shown in Figure 3.1. Due to this quality, cobalt and nickel are primarily used to improve the glass-ceramic coating's adhesive qualities [37], [51]. Because cobalt and nickel have a lower oxygen affinity than iron, which makes them more successful at promoting the attachment of the glass-ceramic to the metallic substrate, these metals were chosen for the coating procedure.

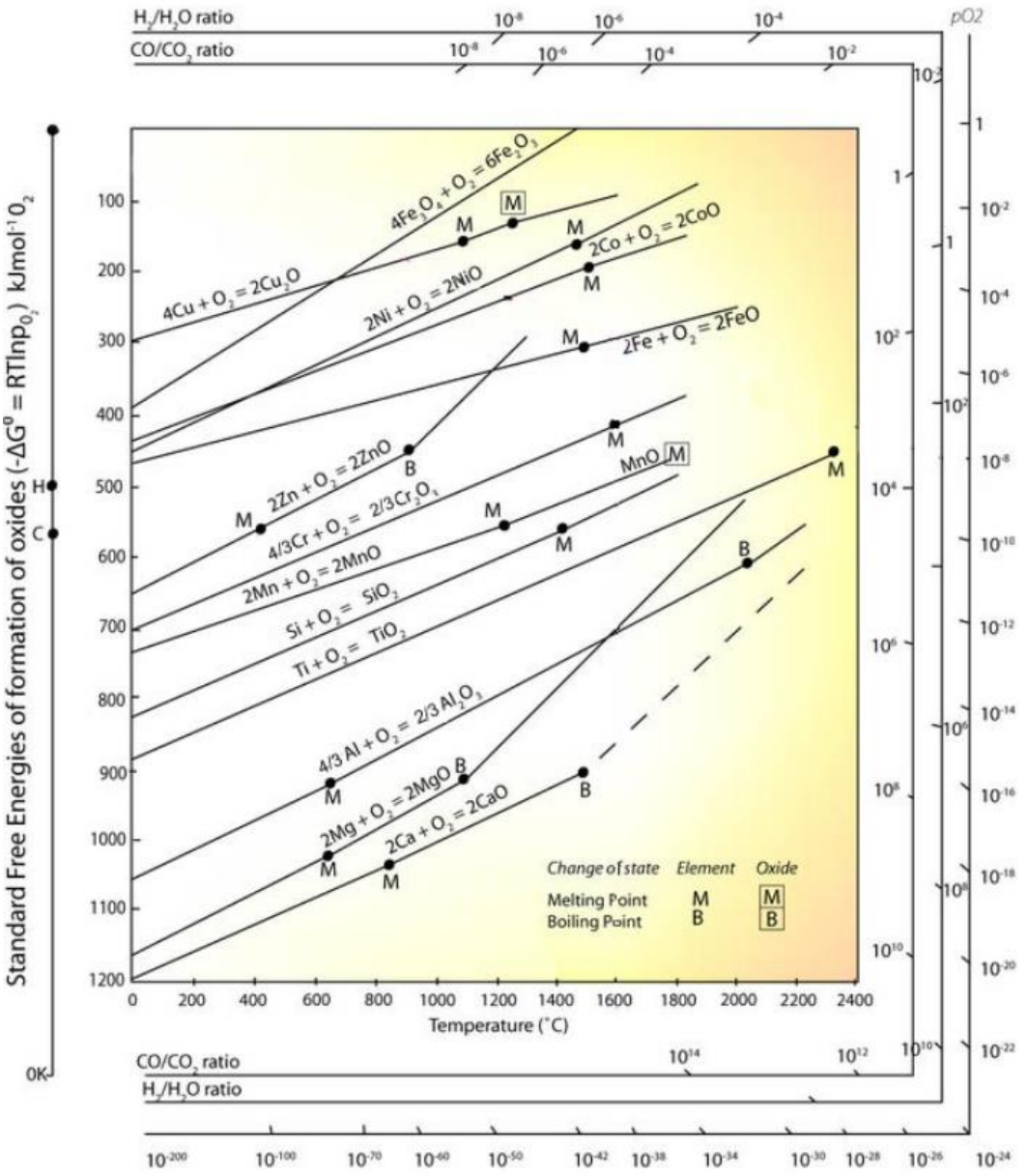


Figure 3.3 The illustration of Elligram Diagrams [52].

Optimizing the contact between these two materials is the mechanical strategy for increasing adhesion between the glass-ceramic layer and the substrate [37]. On the metallic substrate surface, a variety of chemical and mechanical treatments are used to improve this contact. This procedure comprises chemically treating the surface with HCl and H_2SO_4, as well as applying mechanical techniques to improve the interface of the glass-ceramic with the substrate [53]. These combined techniques increase the coating's overall performance and longevity by strengthening the bond between the glass-ceramic coating and the metallic substrate.

3.4 Properties of Glass-Ceramic Coatings

3.4.1 Thermal Properties

3.4.1.1 Thermal Expansion

A material's volume or length increasing as the temperature rises is referred to as thermal expansion. One can determine the total volume or length changes in the material by estimating the changes that take place with each unit of temperature change. The change in unit form multiplied by the temperature difference yields the thermal expansion coefficient.

The material's change in length with each 1 °C rise in temperature is represented by the linear thermal expansion coefficient (). It is computed using the equation shown below:

$$A = \frac{1}{l}\ x\ \frac{\Delta l}{\Delta t} \tag{5}$$

where:

α is the linear thermal expansion coefficient,

ΔL is the change in length of the material,

L_o is the original length of the material, and

ΔT is the change in temperature.

For engineering and design reasons, the linear thermal expansion coefficient gives important details about how a material will expand or contract in response to temperature variations.

The amount that a material changes in volume when its temperature rises by one degree Celsius is measured by its volume thermal expansion coefficient (β). It has an inverse connection with the linear thermal expansion coefficient (α) in isotropic materials, including glasses and amorphous structures.

From a mathematical standpoint, the connection between and is as follows:

$$\beta = 3\ x\ a \tag{6}$$

Here, stands for the linear thermal expansion coefficient, and for the thermal expansion coefficient of volume. For the same change in temperature in isotropic materials, the volume expansion is three times greater than the linear expansion.

In the interaction between glass-ceramic coatings and metal substrates, the thermal expansion coefficient is a key factor. In order to guarantee a perfect fit between the two materials, it is crucial that the thermal expansion coefficients of the glass-ceramic covering and the substrate metal be near to one another. The coating will rapidly shrink during cooling following the firing procedure if the glass-ceramic coating's thermal expansion coefficient is much lower than that of the metal substrate. When the coating's adhesion to the metal is strong, this might result in the growth of stress-induced fissures in the coating.

The structure may develop cracks if the glass-ceramic coating's tensile strength is surpassed as a result of the coating's differential shrinkage from the metal substrate. On the other hand, chipping issues can occur if the glass-ceramic coating's compressive strength is greater than the metal's thermal expansion coefficient. It's vital to remember that in this situation, compressive strength might be 15-20 times more harmful than tensile strength.

Glass-ceramic coatings should typically have a lower thermal expansion coefficient than the metal substrate to prevent these problems. A stronger link is created between the two materials and the danger of cracking or chipping is reduced by matching the thermal expansion coefficients of the metal and the glass-ceramic coatings.

For the purpose of choosing the best material combinations for certain applications, Table 3.3 compares the volume thermal expansion coefficients of various metals and glass-ceramic coatings.

Table 3.3 The coefficients of cubical thermal expansion that several glass-ceramic coatings and some metals exhibit [45].

Material	**Cubical Thermal Expansion Coefficient ($3.\alpha \times 10^{-7}$)**	**Temperature Range (°C)**
Iron	426	0-500
Low Carbon Steel	465	25-760
Cast Iron	378-390	20-500
Ground Coat for Steel	240-300	0-100
Cover Coat for Steel	280-360	0-100
Ground Coat for Cast Iron	250-300	0-100

3.4.1.2 Thermal Shock

The capacity of a glass-ceramic coating to survive abrupt and extreme temperature fluctuations without suffering major damage or failure is referred to as thermal shock resistance. It is a crucial characteristic to take into account, particularly in situations where the coated material is exposed to abrupt temperature changes.

The idea put out by Winkelmann and Schott may be used to mathematically compute the thermal shock resistance. The following equation can be used to determine thermal shock resistance:

$$K = \frac{P}{a.E}\sqrt{\frac{\lambda}{c}.d} \tag{7}$$

where P stands for tensile strength, α for linear expansion, E for elasticity modulus, λ for thermal conductivity, c for specific heat, and d for density.

Glass-ceramic coatings' ability to withstand thermal shock is affected by a number of variables, including internal stresses and thermal characteristics. In comparison to the underlying metal substrate, glass-ceramic coatings often have a lower coefficient of thermal expansion. As a result, when exposed to quick heating, the coating experiences compressive stresses, whereas rapid cooling results in tensile strains.

Compressive forces are often less harmful than tensile strains, which helps explain why glass-ceramic coatings have improved thermal shock protection under fast heating. Because convex surfaces experience larger tensile stresses than concave surfaces, the magnitude of these strains also has an impact on how resistant they are to thermal shock.

Thermal shock resistance is also influenced by the thickness of the metal substrate and the glass-ceramic covering. Since thicker coatings may absorb more energy during sudden temperature fluctuations, they may be more resistant to thermal shock. Similar to this, a thicker substrate metal can offer more stability and support, increasing the overall resistance to thermal stress [45].

During thermal shock testing, the cooling environment is crucial. Since thermal shock with cold water has a more severe effect than thermal shock with cold air, cold water tests are frequently used to evaluate thermal shock resistance. Cold water tests' quick cooling replicates more difficult and harsh circumstances for the glass-ceramic coating, allowing for a more realistic assessment of its thermal shock resistance [45], [54].

In conclusion, internal stresses, coating and substrate thickness, as well as the cooling environment during testing, affect the thermal shock resistance of glass-ceramic coatings. For choosing and creating glass-ceramic coatings suited for applications where rapid temperature swings are predicted, it is essential to comprehend and take these considerations into account [54] .

3.4.1.3 Fusibility and Fluidity

The molten condition of the raw materials for glass-ceramic coatings exhibits two important properties, namely fusibility and fluidity, which become more noticeable throughout the melting and fire process following application. Chemical composition has a major impact on these characteristics, and experimental methods

have been mostly used to accurately determine them. Calculations have worked well for certain composition ranges. In order to evaluate various characteristics of fusibility and fluidity for each glass-ceramic coating mixture, many experiments have been created.

The fusion flow test is used to identify deformation intervals during the melting process, whereas the fusion flow test is used to establish the fusion temperature of glass-ceramic coating compositions. The hardness and softness of the frit as a function of temperature are determined by the fusion flow test. The bead test is also essential for determining the frit's fluidity, surface tension, and fusibility. The interferometer test, last but not least, is very important in establishing the expansion coefficient.

Researchers and producers can learn crucial details regarding the behavior of glass-ceramic coatings in their molten state by carrying out these studies. Understanding the features of fusibility and fluidity enables accurate control and optimization of the coating process, guaranteeing the creation of high-quality glass-ceramic coatings with required qualities for a variety of applications [45].

3.4.1.4 Viscosity

As it is for all glassy materials, the viscosity property of enamel coatings is an important characteristic and it is greatly impacted by temperature. Viscosity may vary significantly with even a modest change in temperature. The glass transition temperature (T_g) in Figure 3.2 denotes the temperature at which the substance turns brittle and reaches a viscosity of 10^{12} N.sec/m^2. In contrast, Ts stands for the melting point, when the viscosity is 10 N.sec/m^2.

The chemical makeup of enamels may be used to determine the values of T_g and T_s. Enamels typically have Tg temperatures below 500 °C and Ts temperatures around 1400 °C. As the viscosity rises, the enamel's firing temperature rises as well, resulting in less gas evolution and better surface flatness. On the other hand, low values of viscosity can lead to enamel flaws and uneven coating thickness. The viscosity of enamels normally ranges between 102 and 103 N.sec/m^2 throughout the firing process.

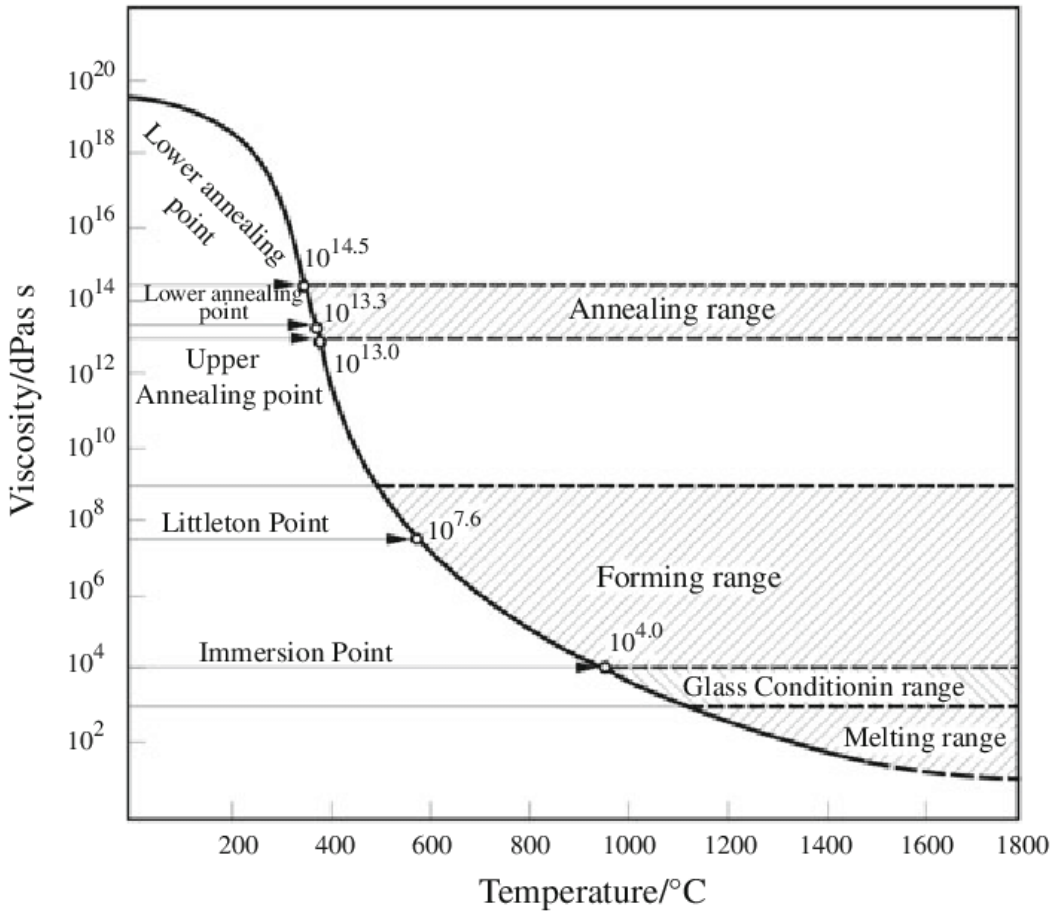


Figure 3.2 Viscosity-Temperature curve for a theoretical glass [55], [56].

Using substances like boric acid, clay, and sodium nitrite, the viscosity of the created enamel slurry may be easily altered for wet applications of the enamel coating process. This makes it possible to precisely regulate the viscosity to obtain the coating qualities and attributes necessary.

3.4.1.5 Thermal Conductivity

Indeed, from a scientific and industrial perspective, the heat conductivity of enamels is a crucial characteristic. It is crucial for enamel coatings to transmit heat effectively in a variety of applications, including household appliances, military equipment, construction, freezers, and ovens. High thermal conductivity enamels can be used in these applications as efficient heat emitters or reflectors.

High thermal conductivity oxides, frequently in the form of metal powders, can be added to the enamel mixture to improve the material's thermal conductivity. These oxides make it possible for the enamel coating to conduct heat effectively, which

makes it a desirable characteristic for applications requiring efficient heat management and distribution.

Enamel producers may specifically tune the thermal conductivity of the enamel coatings to match the needs of diverse applications by carefully regulating the composition and adding certain metal powders. This makes it possible to create enamel coatings that are not only aesthetically beautiful but also very effective at managing and transmitting heat [57].

Thermal conductivity, which measures the size of the thermal conductivity coefficient, is calculated using the formula provided:

$$\lambda = p_1.\lambda_1 + p_2.\lambda_2 + p_3.\lambda_3 \left(\frac{\text{watts}}{\text{m}}.\text{deg}\right) \quad (8)$$

3.4.2 Physical and Mechanical Properties

3.4.2.1 Density

During wet applications, the density (specific gravity) attribute is frequently utilized to regulate the sample's fluidity. It is crucial to obtain the required degree of density dilution for glass-ceramic coatings, which may be tested with a pycnometer.

The following formula is used to calculate the density of glass-ceramic coatings:

$$S = \frac{(w - p)}{(w - p) - (w_2 - w_1)} \quad (9)$$

S is the glass-ceramic coating's specific gravity, w is the weight of the tapered pycnometer and sample, w_1 is the weight of the pycnometer when it is filled with water, and w_2 is the weight of the pycnometer when it is filled with sample and water [58]. P is the weight of the tapered pycnometer.

3.4.2.2 Hardness

Glass-ceramic coatings range in hardness from 5 to 6 on the Mohs scale, with modest variations depending on their chemical make-up. To accurately analyze glass-ceramic coatings, classic hardness testing methods like Rockwell, Brinell, and Knopp are not frequently utilized. Instead, the Mohs scale is used to assess these coatings' scratch resistance [58].

3.4.2.3 Elasticity

Despite being an essential material property, elasticity is not typically used in the field of glass-ceramic coatings. Both mechanical and acoustic methods can be used to analyze it. The mathematical equation for the mechanical technique is given below [58]:

$$A = 4PL^3/bd^3\Delta \quad (10)$$

where P denotes the load, L denotes the material's length, b denotes its breadth, d denotes its thickness, and denotes its deflection [58].

3.4.2.4 Compressive Strength

Although it is frequently ignored, the glass-ceramic coatings' compressive strength might have an impact on other characteristics. Using Winkelmann and Schott's methodology [58], it is possible to determine the compressive strength value of typical glass-ceramic coatings, which ranges from 77 to 81 kg/mm^2.

3.4.2.5 Tensile Strength

The evaluation of tensile strength in glass-ceramic coatings is crucial, although determining it can be difficult. Glass-ceramic coated materials are prone to shattering because of their natural brittle fracture qualities. Different approaches have thus been proposed to examine the tensile strength of such coatings. The tensile strength has a substantial impact on the thermal characteristics of glass-ceramic coatings, particularly in connection to their tensile behavior, while not being the major emphasis or expressly evaluated property [58].

3.4.3 Chemical Properties

3.4.3.1 Acid Resistance

Glass-ceramic coatings are regularly subjected to acidic conditions in a variety of applications, notably in kitchenware. The continuity of the [SiO_4] tetrahedral structure within these coatings plays a significant role in determining their acid resistance, making SiO_2 one of the important oxides affecting acid resistance. In order to cover the areas around [AlO_4]-R^+ and [BO_4]-R^+ in the glass-ceramic coatings from the corrosive effects of acids, tetrahedrons made of [SiO_4] units are strategically used. As a result, the formulation of the glass-ceramic coatings

contains more SiO_2 to strengthen acid resistance. However, the continuity of $[SiO_4]$ tetrahedrons can be disrupted by ions like Li^+, Na^+, and K^+, especially in larger R_2O groups, which lowers acid resistance [59], [60].

3.4.3.2 Alkali Resistance

Depending on where they are used, glass-ceramic coatings may be exposed to alkaline conditions. Alkaline assaults, however, advance more slowly than acidic ones. As a result, testing for alkaline resistance of glass-ceramic coatings often lasts longer. Additionally, in alkaline and acidic conditions, the effects of corrosive chemicals that cause ion exchange leaching in the coating structure of glass-ceramic coatings are substantially less prominent. Test solutions containing sodium pyrophosphate, sodium hydroxide, and sodium bicarbonate are frequently used to evaluate alkaline resistance.

Glass-ceramic coatings that have been exposed to alkaline go through an ion exchange leaching process, where hydrogen ions in the solution react with the coatings' matrix to ionize alkaline ions. At pH 9, this pH-dependent reaction primarily takes place.

Alkaline ions are produced when hydrogen ions interact with a silica network in the presence of two non-bridging oxygen atoms. Alkali metal ions thus easily take the place of hydrogen, resulting in the creation of an aqueous surface layer.

The silicate structure begins to dissolve at a pH greater than 8, and as the pH increases, this process continues. At these pH levels, hydroxyl groups interact with the glass matrix or hydrated layer. As a consequence, Si(OH) groups are produced, which later react with water to produce the reaction $SiO^- + H_2O \rightarrow Si\text{-}OH + OH^-$. Glass-ceramic coatings degrade as a result of these repeated interactions with hydroxyl groups [60], [61].

3.4.3.3 Water Resistance

At room temperature, glass-ceramic coatings show resistance to water and retain their structural integrity. Exposure to hot water has no effect on the coating structure. However, the coating structure deteriorates with extended exposure to harsh environments, such as high pressure and heat at the usage site [60,61]. Tests carried out in compliance with DIN EN ISO 4753-3 state that glass-ceramic coatings shouldn't be more than 8 mg/m^2 following a cumulative exposure of 21 +

21 days, or 6 weeks [62]. Water resistance is especially important for applications like boilers, valves, and thermosiphons.

3.5 The Area of Utilization of Glass-Ceramic Coatings

Glass-ceramic coatings have a wide range of uses, including in the manufacture of water heaters, thermosiphon systems, boilers, ovens, conduits, storage silos, architectural panels, and hot water services. These coatings stand out for their superior technical qualities, which include their ability to tolerate high temperatures, resist chemical corrosion, display strong mechanical resilience, and display visually pleasing qualities. Glass-ceramic coatings are a key element in the culinary and kitchenware industries due to their great technical qualities, aesthetically pleasing attitude, and a wide range of color possibilities. This is in addition to their strong technical capability and visual attraction [42], [44], [63].

3.6 Application Processes

The wet and dry application processes for glass-ceramic coatings are two separate approaches. The decision between these two approaches depends on a number of variables, such as the planned application area, economic reasons, sheet metal substrate characteristics, and unique characteristics of the glass-ceramic material. The best coating strategy is chosen after carefully examining all of these factors.

3.6.1 Coating Process By Wet Method

When applying glass-ceramic coatings, especially in the wet process, mill additives are essential. The frit composition in the mill is mixed with water and mill additives to generate the slurry for the glass-ceramic coating. The ratio of frit to water is 100%, and the amount of mill and water added after that is adjusted accordingly. It is anticipated that the mill will not use all of the raw materials that are introduced. In wet applications, the quality of the water used to create the slurry for the glass-ceramic coating is crucial. Coating quality is adversely affected when dissolved salts, such as calcium, magnesium, and sodium sulfates, are present in the water. Distilled water is good under ideal circumstances, but it might not be useful in an industrial setting. In order to keep the frit particles suspended in the coating slurry, mill additives such as clay are added. Although clay properties might differ

depending on the area, they usually make about 4% to 8% of the mixture. For glass-ceramic coating, electrolyte ingredients such as sodium nitrite ($NaNO_2$), potassium carbonate (K_2CO_3), boric acid (H_3BO_3), and sodium aluminate ($NaAlO_2$) are used to control the fluidity, consistency, flow rate, and infiltration balance of the slurry. The inclusion of quartz to the mill raises the firing temperature and improves resistance to acids [41].

3.6.2 Spraying Method

Glass-ceramic slurry or powder can be sprayed over a metal substrate to coat it. Compressed air is used to push and disperse the coating. The two most common methods for spraying glass-ceramic coatings are manual spraying and automated machine spraying. Due to its increased efficiency, automated machine spraying may be used for large-scale manufacturing [64].

Glass-ceramic coating techniques that use spray technology may be used on both flat and curved components. This process is used in the manufacturing industry to coat a variety of objects, including stove side panels, kitchenware items like pots and pans, chassis, doors, grills, stove plates, and burners. The glass-ceramic slurry used for spray application in the wet process must strike a balance between being sufficiently big to stick to the metal surface and being tiny enough to flow through the spray nozzles efficiently in order to achieve excellent atomization. The nozzle apertures may become blocked by large particles in the slurry that are larger than the nozzle diameter, which might result in uneven or insufficient glass-ceramic deposition. This would lead to an irregular surface and uneven coating thickness. This would lead to an irregular surface and uneven coating thickness. Additionally, painstaking care must be taken to guarantee that the glass-ceramic surface is of a high enough caliber after drying and firing to prevent cracking and shrinkage [65].

The spray method's ability to reuse spilt glass-ceramic powders that don't stick to the components is a benefit. In order to reduce the danger of breakage and shrinkage, it is essential to maintain a higher degree of care to guarantee that the glass-ceramic surface achieves the necessary quality following the drying and fire procedures [65].

Because spilled glass-ceramic powders don't stick to the components, the spray approach has the benefit of making it easier to reuse the powders. In order to

minimize the entrance of environmental pollutants like dust, oil, and dirt into the process, it is crucial to maintain a regulated atmosphere inside the application cabin [46].

3.6.2.1 Dipping Method

Dipping is a basic and easy way to cover glass-ceramics; it works well for products that are only one color. This method is frequently used to cover pots and pans' outside and inner surfaces. Little, round, and simple objects are submerged in a glass-ceramic slurry so that every surface is completely covered. The dipping procedure is used to accomplish coating, then extraction comes next. Using techniques like rotating, hooking, or swinging, excess material that has been taken from the slurry on the components is eliminated. Careful monitoring and control of variables such batch density in the immersion tank, grinding fineness, and set settings are necessary to achieve a consistent glass-ceramic coating [37].

3.6.2.2 Electrophoresis Method

A wide range of industries use electrophoretic deposition (EPD), including the fabrication of solid oxide fuel cells, the assembly of nanoscale particles into nanostructures and micropatterned thin films, the production of textured ceramics with crystalline-oriented microstructures, and the development of biocompatible coatings for metal implants.

Key factors affecting coating quality in the electrophoretic deposition process include the density and particle size of the glass-ceramic material as well as the degree of applied power. In this procedure, charged powder particles are suspended in a reliable colloidal solution. In this solution, electrodes with the proper geometry are used. Electrophoresis and deposition are two different steps in the procedure. Charged powder particles move toward an electrode during electrophoresis as a result of a direct current electric field. These particles then cling to the electrode during the deposition phase, creating a dense mass [67].

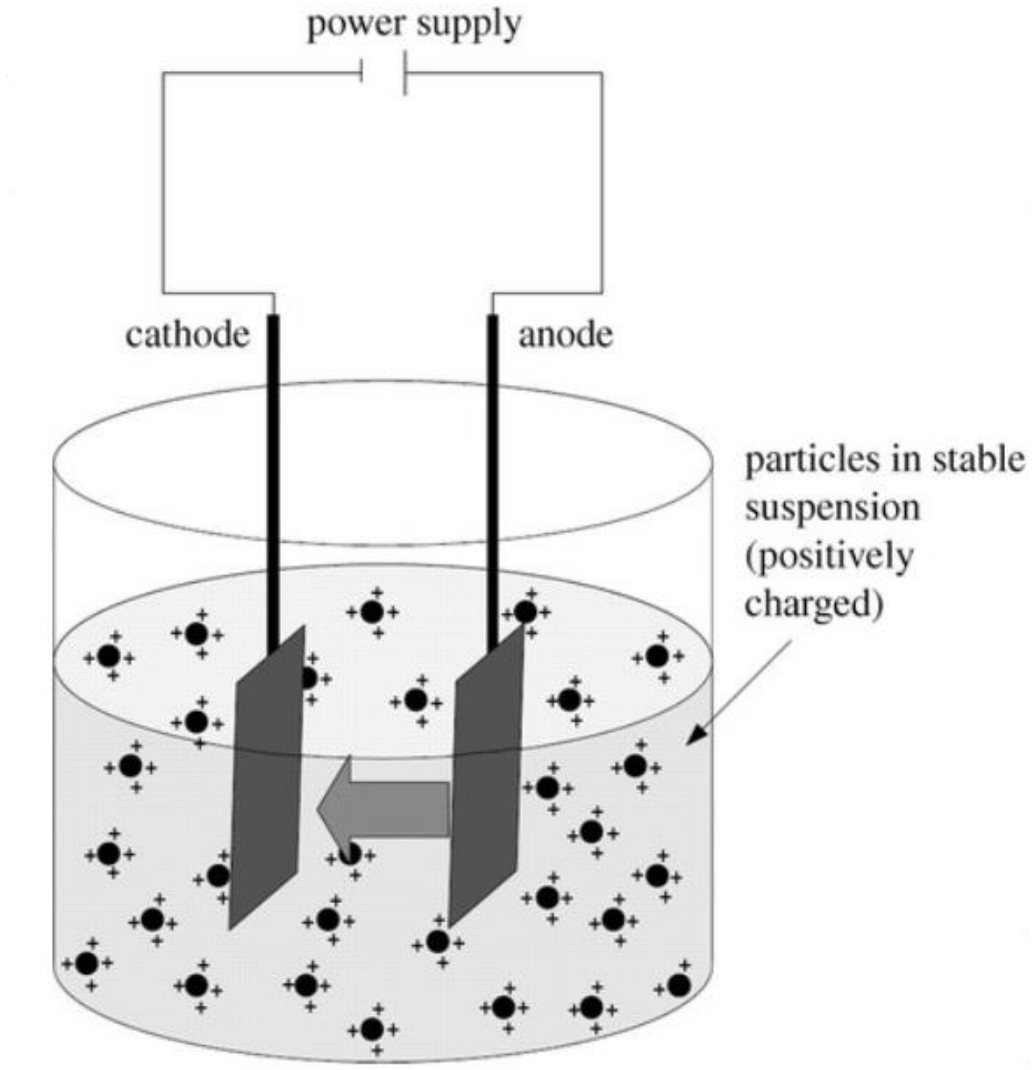


Figure 3.3 The Electrophoresis Method: Electrophoresis and Deposition Procedure [68].

3.6.2.3 Flow Coating

Flow coating is a modified version of the immersion process used in modern industrial settings. The glass-ceramic-coated component is not immersed in the batch while using this modified method. Instead, the process uses one or two nozzles to disperse the batch material over the desired surface for coating. When compared to the immersion approach, flow coating has benefits in terms of cost-effectiveness and application speed [37].

3.6.3 Thermal Spray Method

The term "thermal spraying" refers to a variety of coating methods in which coatings are produced by depositing molten or semi-molten mixtures of finely split

metallic or non-metallic elements. During this process, powder particles are introduced into a hot, high-velocity gas jet, where they are heated, accelerated, and projected onto a substrate to form a coating [69], [70]. This methodology uses a variety of techniques, such as plasma spraying, high-velocity oxy-fuel spraying, D-gun spraying, combustion flame spraying, and arc-wire spraying [71].

Van der Waals forces, diffusion bonds, and mechanical bonds, among others, take place between the substrate and the molten or semi-molten glass-ceramic particles during this process. Depending on the selected technique and material, the coating thickness ranges from 20 micrometers to several millimeters. The material is heated either by combustion heating or electrical techniques like plasma or arc heating. It's crucial to remember that using thermal spraying techniques might produce coatings with a comparatively high porosity. Despite this, these coatings display advantageous features as strong adhesion, high hardness and density, and excellent resistance to corrosion, heat, and wear because of the fundamental composition of glass-ceramic [69].

3.6.4 Powder Electrostatic Application

When passing close to the high-potential electrode, enamel powder made from the mill or frit composition is negatively charged. This creates an electric field between the high-potential spray cannon and the workpiece, which causes the nearby air to ionize locally. As a result, the area's oxygen ions become negatively charged, and enamel powder in the surrounding air does the same. Enamel powder and air are attracted in the direction of the produced electric field, toward the workpiece. Electrical force, mechanical force, air resistance, and gravity are the four main factors that affect enamel particles throughout this procedure. The operation is carried out at 100 kV voltage levels and extremely low amperages. In the end, the procedure produces an enamel covering that is typically consistent. It's important to note that smaller powder particles have a higher propensity to accumulate an electric charge, which improves the metal's adherence to the surface. Additionally, this technique may be used to recycle particles that do not cling to the component or are distributed in the surrounding area [37], [58], [72].

3.7 Toxicological Properties of Enamel Coating

Enamel coatings are commonly used to provide a protective layer on various surfaces, including metal surfaces like those found in boilers or hot water tanks. The toxicity of elements within enamel coatings depends on the specific formulation of the enamel. Here are some common elements found in enamel coatings and their general toxicological properties:

Lead (Pb): Historically, lead was a common component in some enamel formulations, but due to its toxic nature, modern enamel coatings are typically lead-free or contain very low levels. Lead exposure is associated with serious health issues, particularly for children.

Cadmium (Cd): Like lead, cadmium is a toxic heavy metal. Enamel coatings should be formulated to minimize cadmium content, as exposure to cadmium is linked to adverse health effects, including damage to the kidneys and lungs.

Chromium (Cr): Chromium can exist in different oxidation states, and while trivalent chromium (Cr(III)) is generally considered safe, hexavalent chromium (Cr(VI)) is toxic and a known carcinogen. Modern enamel formulations aim to limit the presence of hexavalent chromium.

Cobalt (Co): Cobalt is an essential trace element, but high levels of exposure can be harmful. Enamel coatings may contain cobalt as a component, and the formulation needs to ensure that levels are within safe limits.

Nickel (Ni): Nickel is another element that can be present in enamel coatings. While nickel is considered generally safe for most people, some individuals may be allergic to nickel. Therefore, enamel formulations may strive to minimize nickel content.

Arsenic (As): Arsenic is a toxic element that can be harmful to human health, particularly in its inorganic form. It is associated with various health issues, including skin lesions, developmental effects, cardiovascular diseases, and cancer. Modern enamel formulations strive to minimize arsenic content.

Antimony (Sb): Antimony is a metalloid that can be used in certain enamel formulations. While low levels are generally considered safe, prolonged exposure

to high levels of antimony can cause respiratory and gastrointestinal issues. Enamel formulations aim to keep antimony concentrations within safe limits.

Bismuth (Bi): Bismuth is considered less toxic than some other heavy metals. It is often used as a replacement for lead in certain applications. Enamel formulations with bismuth may be chosen for their low toxicity compared to traditional formulations.

Manganese (Mn): Manganese is an essential element, but excessive exposure, especially through inhalation, can lead to neurological effects. Enamel coatings may contain manganese, and formulations aim to control exposure levels.

Vanadium (V): Vanadium is a transition metal that can have toxic effects on the respiratory system at high concentrations. While it may be present in enamel formulations, efforts are made to keep levels within safe bounds.

Zinc (Zn): Zinc is an essential trace element and is generally considered safe in low concentrations. Enamel coatings may contain zinc for various purposes, and formulations strive to avoid excessive levels that could lead to adverse health effects.

It's important to emphasize that the toxicological properties of these elements depend on their chemical forms, concentrations, and the route of exposure. Strict regulations and standards govern the use of toxic elements in consumer products like enamel coatings, ensuring that they are safe when used as intended. Always refer to safety data sheets (SDS) and consult with manufacturers for specific information about the composition and safety of enamel coatings [73-75].

4
GLASS/GLASS-CERAMIC CORROSION

4.1 Glass Corrosion Mechanism

Glass and water interact r and reach electrochemical equilibrium because they have different potentials. This reaction also occurs during solid-water reactions formed by ion exchange of alkali oxides and glass network-forming species (SiO_2, B_2O_3), hydrolysis, dissolution, diffusion, and adsorption. After equilibrium is reached with precipitated alkali oxides, crystal nucleation and growth occur on the glass alteration surface. The difference in chemical potential between the glass surface and water causes ion exchange from the glass surface to the water shown in Figure 4.1 until potential equilibrium is reached [1], [7-9], [76].

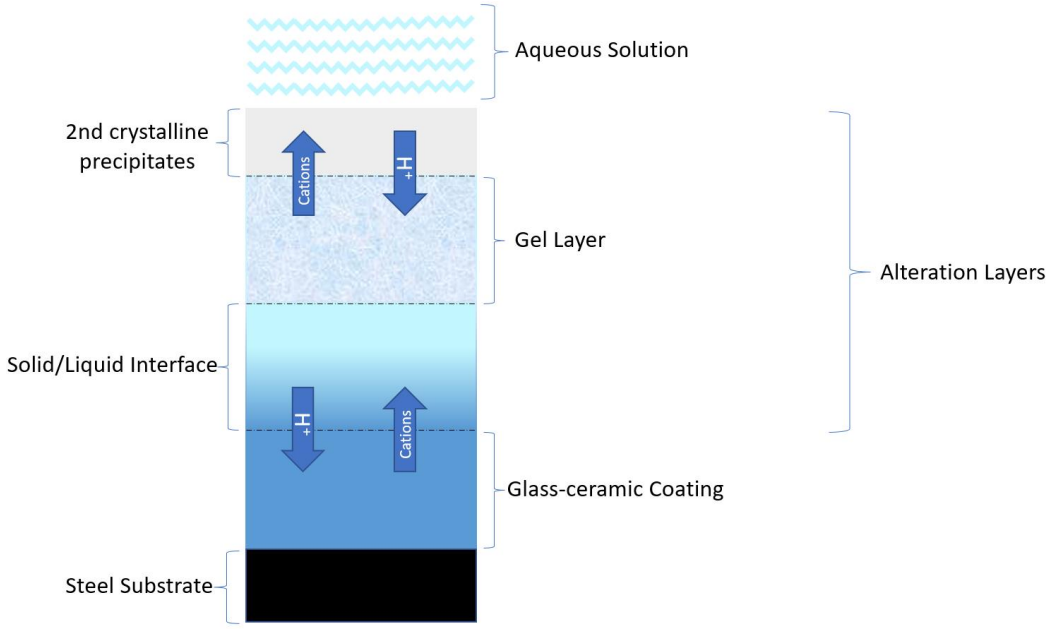


Figure 4.4 Schematic demonstration of ion transfer of between glass and aqueous solution.

Gerald explained the glass corrosion mechanism with the four main reaction steps: ion exchange in water and glass (between H^+ ions in water and Li_2O, Na_2O, K_2O, MgO, CaO, SrO, and BaO alkali oxides in glass); i) hydrolysis of network-forming oxides (SiO_2, B_2O_3, and P_2O_5); ii) dissolution of the hydrolyzed oxides until the water is saturated with hydrolyzed oxides. Also, all reaction processes between

water and glass are influenced by environmental factors, which include temperature, water pH, Eh, and dissolved oxide concentration in the glass [7], [56], [77]. The solid atoms, which are alkaline or earth-alkaline atoms that belong to the glass surface show a tendency to interact with H_2O molecules for the purpose of compensating for the charge imbalance at the surface discontinuity in aqueous solutions. When glass is exposed to the aqueous solution, the solid atoms interact with H_2O molecules, and then the solid atoms, which are located in the glass/aqua interface, are charged with positive, neutral, or negative charges. Because charged solid atoms bond weaker to the underlying glass than uncharged atoms, the surface stability of the glass changes, and it destabilizes according to the aqueous solution (temperature, pH, solution composition, and flow) [77], [78].

In Helmann's study addressing glass corrosion mechanisms, he refers to the glass former and glass network modifier elements' dissolution processes as being characterized by stoichiometric release. When the water reaches saturation with glass-former and glass network-modifier elements, one or more crystalline phases begin to precipitate on the corroded glass surface. Helmann also mentioned a simple chemical mechanism for glass corrosion, which is based on the in situ optional release of mobile glass network modifiers (Li^+, Na^+, and K^+) into water. The corroded glass structure should be electrically neutral and capable of exchanging cations and H ions (H_3O^+) from the bulk solution, as well as the H_2O molecular. The outside of the silica-rich layer, which is a corroded glass surface, continues to let Si and O elements release from the glass surface into the bulk solution [76].

The corrosion of glass exposed to water consists of three main mechanisms depending on the glass composition and environmental parameters, which mechanisms are called stages l to lll. When glass is exposed to diluted water, the corrosion process begins and continues until the solution reaches saturation with the base glass's glass-formers (SiO_2, B_2O_3, and P_2O_5) and glass-modifier species (such as Na_2O, K_2O, Li_2O, CaO, MgO, SrO, and BaO). In this stage, the corrosion kinetics mostly depends on water temperature and pH and are controlled by the hydrolysis of glass network species. A subsequent mechanism of glass corrosion is Stage ll, in which water is saturated with glass-network former species in stagnant water. During that stage, the molecule numbers of the glass-network species

increase in an aqua solution, so the kinetics of diffusion decrease during further processing. When the aqueous solution reaches saturation with glass formers such as SiO_2, B_2O_3, and glass modifier species, such as Na_2O and CaO, this condition provides for massive precipitation of secondary phases such as calcium-silicate hydrates (CSH), magnesium silicates, iron silicates, or aluminosilicate zeolites, triggering an acceleration of alteration in stage III. That forms the passivation of the alteration layer on the corroded glass surface [7], [77]. The stages of the glass corrosion mechanism are depicted in Figure 4.2.

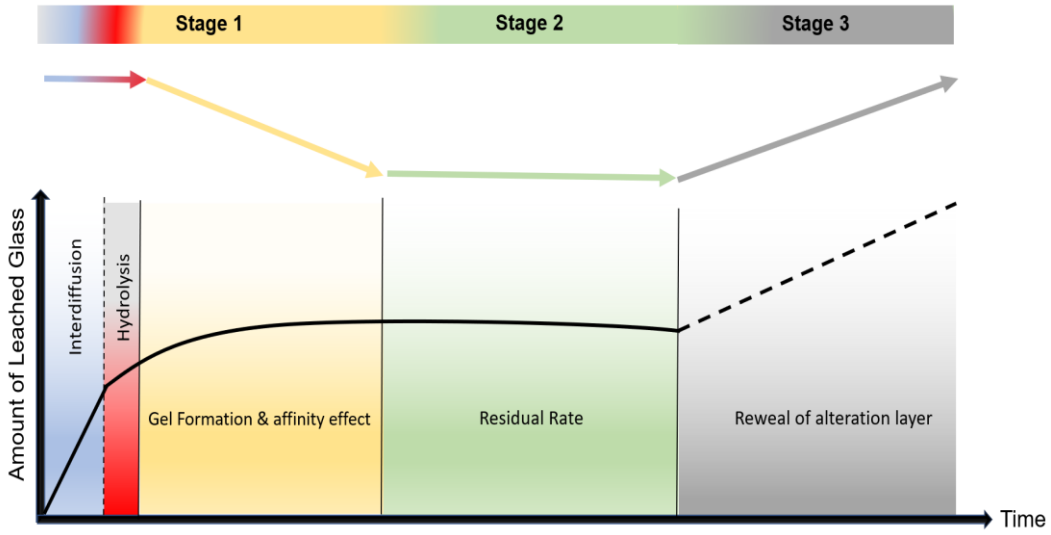


Figure 4.5 Graphic shows corrosion mechanism rates depending on time stages from l to lll.

That forms the passivation of the alteration layer on the corroded glass surface. The alteration layer structure is a reconstruction of glass network species in water that start to change the glass/water interface structure during ion exchange, hydrolysis-condensation dissolution, and finally reprecipitation reaction, and the alteration layer is different from uncorroded glass [79], [80]. The alteration layer is Si-rich, and the structure possesses a porous layer that is semi-permeable for aqueous species, put differently, the alteration layer is a diffusion barrier to the glass-water interface [80]. On the other hand, like the passivation layers that metals have after corrosion, glass has an alteration layer [77]. This layer acts as a protective layer in that changes in porous size and water filling the internal pores slow down corrosion [79]. Information about the structure of the alteration layer is important to predict

the effect of the corrosion mechanism because glass/water interface glass corrosion is affected by so many internal and external parameters.

Because of the difference in chemical potential between the glass surface and the aqueous solution, the glass surface reaches equilibrium in the context of electrochemical reactions before the aqueous solution (H^+/H_3O^+) chemically attacks the glass surface with hydrolysis (B) and ion exchange (mobile elements such as Na and Ca) reactions [7], [80]. As the concentration of glass species in aqua solution increases, the differences in the chemical potential drive down the system's Gibbs free energy. The main glass former, SiO_2, and the aqua solution react as shown in Eq. 11;

$$SiO_2 + 2H_2O \rightarrow H_4SiO_4 \quad (11)$$

Ortho-silicic acid in the aqua solution brings down the dissolution rate of the glass matrix by reaching saturation level with the oxides that diffuse from or are hydrolyzed from the glass. The silanol groups are formed by reactions between the Si reaction zone and the bonded O atoms of the SiO_4 glass former. Also, siloxane bonds can condense to reform siloxane bonds as shown in Eq. 12. [7].

$$= Si - OH + OH - Si = \rightarrow Si - O - Si + H_2O \quad (12)$$

The continuation of corrosion on the glass surface causes the roughness of the glass surface to increase and the thickness of the same surface to increase [70].

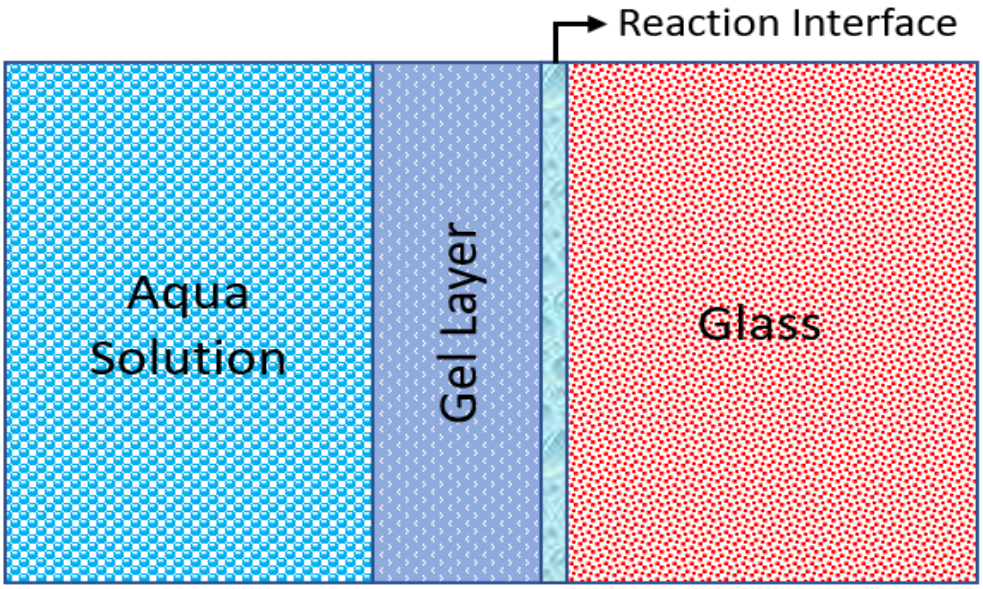


Figure 4.6 Cross-section of glass corrosion layers schematically demonstrated.

If the pH of the aqueous solution provides neutral or zero charges to the glass surface, that is a minimal dissolution rate for single-oxide glass, which have simpler structures than multi-oxide glass. Furthermore, depending on the glass surface speciation, the dissolution rate of the glass surface exposed to the aqueous solution could be changed as a function of the solution pH, the dissolution rate can be used to describe the successful concentration of surface chargeable [78]. For simple alkali silicate glass, NBOs play an important role in the hydrolysis of glass species because glass-modifier cation charges reach a balance toward NBO. The present cations in glass structures, such as Na^{+}, K^{+}, Ca^{+}, or Mg^{+}, are network modifier species for glass, and their presence causes the breaking of some fraction of the Si-O bonds through convoluted NBOs and disruption of silica tetrahedral structures. O atoms that are NBO do not bond to two glass-former or network modifier cations, providing a weak connection between glass formers and network modifiers. The Q^{n} expresses the number of bridging oxygens in the glass, so if a silica tetrahedral atom is bridge-bonded to one oxygen, this indicates Q^{1}. NBOs are present in Q^{3} and Q^{2} areas, and they tend to release from the glass surface into an aqueous solution, reducing crosslink density [82]. For the sodium silicate glass system, which is simple glass, if the amount of sodium increases, the NBO increases in the glass structure so that Q^{2} and Q^{3} areas in the Q^{4} network increase. That change increases the reactivity of alkali silicate glass against aqueous solutions. On the other hand, if alkaline glass possesses the same amount of alkaline oxide but different kinds of

oxide like Na and K oxides exist at the same time in the glass structure, the diffusion rate of the glass couldn't be the same compared with the same content of one type of alkaline and different types of alkali oxides when the glass is exposed to the aqueous solution [82].

A multi-oxide glass corrosion mechanism is more compelling than a simple oxide glass corrosion mechanism because it involves many different internal and external changes. Each glass-former and glass-modifier oxide possesses its own solubility rate in aqueous solutions; their solubility is also affected by each environmental factor, for example, pH. For determining the solubility of multi-oxide glass, differences in the dissolution rate and release rate of oxides should be calculated [78]. For example, Li possesses a small charge-to-radius cation compared to Na and K, so when compared to each other, the solubility ratio to aqueous solutions is different because of the increasing charge-to-radius cation [82]. According to the alkaline existence in the glass network, the distribution of Q species is very varied, and types of Q directly change the corrosion resistance of glass. If the mole fraction of the Q^4 region increases in the glass network, that situation provides resistance to hydrolysis and hydration, and the Q^2 and Q^3 regions negatively affect the corrosion resistance of glass [82], [83].

4.2 Effect of Glass Chemical Composition on Glass Alteration

The addition of alkaline and earth-alkaline oxides to silicate tetrahedra systems decreases chemical resistance and increases the working range while decreasing the melting temperature. The reason for changes in silicate tetrahedra is that alkali concentrates affect oxo-bridges and change ionic nonbridging oxygen bonds (NBOs). The abundance of alkaline, earth-alkaline oxides provides high mobility for their ions, increasing the number and diameter of voids in silicate rings. Without alkaline and alkaline-earth oxides, pure silicate consists of bridging oxygen (BO) bonds, which do not provide rearrangement to accommodate difficult bonds. These silicate ring structures are defect-free, and their strong bonds provide corrosion resistance against chemicals and aqueous solutions; however, the addition of alkaline and earth-alkaline to the glass matrix changes the structure's properties, as previously mentioned. When NBO amounts increase in the network, hydrolysis of the network also increases. Q represents the number of BOs on a silicate tetrahedral,

so the trend of reactivity is $Q^1 > Q^2 > Q^3 > Q^4$ when comparing the number of bridging oxygens. In addition, the existence of glass-modifier elements alters the kinetics and mechanism of network diffusion for silicate glass [1], [82].

When the surfaces of alkali silicate glass were exposed to an aqueous solution, alkali cations were released into the solution because of hydration, hydrolysis, and ion exchange reactions. During these reactions, alkali cations separate from the glass network because those cations stay next to their own NBOs, so water molecules fill the alkali cation's void [82], [83]. Broadly, glass corrosion behavior depends on the composition, especially the SiO_2 content of the structure and other glass-forming and glass-modifying element ratios. In addition to this, alteration layers influence the corrosion rate depending on the exposure time of the aqueous solution [78].

When glass is exposed to an aqueous solution, the size of the voids in the structure controls and limits the diffusion rate due to molecular limitations [82]. The complex glass consists of Na, Li, K, Ca, Mg, and Sr oxide species for glass modifier cations, and the existence of those oxides prevents voids because of the fill of silicate rings. If voids (> 0.7 nm) inside a glass network are larger than the kinetic diameter of the water molecule (0.28 nm), water can diffuse throughout the glass structure. On the other hand, if voids are smaller than a water molecule, water molecules cannot penetrate voids because of the diameter differences. Also, unpenetrated water molecules caused by diameter differences try to break silicate rings, and sometimes they can be successful so water molecules can penetrate into the silicate ring's voids [82].

In the Rebiscoul study [84], the impact of soda-lime borosilicate glass composition and particularly the effect of charge compensators such as Ca and Na and of glass formers such as Si and Zr were investigated in a water solution and tried to be determined with Fourier-transform Infrared Spectroscopy Sample Technic: Attenuated Total Reflection (IRFT-ATR) and X-Ray Reflectometry (XRR) analysis. The composition of glass is as important a parameter in the corrosion mechanism as the hydration of glass or hydrolysis because composition affects the water diffusion coefficient. In addition, Rebiscoul [84], calculated activation energy and determined that water diffusion on the glass matrix was greater than the inert gas, indicating that water molecules react very effectively with the glass matrix.

In the study of Topateş [85], the ZrO_2 effect on glass-ceramic glaze was investigated. The results of the experiment revealed that when ZrO_2 was dissolved in the glass matrix, zirconia accreted to the dissolution of glass-ceramic. On the other hand, if ZrO_2 does not dissolve in the glass matrix, dissolution starts at the zirconia grain boundary, so the glass matrix stands without corrosion.

Fröberh [86] investigated the corrosion behavior of matte raw glaze in acidic and alkaline solutions and firing conditions; the results show the chemical durability of glaze is dependent on the crystal types and shapes. The diopside crystal provides good chemical resistance to glaze in citric acid, HCl, water, detergent, and KOH solutions. The results were investigated with SEM and spinning dish white light confocal microscopy (COM). The reason for providing chemical resistance to the glaze of diopside depends on the elements included, and crystals have good resistance to chemicals thanks to high-strength covalent bonds. On the other hand, wollastonite crystals show different behaviors against both acidic and alkaline solutions. For example, a tiny columnar wollastonite crystal was constituted with a fast-fired process that shows it reacts with all kinds of solutions but especially alkaline aqueous solutions, but dendritic wollastonite shows better resistance to neutral and alkaline solutions.

Dien Ngo's [87] study investigates the surface dissolution of glass networks in silica-saturated solutions using surface-sensitive techniques like LEIS, XPS, and AFM. Despite thermodynamic models predicting no silicate network loss due to initial silica saturation, surface analysis reveals evidence of silicate network dissolution. Mobile elements such as B and Na leaching from the glass may influence silicon species saturation in the aqueous phase, necessitating further study. This suggests no true equilibrium between prepared silicon-containing species and the silicate network at corrosion onset. The study, which conducted short-term (up to 7 days) corrosion experiments, indicates that initial network dissolution may not occur in long-term alteration layers but could influence the layer's structure due to the path-dependence of nonequilibrium reactions. The glass corrosion mechanism can evolve over time, exemplified by UK Magnox-waste glass, which transitioned from ion exchange to hydrolysis control after 28 days at 90°C. The duration of network dissolution depends on the initial silica species concentration relative to saturation, varying with other dissolved species.

Critical analytical proof of a non-uniform element distribution, spanning from a few nanometers to 1 μm, in the surface layers of glass matrices is provided by Roberta Zanini's work [88]. Simulated aging of silica-soda-lime glass mock-ups was investigated using X-ray photoelectron spectroscopy (XPS) and secondary ion mass spectrometry (SIMS). The results showed a markedly non-homogeneous distribution of elements at the glass surface, with a sodium concentration that is noticeably low up to a depth of approximately 500 nm, after which it grows to a plateau. Furthermore, in the first 200 nm of the clean glass surface, hydrogen diffusion from the surrounding environment was seen within the glass network. The chemical state of sodium atoms at the surface changed over time in relation to their bulk state due to aging processes that were impacted by environmental variables including humidity and temperature. The local non-homogeneity of glass composition and change is emphasized in this work, underscoring the significance of examining glass surfaces as areas of environmental interaction. The study highlights notable alterations in the composition of the glass surface, specifically with sodium atoms ranging from a few nanometers to several hundred nanometers. These layers had less sodium than the bulk, perhaps because the sodium volatilized as the glass melted. In the sodium distribution, lateral inhomogeneity was also observed. To get a better understanding and to design conservation techniques, it is necessary to take into account the inhomogeneity that exists non the first few hundred nanometers below the surface for both ancient and current industrial glasses. Current research endeavors to comprehend the progression of surface alterations in glass over extended aging times, specifically focusing on whether the creation of sodium carbonates may serve as a precursor to permanent matrix modification.

4.3 Environmental Factor: Aqeous Solution Parameters for Glass Alteration

Environmental parameters include the pH of the solution of the glass for corrosion mechanisms. The pH directly affects ion transfer, hydrolysis, and diffusion processes between glass and solution. Because the aforementioned mechanisms are dependent on differences in medium concentration, acidic, neutral, and basic solutions contain different types and amounts of ions. During the investigation of

the corrosion of glass, what kind of solution was used should be known. The studies in the literature about different pH values for immersion glass corrosion are given in the following paragraphs.

Antropova's [89] study included the kinetics of corrosion of alkaline borosilicate in acid solutions. That study investigates the acid solutions' effect of corrosion on the glass molar ratio of B_2O_3/SiO_2 with and without stirring. Results show an increased B_2O_3/SiO_2 ratio causes an accelerated increase in network dissolution rate. If the content of SiO_2 is high, glasses will observe a rise in the diffusion processes in the dilute acid solution without stirring conditions. Also, increases in temperature, stirring rate, and concentration of the acid solution improve the formation of the leached layer due to the hydrolysis of the glass network.

International simple glass leaching in acidic and alkaline solutions according to the dynamic leaching Single Pass Flow Test (SPFT) protocol and rate parameters for B, Na, and Si in the basic regime, the Product Consistency Test (PCT), and the Material Characterization Center A Standard Leach Test for Nuclear Waste Forms (MCC-1) protocols with $Ca(OH)_2$ solutions for up to 120 days (PCT) and 720 days (MCC-1) was investigated by Backhouse [88]. His research focused on the behavior of International Simple Glass (ISG) as it changed with different pH values, a temperature range of 40–90 °C, and different days such as 30-720 days. For SPFT protocols, solutions were prepared at pH 7, 9, and 11 at room temperature. PCT-B and MCC-1 hyper alkaline experiments were knocked up in a glovebox with solutions saturated with $Ca(OH)_2$ powder in a flowing nitrogen atmosphere. Also, during his study of alteration layers, the variety of precipitates was examined with back-scattered electron images (BEI) and energy-dispersive X-ray spectroscopy (EDS). The Ca/Si ratio of the alteration products is initially high and decreases with increasing immersion time, while the Ca/Si ratio of the alteration layer starts low and increases when the calcium-silicate-hydrate (C-S-H) alteration products are formed. During the MCC-1 high pH experiments, the Zr band was observed at all immersions in the glass.

Dayhe [91] investigated sodium silicate glass dissolution in high pH aqua media in his study. The static and dynamic test conditions with high pH values, such as 7–17, and temperatures between 30 and 50 °C were examined for sodium silicate glass. The pH also increases the corrosion rate when pH values are between 11 and

13, depending on the glass composition, and the glass improves the extensive reaction layer. The dissolution rate decreases at higher pH values due to corroded product shielding on the glass surface, where a passivation layer forms. On the basis of pH-dependent SiO_2 solubility or a diffusion boundary layer with pH and silica concentration gradients in the leachate at the glass surface, the pH dependency of reaction layer development is described.

In this study, Geisler [92] examined glass corrosion with a different model than traditional models that evaluate chemical and ^{18}O and ^{26}Mg isotope tracer conclusions from a corrosion experiment with borosilicate glass in an acidic solution.The altered glass surface was examined with backscatter electron (BSE), and Inductively coupled plasma atomic emission spectroscopy (ICP-OES) was the preferred analysis of solutions to determine the release of glass into the solution. The release of orthosilicic acid into the solution depends on the nucleophilic character of the solution. The corrosion product has porosity during this study's outputs, a gel layer forms between the glass and aqua solution, the diffusion rate varies depending on the composition of the exposed glass, and non-equilibrium textures can only observe constant and relatively fast long-term corrosion on saturated silica medium.

An investigation of glass-ceramic corrosion behavior against an acidic medium has been done by Ghosh [93]. MgO-Al_2O_3-TiO_2-SiO_2-based glass-ceramic material was chosen for the investigation. X-ray diffraction (XRD) was used for determining crystals, and a scanning electron microscope (SEM) was used to observe the corroded surface. The glass and ceramic were immersed in boiling HCl and HNO_3 solutions to test their corrosion resistance. Results showed that glass-ceramic possesses better corrosion resistance against the different acidic solutions than simple glass, as well as glass-ceramic resistance to the corrosive solution, which has more resistance to boiling water than HCl and HNO_3 acidic medium.

Gin's study [94] explained the residual rate of borosilicate glass corrosion controlled by B. Because B is one of the solubility elements of international simple glass, it controls the residual rate of glass in corrosive mediums with varying pH values because Ca and Na dissolution are imposed by B. The B-O-Si linkage hydrolysis activation energy is lower than that of Si-O-Si linkages at the beginning of passivation layer formation. Dissolution of B is proceeding until a considerable

number of pores are closed at above saturation of solution on the alteration layer of the glass-solution interface. Also, open pores in the passivation layer control water diffusion. In addition to this reduction of B and Ca elements inside, water diffusion is controlled by open pores in the passivation layer.

Kaspar [81] investigate the non-destructive characterization of corroded glass with spectroscopic ellipsometry. That analysis provides information about porosity, alteration layer thickness, surface morphology, and refraction index. The aqueous corrosion on glass was analyzed with SE by glass samples immersion pH 3, 5, 7, 9, and 11 at 90 °C for 7 days, furthermore, the cross-section of the alteration layers were examined with (SEM). In this study, the goal was the non-destructive analysis of alteration layers, so the experiment result shows the investigation cross-section of altered glass with a secondary electron microscope and layer of graded alteration layer modeled according to refractive index with SE. A direct study of the refractive index at the surface of the alteration layer allowed for the direct determination of the porosity of the changed layer, which was found to be lower than expected based on the analysis of the solution data. The alteration layer may have compacted during the corrosion experiment and/or the drying process, as shown by this finding and the disparity in alteration layer thickness. Overall, our findings show how useful a non-destructive SE examination of modified glass coupons may be.

The corrosion behavior of ternary borosilicate glass in acidic aqua solution with fluid-cell Raman spectroscopy examined by Lenting [95] helps to understand glass corrosion at different pH values. If a pH value is higher than 9 further reactions take place, and silica dissolution increase rapidly so water film is observed on the glass. During this study, some evidence was found that a water-rich zone develops between glass and the surface alteration layer despite acidic conditions. Determining gaps and cracks between pristine glass and the border of the alteration layer is common as another study in literature and the reason of occurs those gaps and cracks is explained as shrinkage of the hydrous silica layer.

Glass-ceramic and glass corrosion behavior were examined by Park [96] like a Topateş [85] with different pH values (3 and 10) for 7 and 15 days. Corrosion and dissolution rates were investigated with powder samples, and their immersion in acidic and basic solutions mentioned study. The weight loss of municipal solid waste fly ash glass (SiO_2-Al_2O_3-MgO) and glass-ceramic (main phase is diopside,

Na_2CaSiO_4 crystalline phase), window glass, and marble in pH 3 and 10 were investigated, and the results show that fly ash glass-ceramic materials were the most resistant to both acidic and basic solutions. In an acidic solution that imported the crystal phase of pristine glass ceramic, the diopside ($CaMgSi_2O_6$) was transformed to Na_2CaSiO_4 on the corroded surface of glass ceramic, and the corroded surface of glass ceramic was detected with different crystal phases. Fly ash glass and window glass possess lower weight loss in acidic solutions compared to a basic solution also fly ash glass has better resistance to corrosion than window glass in both pH.

Lumila's [97] study on silica glass corrosion in various aqueous solutions of organic compounds such as citric, oxalic, lactic, ascorbic, tartaric, gluconic, ethylene, and diamine tetra acetic, etc. so powder glass sample immersion to those solutions at 98 °C. When glass powder samples immersion into all compounds, the dissolution of glass was accelerated. The citrate was the most aggressive compound compared to other organic compounds even with a low concentration of it. When the dissolution of SiO_2 increase in citrate solution increases the pH of the solution which provides a higher dissolution rate than citrate-free aqueous solutions.

Calcium-aluminosilicate glass' corrosion behavior at varying pH values was examined by Snellings [78]. At a low pH, a proton-metal exchange reaction was observed, and leaching or proton-metal exchange was the dominant proton consumption process. On the other hand, at a high pH value, all those processes are controlled by proton mass balance, and an alteration layer takes place between the glass and solution interface. Si-rich glass were more resistant to corrosion compared to Ca-rich glass, which is because Ca changes in silicate tetrahedra affect oxo bridges and change ionic (NBOs). As a result, adding alkaline and earth-alkaline oxides to silicate tetrahedra systems decreases chemical resistance [1], [82]. When basicity glass is immersed in the neutral aqua solution, the pH of the aqua solution changes, and the glass's stability against the aqua solution is reduced. Also, the high pH condition for interaction between glass and solution provides a high surface charge, and the polymerization of the glass network decreases for Ca-rich glass.

Vilarigues [98] investigated potash-glass corrosion in an aqueous solution using an ion beam spectroscopy (IBS) and infrared spectroscopy (IR). In that study, potash glass was examined for variations in pH values of the aqua solution under two

different conditions: with and without stirring of the solutions. The results show that the corrosion mechanism was very similar, but the corrosion rate was different compared to each of the conditions. Ca-carbonate occurs on the glass surface at the last step of the glass corrosion, and its kinetics depend on stirring. Because without stirring, the solution condition of the glass is slower than the stirring condition, and calcium carbonate growth takes time. In addition to the stirring condition, the average size of carbonate on the surface is smaller, and the distribution of crystals through the structure is uniform.

The corrosion of international simple glass with the aqua solution was investigated with exogenously added LiCl, KCl, and CsCl by Kaya [99]. Alteration products, which are network formers and hydrous species, occur due to the corrosion of glass from immersion in the aqua solution. The alteration layer was examined with ATR-IR spectroscopy of the corroded surface of the glass and investigated to reveal the effect of exogenously added LiCl, KCl, and CsCl to the alteration of glass with the aqua solution. The result demonstrates that, in comparison to LiCl and NAE conditions, KCl and CsCl conditions had a smaller ratio of molecular water over the surface-bound hydroxyl species, which corresponded to more passivating changed layers.

Arena [8] investigates the effect of glass alteration with minor elements such as Zn, Mg, Ni, and Co in the nuclear glass composition or coming from groundwater. During the Arena study, International Simple Glass alternated for 511 days in an aqueous solution. The four elements were added in the form of XCl_2 chloride salts (X = Zn, Mg, Ni, and Co) to the solution one by one or together to the aqueous solution. Results show the addition of 4 elements in the form of chloride salt increases the alteration of glass, thereby inducing the precipitation of trioctahedral smectites, including the added elements. Also, oxidation accelerated because of the element's change to the pH value of the water solution.

During Collin's [100] research, he investigated the influence of exogenous ions supplied to solutions, which show the effect of gel formation and the properties of the gel formed by passivation of International Simple Glass. ISG was altered at 90 °C and pH 7 in silica-saturated solutions containing various alkaline cations separately (Li^+, Na^+, K^+, and Cs^+). The alteration kinetics observed with Li and Na in the solution are similar to those observed with no ions, while K and Cs in the

solution tend to decrease glass alteration. Furthermore, for K or Cs ions, the kinetics decrease as the ionic strength of the solution increases. The passivation layer formed in these solutions shows selectivity toward cations following the series K>Cs>Na>>Li. These alkalis replace Ca from pristine glass in the altered structures, leading to differences in [AlO_4] unit charge compensation. Importantly, the exchange between Ca and alkali also affects the total quantity of water inside each gel, and this effect is well correlated with the observed drop in glass alteration.

Atomic force microscopy (AFM), X-ray photoelectron spectroscopy (XPS), and inductively coupled plasma mass spectrometry (ICP-MS) were employed in Nathan P. Mellott's [101] work to examine the molecular-scale mechanisms that result in glass surface roughening as a result of water corrosion. The study directly investigated how surface roughness is impacted by dissolving at the atomic and molecular levels by analyzing atomically smooth fiber and melt surfaces. The combined use of both methods showed that cation leaching alone does not produce appreciable roughening; rather, changes in RMS roughness resulting from aqueous corrosion are closely correlated with the concentration of silica liberated from the glass. The study demonstrated how surface roughness at the nano- and microscale affects a number of glass surface characteristics, including strength, optical response, and adsorptivity. It was demonstrated that the amount of silica released corresponds with the surface roughness of silicate glass and is independent of the degree of modifier ion leaching. The results imply that the effect of glass composition on roughening might be a sign of the variability of the glass network structure at the nanoscale. The spatial consistency in RMS roughness of melt surfaces was validated by AFM imaging of more than 25 distinct locations on a single sample surface and RMS measurement of several 1 μm x 1 μm areas. The study also proposed that when the local environment is far from chemical equilibrium with the glass, the roughening associated with glass composition in the early stages of corrosion may be caused by the structural heterogeneity of the silicate network.

In Dien Ngo's [102] study, the chemical composition, porosity, pore-size distribution, and thickness of alteration layers formed on International Simple Glass (ISG), a model nuclear waste glass, after corrosion in aqueous solutions of pH 7 and pH 9 at 90 °C for durations of 7 days and 2046 days were analyzed using X-

ray photoelectron spectroscopy (XPS) and spectroscopic ellipsometry (SE). These pH values correspond to pH levels buffered by boron species emitted from the glass and aquifers of the granitic type, respectively. Hydrogen bonding interactions on these layers were examined further using sum frequency generation (SFG) spectroscopy and attenuated total reflectance infrared (ATR-IR) spectroscopy. To comprehend how pore size affects hydrogen bond length distributions in nanoporous gels, molecular dynamics (MD) simulations were performed. The elemental compositions of the alteration layers generated in various pH solutions were found to be quite comparable by the results, and the SE indicated that the pore size increased with corrosion time. Strongly hydrogen-bonded hydrous species predominated in the alteration layers, according to ATR-IR spectroscopy, and SFG spectroscopy showed variations in hydrogen bonding interactions on ISG corroded at pH 7 and pH 9. These results advance our knowledge of the hydrous species on alteration layers, which benefits our comprehension of the process behind glass corrosion. In conclusion, ISG alteration layers that arise in silica-saturated solutions at pH 7 and pH 9 have comparable chemical compositions, but they vary in terms of hydrogen bonding interactions and nanoporous structure. To relate these variations to the rates of glass dissolution and the mobility of hydrous species, more investigation is necessary.

4.4 Glass-Ceramic Corrosion

Glass-ceramics, which are defined by the coexistence of a crystalline and an amorphous phase, have several beneficial features that are necessary for a variety of applications. These include ideal dielectric constants, mechanical strength, chemical durability, a lower thermal expansion coefficient than typical glasses, and effective electromagnetic radiation transmittance. Glass-ceramics have been widely used in a variety of disciplines, such as electronics, vacuum technology, military applications, domestic items, industrial operations, and even biology, because of their diverse range of qualities. Given that glass-ceramics are multiphase materials, it is essential to approach their corrosion behavior with a comprehensive understanding. The crystalline phase is made up of a configuration of individual grains, whereas the glass phase is typically thought of as a homogeneous system. Examining the dynamics of the grains and their boundaries is essential to assessing

the crystalline phase's propensity for corrosion. Grain borders are more reactive than the grains themselves, which is noteworthy. This increased reactivity shows up as galvanic couple formation, in which the grains operate as cathodes and the more active grain borders as anodes. Glass-ceramics' corrosion behavior is shaped by the complex interactions between their crystalline and amorphous constituents, which affects how well they function and how long they last in practical applications [103].

Five different mechanisms are taken into account when analyzing the corrosion of the glass phase: ion leaching, dissolution, precipitation, pitting, and weathering. The process known as ion leaching, which was previously covered in relation to glass corrosion, involves exchanging alkali ions found in glass for H^+ and H_3O^+ ions found in the corrosive media. Dissolving is a noteworthy mechanism that entails the dissolving of silica through the breaking of the silicate structure. Precipitation develops on the glass surface when the dissolved species concentration approaches saturation. Pitting develops in areas where the precipitate layer has pores, allowing the corrosive medium to attack and penetrate. Pits occur on the surface of the glass as a result of this contact through the pores. Moreover, weathering results from the glass surface's sporadic contact to water vapor. Ion exchange between the vapor and the surface happens during this process, which adds to the overall weathering impact. Each of these complex processes has a unique effect on the surface integrity and long-term durability of the glass material, and together they affect the corrosion behavior of the glass phase [103].

The $Li_2O–SiO_2$ system provides the basis for a significant class of glass-ceramics that are used in commerce [104-106]. This system has been the subject of extensive corrosion research, the results of which are summarized. The lithia-silica system's corrosion dynamics are significantly impacted by the crystallization process. The least amount of damage is shown in settings with an acidic content, whereas basic conditions show the highest damage. In areas where glass predominates, high and uniform dissolution is more likely to happen. Both intracrystalline and interphase assaults are applicable in neutral or basic media [103].

The influence of grain boundaries on water corrosion in glass ceramics is evident through the dissolution behavior observed when ZrO_2 is present in the glassy phase which was examined by Topateş. The introduction of ZrO_2 accelerates corrosion by

promoting the formation of soluble Zr-containing components, leading to increased dissolution of the glassy phase. In contrast, when the glassy phase does not contain ZrO_2, corrosion primarily takes place through the dissolution of the grain boundary phase surrounding the zircon grains, rather than the glassy phase itself. This distinction in corrosion mechanisms highlights the role of ZrO_2 and the significance of grain boundaries in influencing the overall corrosion behavior of glass-ceramic materials [85].

4.5 Boiler and Hot Water Storage Tank

The hot water tank, commonly found in home heating systems, serves as a storage unit for hot water, ensuring users have access to it when needed. There are two primary types: pressurized and unpressurized hot water storage tanks.

Pressurized hot water tanks, typically used in homes connected to city water supplies, maintain water under city water pressure. Made of steel with an enamel-coated interior, these tanks include a heater to quickly heat the water. On the other hand, unpressurized hot water tanks, common in homes connected to local water wells or low-pressure sources, can use a water pump to increase pressure. Often made of plastic for lighter construction, these tanks store water heated by a water heater or boiler [107-110].

Boilers may experience internal corrosion, particularly when oxygen and minerals in water react with the steel surface inside the tank, a process accelerated during hot water production. Enamel coatings, derived from glass, are often applied to the interior of boiler tanks. These coatings create a durable, corrosion-resistant barrier, preventing direct contact between water and the steel surface, thus extending the lifespan of the boiler and preventing rust [107-110].

The effectiveness of enamel coatings can be influenced by factors such as operating conditions and water hardness. Minerals like lime, magnesium, and calcium in water can challenge enamel coatings, leading to accumulation and potential corrosion. Water hardness, determined by mineral concentration, especially in hard water with higher lime content, can impact enamel coatings negatively, reducing heat transfer efficiency [108-110].

Working conditions, including the expansion and contraction during hot water production, can stress enamel coatings, resulting in cracks or fractures on the tank's interior surface. This creates potential entry points for corrosion to initiate [108].



Figure 4.7 Image of domestic hot water boiler

5
EXPERIMENTAL PROCEDURE

5.1 Production of Precursor Glass, i.e., Frit

Raw material sources were chosen as Quartz, Boric Acid, Sodium Hydroxide, and Cobalt Oxide (72%); in addition to them, earth-alkaline oxides were preferred in carbonate forms, which are $CaCO_3$, $SrCO_3$, and $BaCO_3$. Also, other oxides were added to the exact molar% value in each frit formula; there were the oxides SiO_2, B_2O_3, Na_2O, CoO, and MO, respectively 59:13:13:2:13. Frit and enamel-quality mill additives were supplied from Akcoat Advanced Chemical Coating Company. The Seger method was used to formulate the frit design, which corresponded with the intended qualities and resulted in the creation of the formula. Accurate measurements of the raw components were made in compliance with the prescribed formula, and they were then put into an alumina-silica crucible. For one hour, the melting process took place at a temperature of 1300±50°C. Once the resultant molten materials were submerged in water, a quick cooling procedure caused the material to solidify as frit. Following this process, the granular frits were filtered and let to sit at 100°C for a day, which successfully eliminated the water content. The chemical composition of the frits and batch (mill) enamel experiments, as well as whether the frit formulas calculated in % molar were at the values calculated in molar after melting, were analyzed with a Bruker S8 Tiger X-ray fluorescence (XRF) device. Molar frit formulas are listed in Table 5.1. Also, mill additive ratios are given in Table 5.1.

Table 5.4 Chemical composition of frits (molar%)

Component	F-Ca	F-Sr	F-Ba
SiO_2	59	59	59
B_2O_3	13	13	13
Na_2O	13	13	13
CoO	2	2	2
CaO	13	-	-
SrO	-	13	-
BaO	-	-	13

Table 5.5 Batch (mill) recipe of the samples.

Material	**Weight (g)**
Frit	100
Clay	6
Sodium Nitrite	0,2
Acid Boric	0,2
Water	40

For the milling procedure, an alumina ball mill with a 300-gram capacity was used. The RTU enamel powder was calibrated to a value of 13±1 on the Bayer scale, with the residual amount remaining above the 150-mesh filter. Once the required particle size for RTU was reached, 40% water was added and well mixed to guarantee homogeneity. The enamel slips' density as a consequence was around 1.91 g/cm^3.

An enamel-grade steel plate of S235JR+AR (EN 10025 & EN 10011) measuring 105x105x2 mm is used as a standard. Specimens are produced following ISO 28764 standards. First, one side is covered with a 10–20µm ground coat enamel, which is fired for two minutes at 790°C. The uncoated surface is next prepared for enamel application by sandblasting it with silica sand for one to two minutes at a pressure of six bar. Weight gain in the corrosion test results is intended to be eliminated by the ground coating on one surface. The scale-carbon combination created during the background coat firing is cleaned by sandblasting. After applying the enamel slurry to the steel surface using the Dip Coating process, it is dried for ten minutes at 320°C in an oven and fired for ten minutes at 860°C in a box furnace. After firing, the sample is let to cool to room temperature. A final cover coat thickness of 250µm ± 50µm has been determined.

5.2 Hot Water Corrosion Test

Enamel surfaces can be corroded by hot water solutions. For the most part of their lives, they were exposed to corrosive environments, particularly in water heaters, boilers, and hot water storage tanks. The rate of corrosion rises in tandem with environmental temperature. These conditions have the potential to quickly inflict major damage, particularly to pipelines, chemical reactors, and water heaters. To avoid this, certain enamel coatings that are resistant to heat have been created. The aim of the study is to ascertain how alkaline-earth oxides affect the way steel's enamel coatings change when exposed to hot water. The exploration of this fundamental impact on the corrosion process will help develop broad standards for the enamel coatings in contact with the hot water solution. DIN 4753-3 was followed in the preparation and testing of enamel-coated steel samples. Part 3: Corrosion protection on the water side by enamelling and cathodic protection - Requirements and testing. Also, test equipment was used according to ISO 28706 during all tests. For 42 days, each sample was subjected to a test with the solution

temperature maintained at 95°C ±1. Every enamel formula experiment was run three times with various sample plate specimens. The specimens' surfaces were washed with water, dried for two hours at 110°C, and stored in a desiccator for two hours before to the corrosion test. Subsequently, the initial mass of every specimen was measured using the closest sensitive scale, measuring 0,2×10-3 g. Specimens were positioned face up at the bottom of the cylindrical cylinder in preparation for a liquid phase test. The cylindrical vessel's upper surface was covered with borosilicate glass, which was provided in compliance with ISO 3585:1998. The vessel was secured once the wing nuts were tightened. After 450 milliliters of clean water were added to the vessel, the heating mechanism was activated. After 21 days, the heating system was turned off, and the specimens' surfaces were washed with water, dried for two hours at 110°C, and then placed in a desiccator for another two hours. Each specimen's second weight was determined, and the first 21-day weight reduction was computed. In order to ascertain the elements release from the enamel layer to water, a test solution was also obtained. Following that, specimens were put into the testing apparatus, and for the last 21-day test, the heating system was activated once again. Following the same procedure, the test was terminated by turning off the heating system, washing the specimens' surfaces, drying them for two hours at 110°C, and storing them in a desiccator for two hours. Each specimen's ultimate weight was recorded, and an ICP-MS analysis of the water sample was conducted from the vessel to ascertain elemental migration. Throughout these procedures, all safety regulations were adhered to.

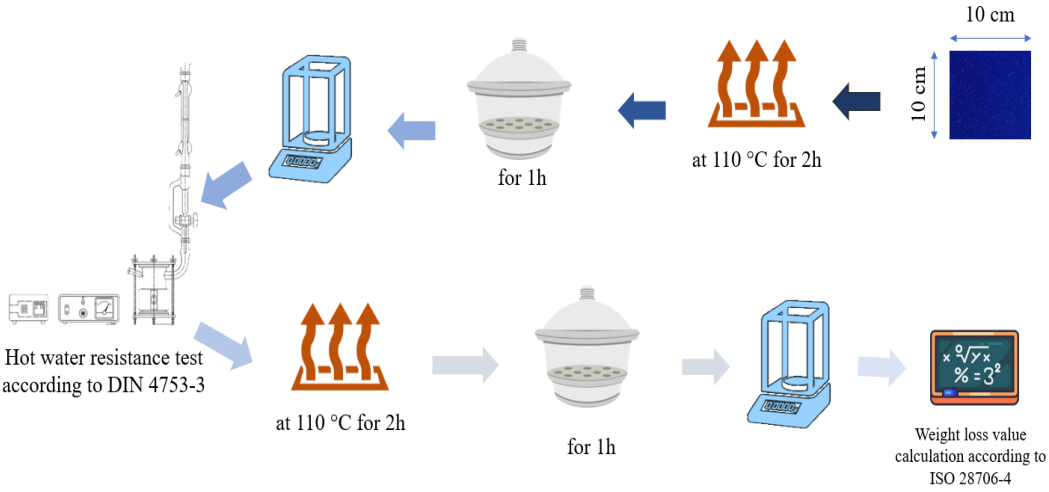


Figure 5.1 Schematic illustration of DIN 4753-3 hot water corrosion test procedure.

6

CHARACTERIZATION PROCEDURE

As illustrated in Figure 6.1, a flow chart was used in this investigation to illustrate the characterisation process for each frit, bulk glass or glass-ceramics, and glass or glass-ceramic coatings. The successive stages involved in characterizing the glass and coatings investigated in the research are visually represented by the flow chart.

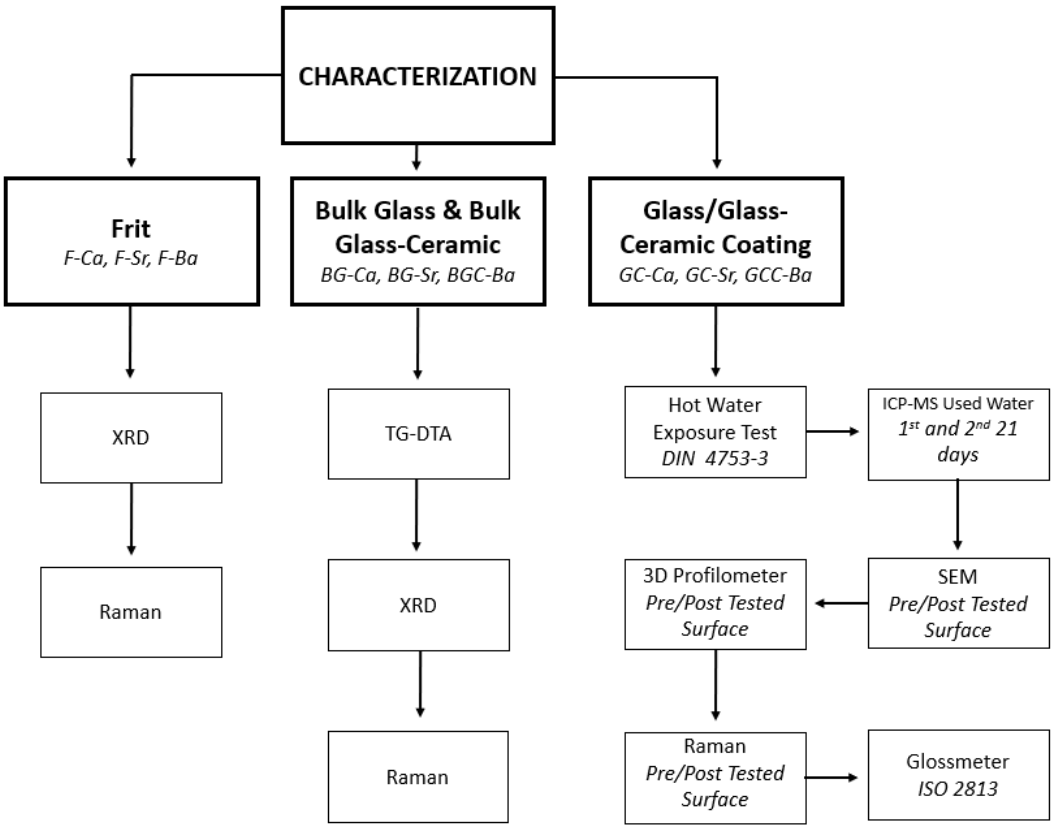


Figure 6.1 Chart of the characterization procedure conducted in the study.

6.1 Preparation of Glass-Ceramic Coatings

Using the wet spray-gun method, amorphous frit powders with a particle size distribution of D90: 110 μm were applied on S 235JR+AR (EN 10025 & EN 10011) enamel grade steel plates, which had a thickness ranging from 225 to 325 μm. Glass-ceramic coatings, also known as enamel coatings, were created on the steel substrates by sinter-crystallization procedures carried out for eight minutes at 860 °C in a Protherm-PLF110/30 furnace after the spray coating was applied.

6.2 Chemical Analysis

Bruker AXS S8 Tiger XRF (USA) equipment was used to perform X-ray fluorescence (XRF) analysis to determine the chemical composition of the produced frits. The purpose of this investigation was to verify the frit's chemical composition and amounts. The oxide percentages of the frit were also closely examined in order to ensure proper interpretation of the data.

6.3 Crystal Phase Analysis

Frit powders for F-Ca, F-Sr, and F-Ba were pelletized using 15 g and 1 cc isopropyl alcohol. The resulting bulk glass-ceramics were BG-Ca, BG-Sr, and BGC-Ba, which were obtained using sinter-crystallization operations conducted at 550 °C for 8 minutes, 860 °C for 8 minutes, and 550 °C for 8 minutes. Using an X-ray diffractometer (Bruker XRD D8 Advance), the crystalline development of the glass-ceramics was examined following the milling of the sinter-crystallized pellets. Cu K_{α} radiation was used to record the patterns, and the x-ray generator was adjusted to 40 kV and 25 mA. The scanning range was 2θ: 5°-85°, with a step size of 0.02°.

6.4 Raman Spectrometer

A Raman spectrometer (Kaiser Optical System, model Raman RXN1, MR Probe) with wavenumber ranges of 100–3450 cm^{-1} was employed for the investigation of network structure. Depending on the material, the Invictus Diode Laser 785 nm light source might provide 4 mW to 400 mW of power. Glass-ceramic samples were examined using Raman Spectra both before and after they were exposed to hot water. A power of 50–60 mW was used, with an exposure duration of 180 s^{-1}.

6.5 Thermal Analysis

Phase transitions, breakdown, and exothermic and endothermic processes were all investigated using differential thermal analysis (DTA). The equipment used for the tests was a Netzsch STA 449 F5-Jupiter. We studied the thermal changes of various compositions of glass including earth-alkaline oxide by heating 15 mg of glass

powder in an alumina crucible at a rate of 10 °C/min up to 1200 °C in an environment of nitrogen (N_2).

6.6 Hot Water Resistance Test

We evaluated the coatings' resistance to water corrosion using the equipment and the test protocol described in DIN 4753-3. For 42 days, water that was 95 °C in temperature was applied to the plates. This study did, however, differ in that clean water was not replaced every 24 hours for the length of the test. This change was made to make it possible to analyze the quantities of migrant elements (SiO_2, B_2O_3, Na_2O, CaO, SrO, BaO, and CoO) that were incorporated into the aqueous solution from the glass covering surface. By comparing the pre-and post-water exposure weights, the DIN 4753-3 standard test calculated the weight loss of the coated plates. Loss of weight revealed information about the degree of corrosion the coatings underwent throughout the test.

6.7 Inductively Coupled Plasma Mass Spectrometry (ICP-MS)

The quantity of leached elements from the coating to the aqueous solution, which was taken from the cylindrical vessel just after the tests were completed, was measured with an Agilent 7800 ICP-MS, an inductively coupled plasma mass spectrometer.

6.8 Scanning Electron Microscope (SEM)

A ZEISS EVO 10 Scanning Electron Microscope (SEM) with an acceleration voltage of 15-20 kV and a working distance of 7-10 mm at x150, x250, and x500 magnification was used to investigate changes in the microstructure and surface morphology of the glass/glass ceramic coating by d-H_2O at 95°C before and after the hot water attack. This allowed for a thorough analysis of any microstructure modifications caused by the hot water attack.

6.9 Surface Profilometer

According to ISO 2813, ASTM 523, and DIN 67530 standards, gloss is measured using the TQC Polygloss Gloss-Meter at 60° from several spots on the coated

surfaces, both in their original condition and their state after being exposed to hot water. Any changes in the coatings' reflecting qualities and surface appearance may be assessed by comparing gloss values, which can offer important information on the degree of aqueous corrosion-related damage to the coated surfaces.

6.10 Gloss Determination

In order to assess the glass-ceramic coatings' surface qualities, factors including gloss, topography, surface morphology, and roughness were looked at both before and after the coatings were exposed to hot water. The breadth of the leached surfaces and the values of Ra and Rz were measured using a 3-Dimensional optical surface profilometer that complied with ISO 4287 criteria (ZEISS Smartzoom5). This study made it possible to identify any physical changes brought on by water corrosion.

7

RESULT AND DISCUSSION

The basic glass system selected for the frit was specifically sodium-borosilicate, which was used to accomplish a harmonious integration of earth-alkaline oxides within the borosilicate glass matrix. The purpose of choosing sodium-borosilicate as the primary glass system was to enable the smooth integration of earth-alkaline components in a way that guarantees compatibility and optimal compositional synergy. Following the melting-quenching processes, the chemical makeup of the resultant frits, which are called precursor glass, was carefully examined and is presented in Table 5.1. Of the various elements of the glass composition, silicon dioxide (SiO_2) stands out as the most molar percentage. This large presence has a major role in the overall amorphous network structure that defines the glass matrix. Boron trioxide (B_2O_3) serves as a dual-purpose network former and modulator, contributing a subtle complexity to the glass's structural dynamics. Sodium oxide (Na_2O), which functions as a flux, is an essential moderator that aids in the melting process and encourages the glass's fluidity throughout the several processing phases. Interestingly, it coincides exactly with the molar ratio of B_2O_3, highlighting its essential role in the compositional balance. Furthermore, a little amount of cobalt oxide (CoO) added wisely acts as an adhesion agent, strengthening the link between the coating and the substrate underneath [34], [45]. Entering the domain of earth alkaline components examined in this extensive analysis, it is apparent that the barium ion (Ba^{+2}), with its comparatively greater radius of 1.34 Å, exceeds its equivalents, which are the sodium ion (Na^{+}, radius 0.97 Å), calcium ion (Ca^{+2}, radius 0.99 Å), and strontium ion (Sr^{+2}, radius 1.12 Å) [111]. One of the most prominent characteristics of the Ba^{+2} ion is that it has a somewhat smaller propensity to form chains in silicate structures, which gives its contribution to the composition of glass a unique quality [111]. Additionally, the difficulty comes from the fact that silicon (Si) and boron (B), which are essential network formers in the silicate structures, are difficult for alkali and alkaline earth ions to replace. Rather, by settling into interstitial places within the network, these ions become network modifiers with ease. When the coordination number of these cations is more than 6, they participate in the weaker bond formation with oxygen than network formers,

which is essential for preserving the electroneutrality of the negatively charged borosilicate network [112]. The foundation of the glass system is this complex interaction of carefully considered compositional materials that are strategically integrated. Each component influences the structural and chemical properties of the resulting frit in a subtle but important way.

The existence of tetrahedra and trigonal species joined by bridging oxygen bonds (BO) characterizes the complex structure of silicate networks in glasses. Non-bridging oxygen (NBO) atoms, which have a negative charge and may form ionic interactions with positively charged cations such as Na^{+}, Li^{+}, Ca^{+2}, or Ba^{+2}, are important components of this network. An intriguing theory of the glass structure is presented by the modified random network (MRN) model, which postulates the existence of two entangled sublattices: (i) the network region made up of tetrahedra, and (ii) regions rich in atoms that do not integrate into the network, like network modifiers. Percolating channels may arise in these locations at greater concentrations of network modifiers. The NBO atoms define depolymerized areas that can create percolation channels, whereas the tetrahedra define the structured network regions. Located at the periphery of these intricately structured network areas, NBO atoms form ionic connections with alkali, alkaline earth, or other glass-modifying species while also paving the way for percolation channels. These channels, which include NBO atoms in them, could serve as ion exchange channels, especially for elements that have weaker connections with the NBO [112]. This model sheds light on the creation of percolation channels and their possible function in ion exchange processes in glasses, offering insightful information about the dynamic interplay of structural components within the silicate network. The features of the glass structure are greatly affected by the addition of alkaline and earth-alkaline oxides to silicate tetrahedral systems. These effects are mainly felt on oxo-bridges and ionic non-bridging oxygen (NBO) sites. These oxides increase the number of gaps in silicate rings, which lowers the melting point, widens the range of operation, and lessens the chemical resistance of silicate tetrahedral structures. Q stands for the number of bridging oxygens in a silicate tetrahedral, and the order of the silicate tetrahedra's reactivity trend is $Q^{1} > Q^{2} > Q^{3} > Q^{4}$ [1], [82].

7.1 Analysis of Frits and Bulk Glass/Glass-Ceramics

7.1.1 Thermal Analysis

The frit powders, F-Ca, F-Sr, and F-Ba, underwent differential thermal analysis (DTA), which showed both exothermic and endothermic reactions. These reactions might be related to processes such phase formation, structural alteration, or breakdown within their compositions. Figure 7.1 shows the DTA patterns of the F-Ca, F-Sr, and F-Ba frit powders, giving an overview of the typical reactions and thermal behavior seen during the analysis.

For every frit sample, peaks in the 140–150 °C range were seen, indicating the volatilization of physically attached moisture and possible organic contaminants. An endothermic peak between 462 and 526 °C, depending on the sample, is observed in the DTA curves as the temperature gets closer to 460 °C, which is thought to be the consequence of the breakdown of crystalline water [113]. At around 660 °C, which is the glass transition temperature (T_g) for all frit samples, there is a notable change in specific heat. With an onset Tg of 673 °C, F-Ca had the highest of the frit samples; F-Sr and F-Ba had onset Tg's of 661 °C and 664 °C, respectively. According to the DTA curves, the offset point of Tg also exhibits the same tendency, with F-Ca having the greatest offset temperature (697 °C) and F-Ba having the lowest (685 °C).

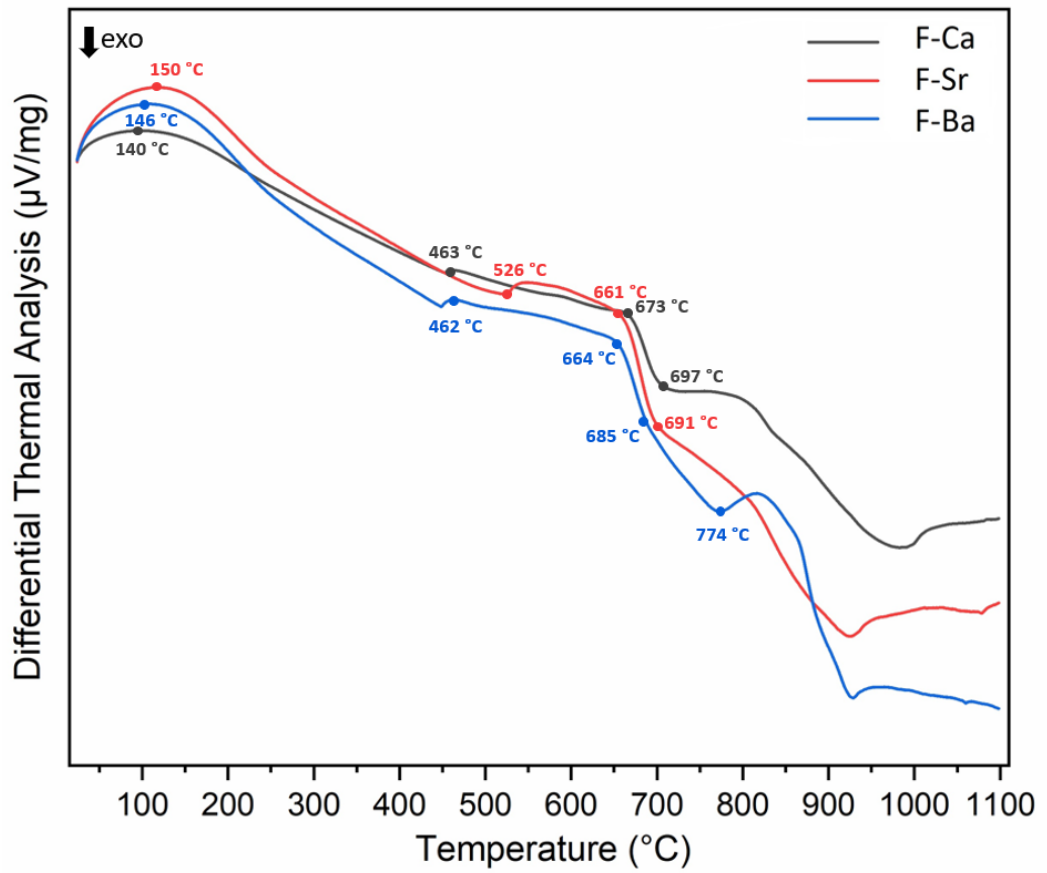


Figure 7.8 DTA analysis of frits; F-Ca, F-Sr, and F-Ba.

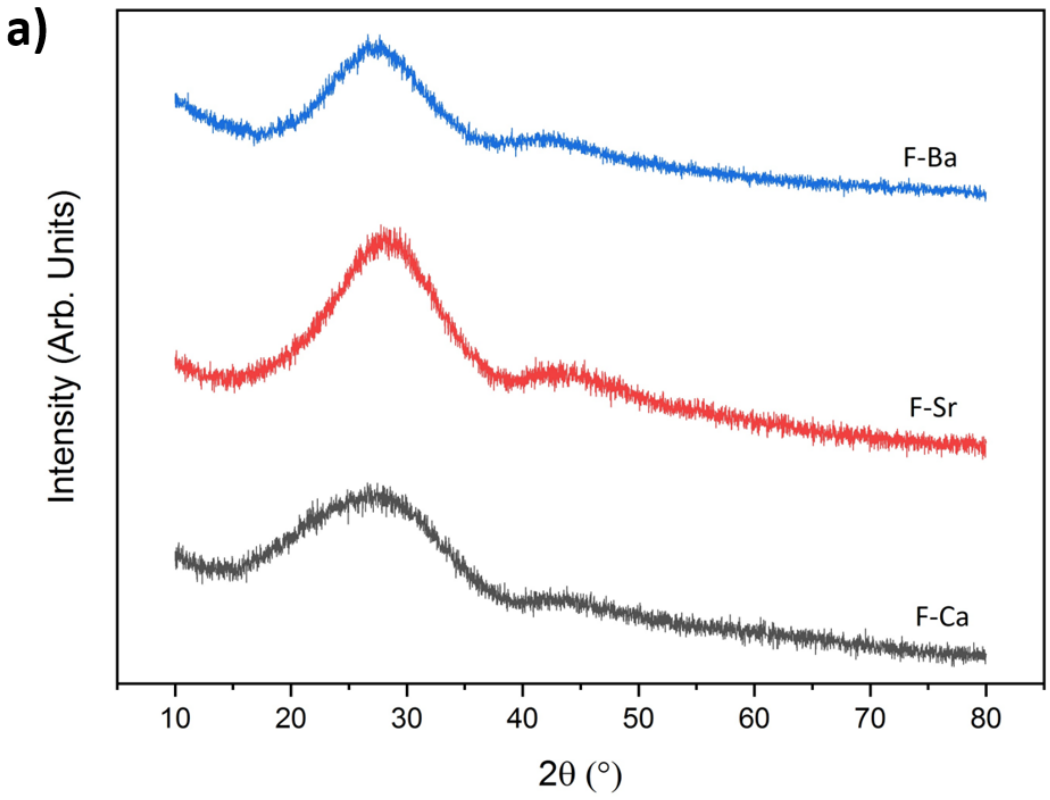
7.1.2 Crystallographic Analysis

The effects of several earth-alkaline oxides on sodium-borosilicate glass with respect to their influence on densification and crystallization behavior were thoroughly investigated at increased temperatures. The results show that the BaO content acts as a catalyst for the formation of crystals, resulting in the exothermic process that is observed at 774 °C. X-ray Diffraction (XRD) analysis, as shown in Figure 7.2, provided evidence for this crystallization occurrence by identifying the creation of a Ba-Si-containing crystalline phase in the F-Ba sample. In contrast, at the specified circumstances, the addition of CaO and SrO to the sodium-borosilicate glass system did not result in any appreciable crystallization behavior. The X-ray Diffraction (XRD) investigation presented in Figure 7.2 revealed that the F-Ba sample underwent the development of a crystalline phase containing Ba and Si.

It is possible that insufficient oxidic content in the F-Ca and F-Sr samples resulted in an unsuitable temperature environment for nucleation, which is why no crystals formed in those samples. For example, prior research suggests that at 1567°C, a

crystal phase in the SrO-SiO glass system may form with 50.7 mol% SrO [114], [115]. Similar to this, a crystal phase containing SiO2 and CaO may form in the $CaO\text{-}SiO_2$ system at 1497°C and 54 mol% CaO [116]. The heat treatment that was performed on the F-Ca and F-Sr samples did not cause any discernible crystal formation in spite of these factors.

In contrast, no notable crystallization behavior was induced by the integration of CaO and SrO into the sodium-borosilicate glass system. It is possible that insufficient oxidic content in the F-Ca and F-Sr samples resulted in an unsuitable temperature environment for nucleation, which is why no crystals formed in those samples. For example, prior research suggests that at 1567°C, a crystal phase in the SrO-SiO glass system may form with 50.7 mol% SrO. Similar to this, a crystal phase containing SiO2 and CaO may form in the CaO-SiO2 system at 1497°C and 54 mol% CaO. The heat treatment that was performed on the F-Ca and F-Sr samples did not cause any discernible crystal formation in spite of these factors [114-116].



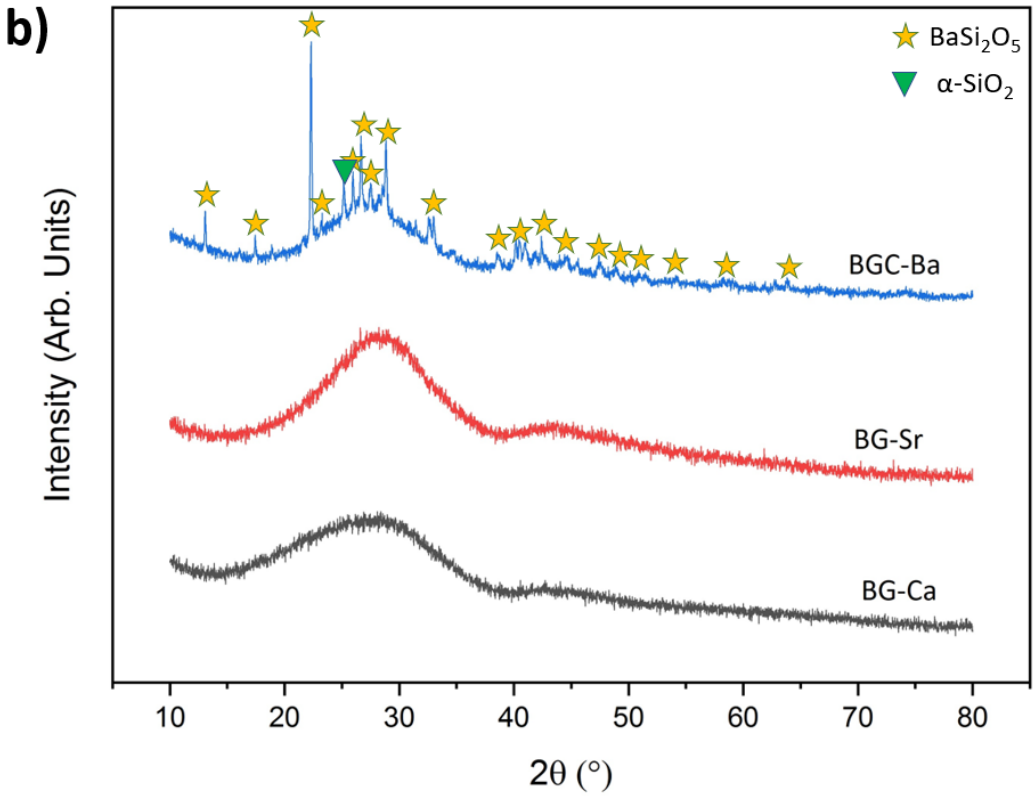


Figure 7.2 XRD patterns of the studied a) frits F-Ca, F-Sr, and F-Ba b) after crystallization of bulk glass BG-Ca, BG-Sr and bulk glass-ceramic BGC-Ba.

The X-ray Diffraction (XRD) phase analyses of the frits and the frits that underwent heat treatment based on the findings of the Differential Thermal Analysis (DTA) are shown in Figure 7.2. Three different frits were examined: F-Ca, F-Sr, and F-Ba. The results of the analysis indicate the existence of an amorphous phase, which indicates that all of the raw materials have completely melted and that the quenching process has prevented the development of crystals in the glass system. After the DTA findings were analyzed (as shown in Figure 7.1), the frits were heat treated to simulate the temperature at which F-Ba crystallizes and the boiler enamel firing range of 840–880 °C. The bulk sample XRD studies confirmed the BaO-containing sample's crystallization, which was consistent with the DTA findings.

Sanbornite, or $BaSi_2O_5$, peaks were seen in the BGC-Ba sample's structure when the right temperature and chemical makeup were used to cause the $BaSi_2O_5$ crystal phase to crystallize. The nucleation of barium disilicate glass ($BaO.2SiO_2$-BS2) is prone to occur even in the absence of exogenously introduced nucleation agents. Being one of the few silicate glass compositions that may undergo volume nucleation makes it noteworthy [117], [118]. For the SiO_2 and BaO binary phase

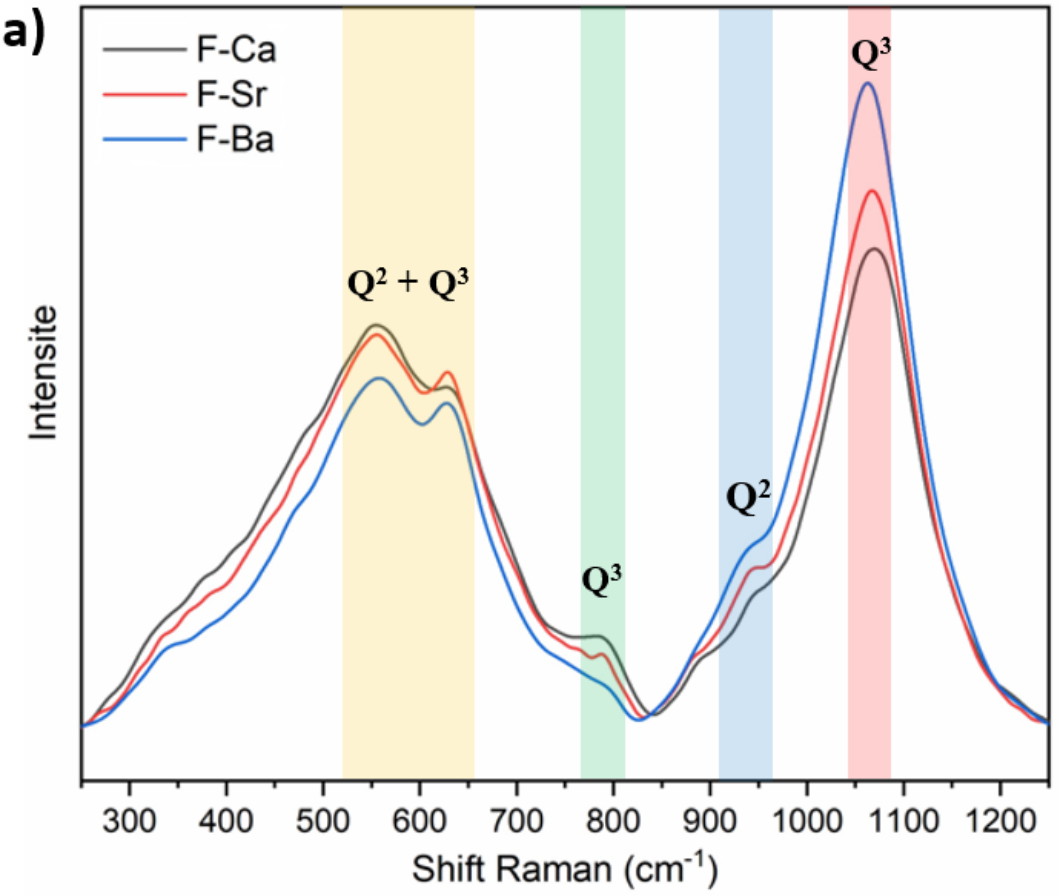
diagrams, the SiO_2 mol fraction should range from 0.67 to 1 mol fraction in order to produce the $BaSi_2O_5$ crystal phase. Reaching a crystallization temperature that is favorable to the particular crystal phase in issue is essential to achieving the appropriate crystal phase. Temperatures for $BaSi_2O_5$ crystallization usually vary from 800 to more than 1400 °C. Notably, an 860 °C firing temperature was used to the BGC-Ba sample, which has a SiO_2 mol percentage of 0.82 between SiO_2 and BaO. This selected temperature is in accordance with the conditions necessary for the $BaSiO_2$ crystal phase to crystallize.

There were quartz peaks seen in the BGC-Ba sample. The ionic-atomic composition of the Si-O bond makes it a strong bond type, which explains why. The angles of this connection vary remarkably, ranging from 132° to 180°, which contributes to the inherent flexibility of the silicate structure. This flexibility is crucial for silica glass's exceptionally low tendency to crystallize and is a key factor in SiO_2's unique glass-forming properties. On the other hand, SiO_2 may assume a wide range of polymorphic forms due to the malleability of its chemical bonds. Examples of these forms are the three low-pressure forms of quartz, tridymite, and cristobalite, which have distinct high- and low-temperature structures. Higher temperatures allow the more mobile atoms of the mixture to be removed and rearranged within the quartz structure. Furthermore, with increasing temperature and mobility, the glass network structure with a high SiO_2 content may tend to crystallize into quartz since it is a saturated solid solution [119], [120].

7.1.3 Raman Spectrometer Analysis

An essential method for exploring the complex bonding patterns and network structure units found in the glasses under investigation was to perform room-temperature Raman spectroscopy spectra, as seen in the detailed Figure 7.3. Raman spectroscopy is well acknowledged for its potent role in examining structural details, as it may provide vital insights into coordination states, chemical bonding, and glass networks via inelastic light scattering [121], [122]. Glassy matrices undergo a fundamental transition when they undergo network modification. Specifically, this conversion of BO_3 units into BO_4 units is largely dependent on the addition of network modifier ions like Na^+ and Ba^{2+}. This transition occurs before nonbridging oxygen (NBO) is formed inside the glass network. The complex interaction between an increase in silica concentration and a decrease in the Na/Si

(or Ba/Si) ratio becomes important, impacting the silicate network's depolymerization once BO_4 units are synthesized. This dynamic interaction highlights the important role that the silica content and ratio play in borosilicate glasses. It also shows that a greater concentration of SiO_2 in borosilicate glasses leads to a more polymerized silicate network than in boron-rich glasses [121], [123].



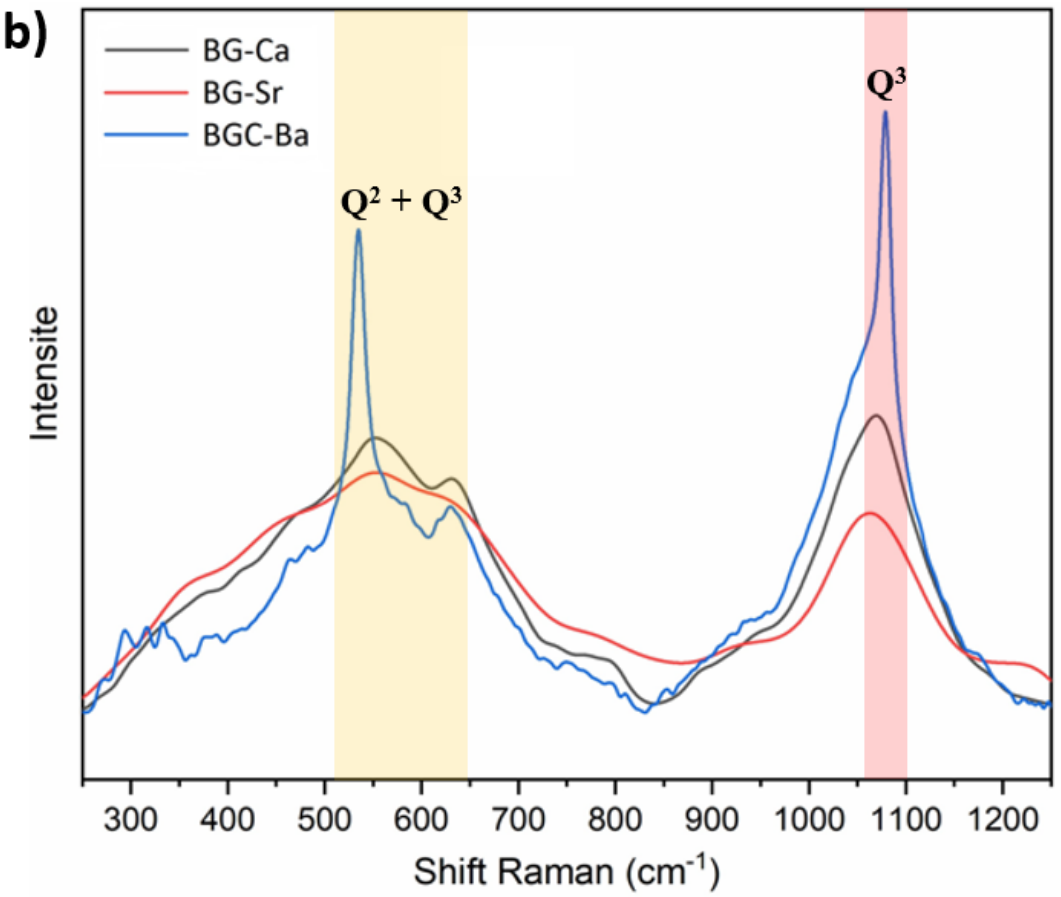


Figure 7.3 Raman spectrum curves of a) frits and b) after crystallization heat treatment of frits, resulting bulk glasses and bulk glass-ceramics.

In addition, the replacement of earth alkaline cations with modifiers such as Ca, Sr, and Ba results in a significant increase in the Raman peak intensity at 960 cm^{-1} along with a change in frequency towards lower values. Characteristic bands appear in the Raman spectra of the Na_2O-B_2O_3-SiO_2 glasses at around 430, 485, 600, 800, 1060, and 1200 cm^{-1}. Of these, the bands located at 485 and 600 cm^{-1} are clearly linked to the three-membered and four-membered silicate rings' ring breathing modes, respectively [123].

Glass networks are shaped in large part by modifiers such as Ba, Ca, Mg, Sr, and La, which break B-O or Si-O bonds and take up interstitial or substitutional places in the network. According to Fajan's rule, the effect of these modifier ions on the glass network is closely related to their ionic radii. Interestingly, the order of increasing ionic radii is Ba>Sr>Ca>Mg, where Mg has less polarization and Ba has more polarization [123].

The Si-O-Si bonding-related delocalized vibrations, which result from a mix of stretching and bending modes, give rise to noticeable peaks within the spectral area between 500 and 850 cm^{-1}. An n-membered ring consisting of silicate units (n = 3, 4, or 6), a silicate unit with two bridging oxygen atoms (Q2), and a silicate unit with three bridging oxygen atoms (Q3) is responsible for the significant Boson peak that was observed in the lower wave number range, specifically below 250 cm^{-1} [121], [122], [124].

The band at around 550 cm^{-1} represents the B-O-B stretching seen in BO_4 units, pyroborate groups, and B-O stretching. It is closely associated with B-O-B structures. Furthermore, bands at 630 cm^{-1} (equivalent to Q2 and Q3) and 780 cm^{-1} (related with Q3) are intimately connected to Si-O structures. To go more precise, the Q2 band is located at about 934 cm^{-1}, while the Q3 band is visible about 1,040 cm^{-1} [121], [125].

The heat-treated and crystalline sample (GCC-Ba) showed a simultaneous sharpening of the Raman bands and a decrease in the Boson peak, indicating a glass-crystal phase transition. This discovery is consistent with the results of DTA and XRD investigations, offering a thorough comprehension of the structural changes that occurred during the heat treatment [124].

The heat-treated BGC-Ba sample has a sharper Raman band than the BG-Ca and BG-Sr samples, suggesting a more prominent glass-crystal phase transition or crystallization. This observation supports the possibility of a glass-crystal phase transition and is consistent with findings from DTA and XRD experiments for GCC-Ba. Furthermore, the spectral profile of the smooth Raman spectra of all the amorphous samples is similar to that of the crystalline sample (BGC-Ba). Further evidence that the glassy sanbornite silicate structure resembles a sheet comes from the existence of Q2 and Q3 units, where Q2 units match the edges of the silicate layer created by joining Q3 units [124].

The BGC-Ba sample showed quartz peaks, which are indicative of the strong Si-O bond as defined by its ionic-atomic composition. Interestingly, this connection has a broad range of angles, from 132° to 180°, which adds to the silicate framework's natural flexibility. This flexibility is a key component of SiO_2's special glass-forming qualities and accounts for the very low crystallization propensity of silica

glass. On the other hand, because of the flexibility of the chemical bonds, SiO_2 may take on a variety of polymorphic forms. These forms include the three low-pressure forms of quartz, tridymite, and cristobalite, which have different structures at high and low temperatures. Admixture atoms become more mobile at high temperatures, which makes it easier for them to be removed and rearranged inside the quartz structure. Additionally, when temperature and mobility rise, the glass network structure with a high SiO_2 content may show a tendency to crystallize into quartz as a saturated solid solution [124], [125].

7.2 Enamel Coating Analysis

7.2.1 Hot Water Corrosion Test

The evaluation of glass or glass-ceramic coatings' susceptibility to corrosion entails calculating weight variations that are seen both before and after exposure to hot water. According to DIN 4753-3 standard rules, the corrosion testing on the coatings, as shown in Figure 7.4, offers a thorough overview of weight loss values after 21 and 42 days of hot water exposure at 95 °C. These weight loss data provide important information about the degree of corrosion that the coatings underwent throughout the designated time periods.

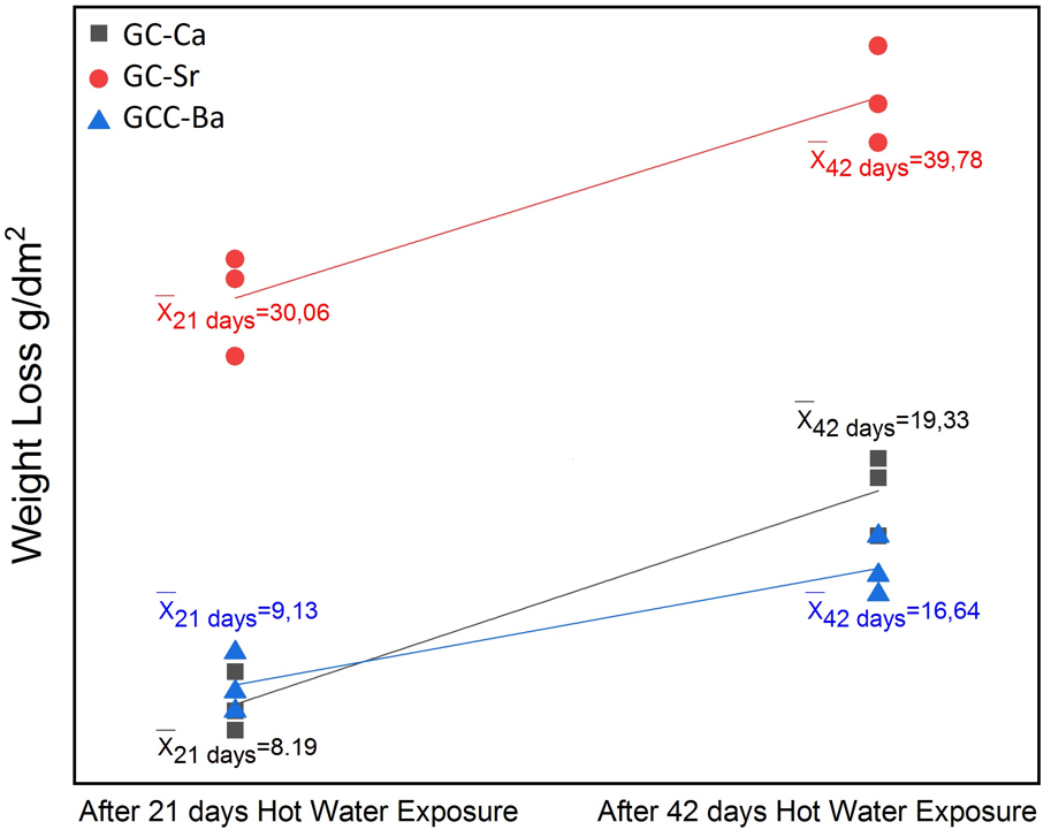


Figure 7.4 According to DIN 4753-3 corrosion testing the glass/glass-ceramic coatings were exposed to hot water (95 °C) after 21 days and after 42 days weight loss values

Important findings surfaced after a careful assessment of the weight loss across various coatings. After 21 days in hot water, the GC-Ca coating-enriched with calcium (Ca) in its glass composition-showed the best result, losing the least amount of weight (8.19 g/dm^2). The addition of calcium could have made it easier for silica condensation to produce a thick gel layer on the glass surface. By acting as a barrier, this gel layer prevented ions from passing through the glass and into the water [126].

Comparable weight loss results of 9.13 g/dm^2 were also shown by the GCC-Ba coating, which nearly matched the GC-Ca coating's effectiveness. The XRD examination (Figure 7.4) revealed the existence of $BaSi_2O_5$ ceramic crystals within the glass matrix, which resulted in an increased corrosion resistance for alkaline or earth-alkaline borosilicate glass-ceramic coatings. The mechanisms of change in ceramic crystalline materials in aqueous solutions, such as ion exchange, hydrolysis, and diffusion, reinforced the coating's overall resistance to corrosion

against the corrosive impacts of hot aquatic environments by mirroring the processes of glass alteration.

In contrast, the GC-Sr samples showed worse findings for corrosion resistance, which were especially noticeable in the weight loss measures during a 21-day period. This lower resistance could be explained by the fact that Sr has a bigger ion radius (1.12 Å) than Ca does (0.99 Å). Because Sr has a higher ion radius than other elements, it is less likely to form chains inside silicate structures, which reduces corrosion resistance in aqueous solutions, especially when weak silicate structures are present [111].

When the GCC-Ba coating was exposed to water for 42 days, it showed that it was still performing better than the other coating samples, with the lowest weight loss value of 16.64 g/dm^2. However, after 42 days of testing, the weight loss value of 39.79 g/dm^2 showed that the GC-Sr coating was the least resistant to hot water. These results confirmed the patterns seen in the first 21 days of exposure.

A comprehensive analysis of Figure 7.4 highlights that, in contrast to the presence of Sr, the presence of Ca in the glass structure contributes to improved corrosion resistance. The weight loss findings obtained following the hot water exposure durations of 21 and 42 days demonstrate this, with the GC-Ca coating consistently exhibiting lower weight loss values in comparison to the GC-Sr coating. With its glass-ceramic properties, such as a crystalline structure imbedded in the glass matrix, the GCC-Ba coating stood out as having the lowest weight loss value. The observable variations in corrosion resistance between the coatings can be ascribed to the unique impact of the corresponding earth-alkaline components on the crystalline structure and glass structure.

7.2.2 Element Migration Analysis

When glass or glass-ceramic coatings come into contact with hot water, a process known as corrosion occurs. As a result, elements are released from the coating surface and diffuse into the surrounding aqueous solution medium. The diagrams shown in Figures 7.5 and 7.6 provide a clear explanation of this complex releasing process. The dynamics of several elements, including Silicon (Si), Boron (B), Sodium (Na), Cobalt (Co), Calcium (Ca), Strontium (Sr), Barium (Ba), and Iron (Fe), that emanate from the coating itself as well as from the metal substrate and

seep into the surrounding aqueous solution are meticulously detailed in these figures. After a thorough analysis of the first and second 21-day corrosion tests on GC-Ca, it was determined that Silicon (Si) was the element that leaked the most, with amounts of 202740 ppb and 287280 ppb, respectively. Cobalt (Co) on the other hand showed the least amount of material release, with quantifications of 17.8 ppb and 4 ppb across the respective testing durations. A careful examination of the graphical depictions shown in Figures 7.5 and 7.6 identifies a consistent sequence of elements released, ranked from highest to lowest concentrations, as Si > B > Na > Ca > Fe > Co, following the first and second 21-day corrosion assessments. In the case of GC-Ca, the release of Si, which was determined to be the glass-forming element, increased by around 41% between the first 21 days and the second 21 days, as Figure 6 makes evident. At the same time, B's release increased by 68%, while Na showed a significant increase of 82% between the first 21 days and the second 21 days. SiO_2 and B_2O_3 have the largest molar values of all the components, indicating that they are the most prevalent network formers and that they have a major role in the overall amorphous network structure. When it comes to aqueous corrosion, the hydrolysis of oxides that form networks is a crucial step that leads to the most notable elements, Si and B, being released. The ion exchange process, which plays a crucial role in the early phases of corrosion when the coated surface contacts with water at 95 °C, is responsible for the significant increase, specifically 82%, in Na release into the aqueous solution. One hypothesis is that if reactions are allowed to run longer, the ion-exchange process becomes more and more prominent and eventually eclipses glass hydrolysis reactions. The network modifier element of GC-Ca, or calcium (Ca), as shown in Figure 7.6, significantly increased by 218% when exposed to hot water, going from 1,064 ppb in the first 21 days to 3,392 ppb in the second 21 days. Even with the very little amount of Ca discharged into the water, the rate of corrosion showed an increasing trend over time. Ca's ion radius is 0.99 Å, which means that it has a stronger tendency to form a chain with a silicate structure. This increases corrosion resistance relative to aqueous solutions, provided that chained silicate structures are present. However, because of their small ion radius, the length of exposure determines whether Ca migration from the coating's broken silicate chain is facilitated by hydrolysis. Following a detailed examination of the first and second 21-day corrosion tests on GC-Sr, Silicon (Si) was clearly the element most noticeably liberated, with concentrations of 232,268

ppb and 285252 ppb throughout the corresponding testing intervals. Conversely, Cobalt (Co) showed the least amount of material release, with just 2.9 ppb and 1.4 ppb recorded in the respective studies. After Cobalt (Co), Iron (Fe) was the next least amount of material released from the metal substrate; the release amounts were 3.8 ppb and 32.8 ppb for the defined testing times. A thorough analysis of the graphical representations contained in Figures 7.5 and 7.6 reveals that the elemental release sequence followed the hierarchical order of Si > B > Na > Ca > Fe > Co. This was consistently observed following the first and second 21-day corrosion evaluations. As shown in Figure 7.5, there was an approximate 22.8% increase in Si release for GC-Sr, an elemental cornerstone of glass composition, during the first and second sets of 21 days. During this designated period, there was a noticeable decrease in B release of 32.47% and a substantial fall in Na release of 49.9%. The components with the highest molar amounts were silicon dioxide (SiO_2) and boron trioxide (B_2O_3), which highlighted their critical function as network formers in the non-uniform network structure. Water-induced corrosion began to hydrolyze the oxides that constitute the network, which in turn caused Si and B to precipitate out as the main constituents. The ion exchange mechanism was crucial in the early phases of corrosion when the coated surface came into contact with water at 95 °C. This led to a more noticeable percentage drop in Na release into the aqueous medium-49.9%, to be exact. Ion exchange processes became more prominent as the reaction's duration lengthened, often replacing glass hydrolysis events in terms of frequency and significance. The complex behavior of strontium (Sr), the network-modifying element included in GC-Sr, was seen to decrease by 52.55% when it was exposed to hot water between the first 21 days (28975 ppb) and the second 21 days (13747 ppb), as Figure 7.6 explains in detail. Over a prolonged period of time, there was a commensurate fall in the corrosion rate for GC-Sr in tandem with this notable reduction in Sr release into the water. The primary cause of the decrease in the rate of corrosion may be ascribed to the development of a surface modification layer that essentially stops weight loss. Sr's higher ionic radius (1.12 Å) is essential in lowering the possibility of chain formation with a silicate structure and, as a result, corrosion resistance as compared to aqueous environments, especially when chained silicate structures are present. Due to the weak bonds that cause Sr and silicate to form chains, there is an increased likelihood that Sr will migrate by hydrolysis from broken silicate chains inside the coating as the exposure duration

lengthens. Silicon (Si) was the most common element released in the first and second 21-day corrosion evaluations on GCC-Ba. During the corresponding experimental intervals, Si concentrations were recorded at 127758 ppb and 182030 ppb, respectively. Conversely, in the equivalent experimental settings, the minimal material release values for Cobalt (Co) and Iron (Fe) were 3.6 ppb and 0.3 ppb, respectively, and 7.8 ppb and 12.2 ppb, respectively. After the first 21-day corrosion interval and the second, as carefully shown in Figures 7.5 and 7.6, the elemental release sequence continued in a uniform and oriented fashion as Si > B > Na > Ca > Co > Fe. The detailed information from Figure 7.5 revealed that during the next two 21-day periods in GCC-Ba, there was a significant rise of approximately 42.48% in the release of Si, a crucial glass component. Concurrently, there was a noticeable decrease of 24.25% in the release of B, and a remarkable decrease of 17.08% in the release of Na within the same time period. The complex interaction between elemental release dynamics and corrosion behavior of GCC-Ba illuminates the subtle variations in Si, B, and Na concentrations during long exposure times. The components' elevated molar concentrations of either silicon dioxide (SiO_2) or boron trioxide (B_2O_3) highlighted their critical function as network formers in the complex amorphous network structure. The hydrolysis of these network-forming oxides worked as a catalyst during the corrosion process in the presence of water, causing the main components, silicon (Si) and boron (B), to be released. Especially, the significant decrease of 17.08% in the release of Sodium (Na) into the aqueous medium became significant. This may be attributed to the ion exchange mechanism, which is an important factor in the early stages of corrosion when the coated surface comes into contact with water at 95 °C. Glass hydrolysis reactions were increasingly replaced by ion exchange processes as the reaction's time dimension increased. One striking finding in Figure 7.6 showed that after being exposed to water at a higher temperature, Barium (Ba) release—the GCC-Ba component that was crucial in altering the network—decreased by 79.01%, from 819 ppb to 221 ppb in the first 21 days. Interestingly, throughout this extended period, there was a noticeable drop in the corrosion rate for GCC-Ba, which was ascribed to the dynamic change in Ba release into the water. The possible emergence of a temporary, unstable modification layer on the surface was connected to the observed increase in the rate of corrosion. Because of their dual composition, which consists of an amorphous phase and a crystalline phase coexisting, glass-ceramics

are complicated materials that require careful consideration when examining their corrosion properties. This study explores the interactions between the different grains placed in a certain pattern inside the crystalline phase and the glass phase's homogeneity. The evaluation goes beyond individual grains to include their margins, or grain borders, and finds that the latter have a higher level of responsiveness, as has been noted in the literature [127]. On the other hand, Barium (Ba) has a significant ionic radius of 1.34 Å, which makes it difficult for bigger ions to migrate relative to smaller ones. As a result, the $BaSi_2O_5$ crystal phase's presence in aqueous settings reduces the corrosion resistance of GCC-Ba. Nevertheless, this disadvantage is offset by the barrier that prevents big ions from migrating from the coating into the aqueous solution, hence offsetting the reduced water resistance linked to crystal grain boundaries.

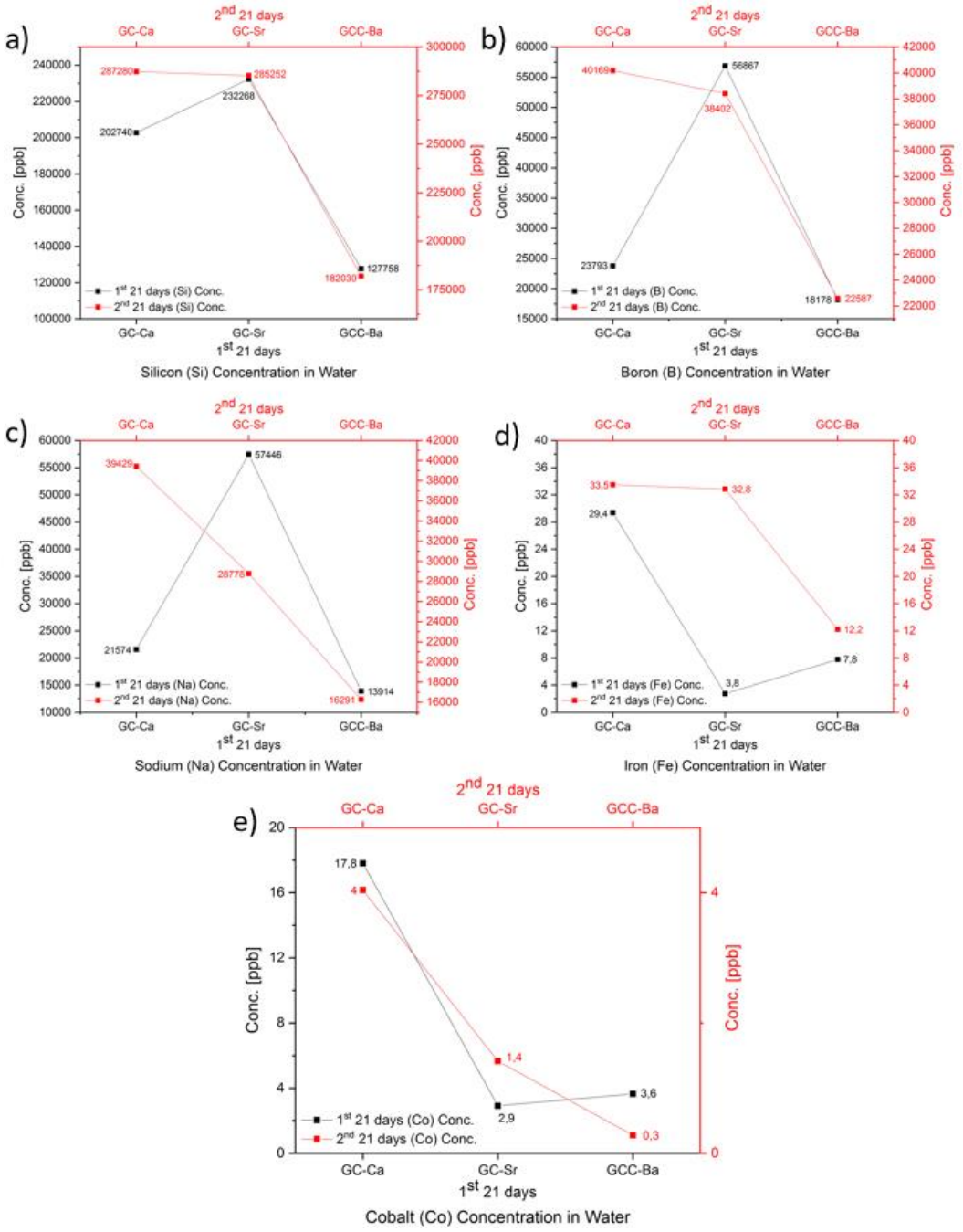


Figure 7.5 ICP-MS analysis results (Figure out of black lines for the first 21 days, red lines for the second 21 days) for determining elements released from coating to water a) Silicon, b) Boron, c) Sodium, d) Cobalt, and e) Iron. The determined Iron element could be released from the steel substrate into water.

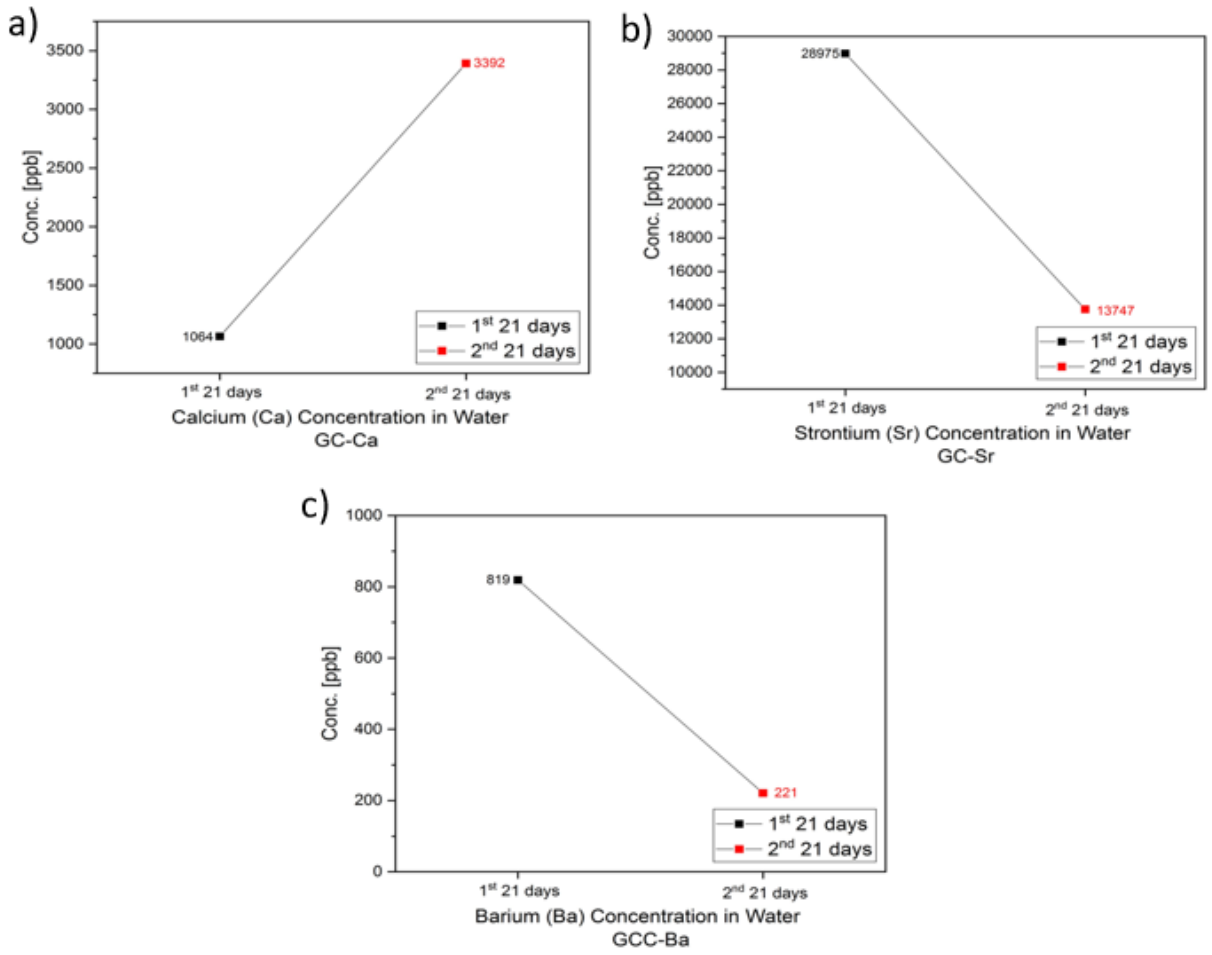


Figure 7.6 ICP-MS analysis results (Figure out of black dot for the first 21 days, red dot for the second 21 days) for determining each coating formula which is specific to samples, elements released from coating to water for GC-Ca a) Calcium, for GC-Sr b) Strontium, and c) Barium for GCC-Ba.

Silicon (Si) was the most often released element across all coatings in the first and second 21-day corrosion tests of the coating samples, with cobalt (Co) showing the least consistent release. The graphical depictions presented in Figures 7.5 and Figure 7.6 make it evident that silicon was the most often released element in all coatings throughout the first and second 21-day corrosion tests, whereas cobalt had the lowest release levels in all cases. The significant molar ratio of silicon in the formulation is responsible for its enhanced release. The formation of the amorphous network structure is largely dependent on silicon dioxide (SiO_2) since the glass system takes on an alkali-borosilicate composition. Cobalt, on the other hand, plays a less significant part in the formulation due to its relatively smaller molar concentration. Its purposeful addition to the mixture is to serve as a bonding agent, encouraging the metal substrate and other ingredients to create a dendritic structure.

A pattern becomes apparent when examining the migratory patterns of all the elements: Si > Na > B > Sr > Ca > Ba > Fe > Co.

The order in which these components are released throughout the corrosion testing phase is shown by this sequence. The prominent position of silicon emphasizes its fundamental function within the glass matrix, and the elemental order reveals the subtle differences between each component's influences on the coatings' corrosion behavior.

The release of silicon (Si) and boron (B) elements oscillates significantly in the GC-Sr example, with values of 517520 and 95269 (ppb) respectively. This increased Si and B element release is consistent with the significant weight loss of 39.78 (g/dm^2) in GC-Sr. Since silicon and boron are essential elements for glass-forming, their significant release has a greater impact on corrosion behavior than other elements. After the significant release of glass-formers, flux oxide, or sodium (Na), exhibits the third-highest release in all samples. GC-Sr shows the largest release for the Na flux element relative to other elements, just like silicon and boron do. In the corrosive media, alkali ions, such Na in the glass, exchange with H^+ and H_3O^+ ions. Of particular note is the fact that sodium migrates from the coating to the aqueous solution more quickly than other elements because to its tiny atomic radius (0.97 Å) in formulae. When comparing other coating samples, cobalt (Co) shows the largest release in contrast to other elements released in GC-Ca (21.8 ppb). Corrosion is closely related to the release of iron (Fe). The observed release of iron occurs when the aqueous solution comes into direct contact with the metallic substrate when the glass or glass-ceramic components are removed from the coating. These complex elemental release patterns provide insight into the complex interactions between the dynamics of corrosion, the composition of the glass, and the elemental migration from the coating into the aqueous solution. After assessing the total element release in water samples from the coatings, GC-Sr (741775.9 ppb) > GC-Ca (619525.7 ppb) > GCC-Ba (381821.9 ppb) shows a clear mass loss hierarchy. The reduction in the quantity of Si-O and B-O covalent connections explains GC-Sr's worse resistance to corrosion in hot aqueous solutions. Concomitantly, the presence of SrO weakens the glass network by increasing the amount of nondirectional ionic connections between cations and borate or silicate anions, leading to a greater weight loss in comparison to other coatings [128], [129].

This little effect is different from how SrO and CaO affect corrosion in hot aqueous solution in sodium-borosilicate glass matrix [130]. On the other hand, at higher temperatures, the energetically constrained diffusion of the big Ba^{2+} ion (1.34 Å) is responsible for the better stability of the coating containing BaO. This limited diffusion enhances extraction and creates a channel for leaching, especially when combined with the comparatively simpler passage of the smaller earth-alkaline oxide ion through the leached layer [131]. Furthermore, the stability of the coating is further improved by the presence of a crystalline phase in the glass matrix that XRD analysis revealed as sanbornite. This phase adds to higher corrosion resistance.

7.2.3 Macro and 3D Surface Topography Image Analysis

Macroscopic pictures of coating samples for GC-Ca, GC-Sr, and GCC-Ba are shown in Figure 7.7 before and after corrosion. These photos demonstrate changes in surface conditions brought on by exposure to hot water. The comparison of pre- and post-corrosion photographs in Figure 7.7 facilitates better understanding of the weight loss data in Figure 7.4 by directly assessing the increase in weight loss associated with surface flaws. Remarkably, the macro photos indicate that, following corrosion, GC-Sr suffered the most surface damage, whereas GCC-Ba showed the least. Figure 7.8's 3D surface topography give more information on the surface properties. The observations are supported by these visualizations, particularly when GC-Sr is examined on the 3D topography data, which show a significant increase in surface flaws following hot water exposure in comparison to other samples.

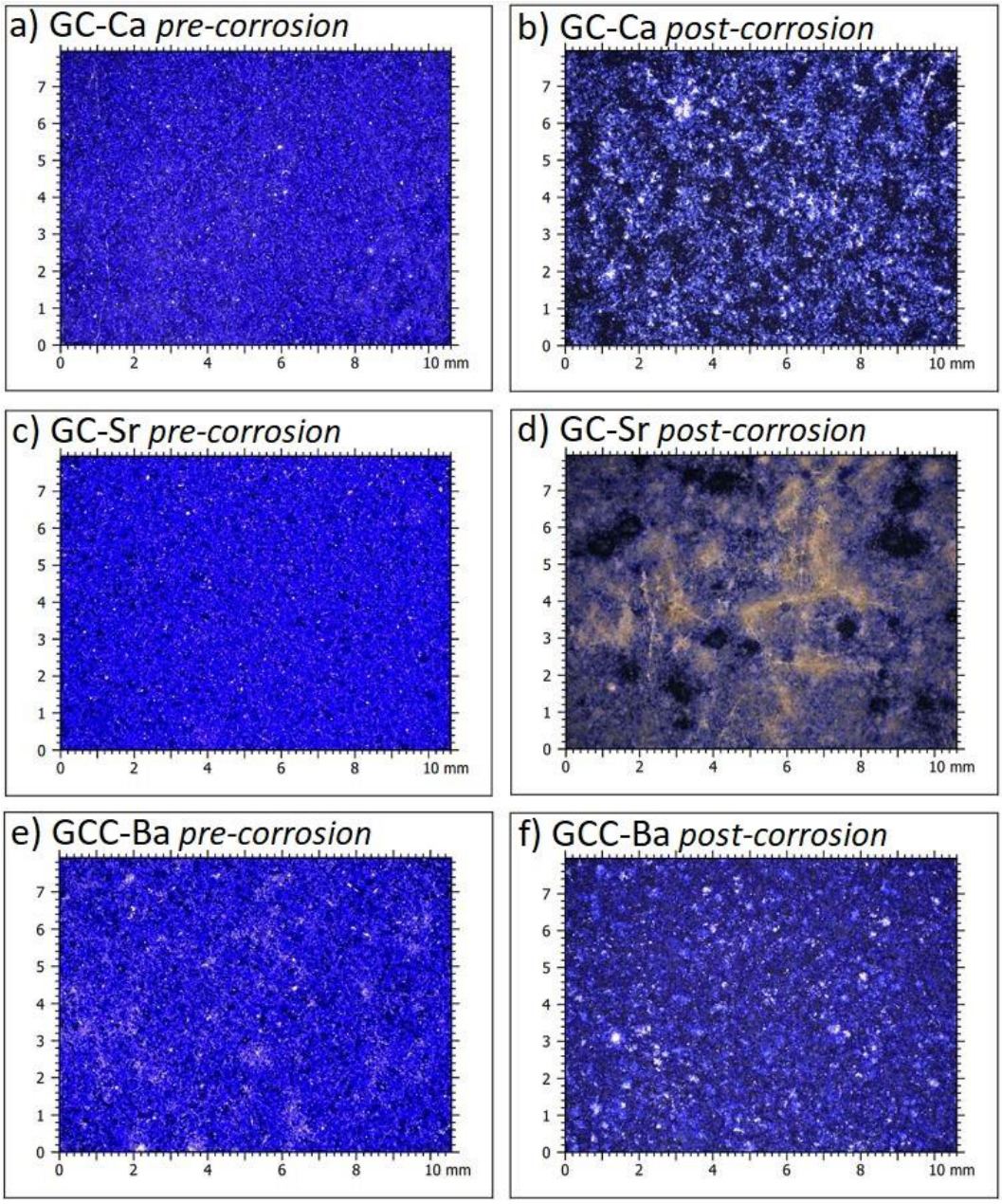


Figure 7.7 Macro images of coatings pre- and post-hot aqueous corrosion

In surface-focused scientific investigations, where wear-induced, chemical, and mechanical deteriorations are critical factors, roughness evaluation is critical. A smart zoom profilometer stands out as one of the most important assessment tools for the thorough examination of topography and surface quality. With the use of both transmitted and reflected light, the surface is carefully analyzed by means of algorithms that have been designed. For surface evaluation in this study, the specialist Mountains 3-D application was used. Non-contact profilometers were used to do three-dimensional scanning of glass-ceramic coated surfaces. A roughness meter was used to extract important characteristics and create three-

dimensional surface topography maps, such as the arithmetic mean roughness (Ra) and the distance between the maximum peak heights (Rz). The 3-D surface topography maps of coatings subjected to hot water for 42 days, as per DIN 4753-3 standard, and coatings that did not receive any corrosive treatment are shown in Figure 7.8 and Table 7.1 displays the outcomes of the roughness parameters, including Ra, that were determined using profile lines in compliance with ISO 4287.

In particular, the 3D topography for the three coating samples are shown in Figure 7.8. The blue, green, and yellow chromatic changes that are visible on the scale characterize the surface morphology of pre-corrosion specimens that were not subjected to any further processes or hot water treatment. When it comes to GC-Ca, a lot of yellow-colored peaks are seen along with occasional localized red-colored roughness. Although GC-Ca surfaces often lack prominent voids and depressions, GC-Sr and GCC-Ba show reddish peaks and sporadic, locally elevated white-colored roughness. After being in hot water, GC-Ca exhibits a restricted appearance of white peaks and an increase in the frequency of red peaks. Examining the 3D morphology of GC-Sr after the hot water corrosion evaluation, we find that the quantity of high-altitude white-colored peaks increases for GC-Ca and reduces for GCC-Ba coating. The red-colored peaks of GCC-Ba show the least amount of divergence from pre-corrosion values during post-corrosion. Interestingly, a left-side scale analysis for each coating shows a decrease in scale bar width following immersion in hot water, suggesting that 3D surface topography measurements might not be very sensitive in these specific circumstances.

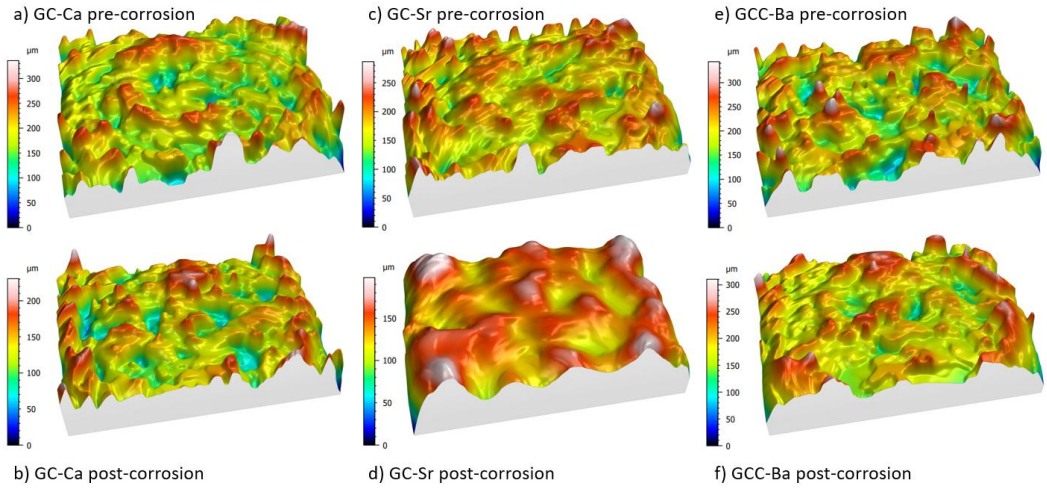


Figure 7.8 3D surface topography and 2D surface plot for three different glass/glass-ceramic coatings; a) GC-Ca pre-corrosion, b) GC-Ca post-corrosion, c) GC-Sr pre-corrosion d) GC-Sr post corrosion e) GC-Ba pre-corrosion f) GCC-Ba post-corrosion.

Table 7.6 Roughness values of three different glass/glass-ceramic coatings pre- and post-corrosion.

	Pre-Corrosion		**Post-Corrosion**			
	R_a	**R_z**	**R_a**	**R_z**	**$\%\Delta R_a$**	**$\%\Delta R_z$**
GC-Ca	0.90	3.88	1.44	6.29	60	62
GC-Sr	0.75	3.44	1.33	7.81	77	127
GCC-Ba	1.13	6.10	1.27	7.66	12	25

Roughness values were carefully evaluated using a roughness meter in order to precisely ascertain the changes in roughness caused by hot water corrosion in the coatings. According to Table 7.1, the pre-corrosion roughness values for GC-Ca were Rz: 3.88 and Ra: 0.90. Following the corrosion test, these values rose to Ra: 1.44 and Rz: 6.29, suggesting an increase in roughness and supporting the effect of hot water exposure on corrosion on the coated surface. The results of calculating the %R-value for GC-Ca coating were 62% for %Rz and 60% for %Ra. Similarly, Ra: 0.75 and Rz: 3.44 were the pre-corrosion roughness values for GC-Sr. These readings increased to Ra: 1.33 and Rz: 7.81 after corrosion, indicating an increase

in roughness. For GC-Sr, the percentage R-values were 77% for Ra and 127% for Rz. Notably, the starting values for Ra and Rz were 1.13 and 6.10 for roughness values for GCC-Ba, which showed greater resilience to hot water than other coatings. Roughness values increased to Ra: 1.27 and Rz: 7.66 after 42 days in hot water, yielding %ΔR-values of %ΔRa: 12% and %ΔRz: 25%. The following is a comparison of roughness %ΔRa change values for coatings that are ranked similarly to mass loss and element release: GCC-Ba (%ΔRa: 12%) > GC-Sr (%ΔRa: 77%) > GC-Ca (%ΔRa: 60%). With GC-Sr (%ΔRz: 127%) > GC-Ca (%ΔRz: 62%) > GCC-Ba (%ΔRz: 25%), the %ΔRz numbers reflect this pattern.

7.2.4 Gloss Measurement Analysis

The coating gloss values and delta gloss variations for the examined coating samples are shown in Figure 7.9, together with the pre- and post-corrosion testing. The diffused light alteration on the surface caused by hot water corrosion in glass or glass-ceramic coatings is shown by a change in gloss in this investigation. Hot water in contact with the coated surface causes changes due to processes such as diffusion of glass-former components and ion exchange of alkaline or earth-alkaline elements. As a result, these modifications cause solid particles to be transferred from the surface to the solution, which affects the coating's capacity to reflect light. Prior to the corrosion tests, the coatings' gloss measurements showed that GC-Ca had the highest gloss value, at 83, followed by GC-Sr, at 81, and GCC-Ba, at 66. The gloss values for the studied samples dropped to 22 for GC-Ca, 17 for GC-Sr, and 10 for GCC-Ba after 42 days of exposure to hot water. The calculated gloss change from pre- to post-corrosion for GC-Ca was 60, for GC-Sr, 64, and for GCC-Ba, it was 56. Following 42 days in hot water, the delta gloss change (ΔG) is ranked as follows: GC-Sr (ΔG=64) > GC-Ca (ΔG=60) > GCC-Ba (ΔG=56). According to this ranking, GC-Sr saw the greatest delta gloss change, indicating a more substantial modification in gloss values in contrast to the other samples. One important thing to keep in mind is that gloss and roughness have an inverse connection. The corrosion-related gloss values tend to decrease with increasing roughness [132-134]. The reason for this association is because parallel light rays are reflected in the same direction on a smooth, mirror-like surface. Across the other hand, light beams are diffusely distributed across an uneven surface, giving the impression of enhanced opacity [135]. Together with implications for surface

smoothness and light reflection characteristics, the assessment of gloss values and delta gloss variations, in summary, offers important insights into how hot water corrosion impacts the optical properties of GC-Ca, GC-Sr, and GCC-Ba coatings.

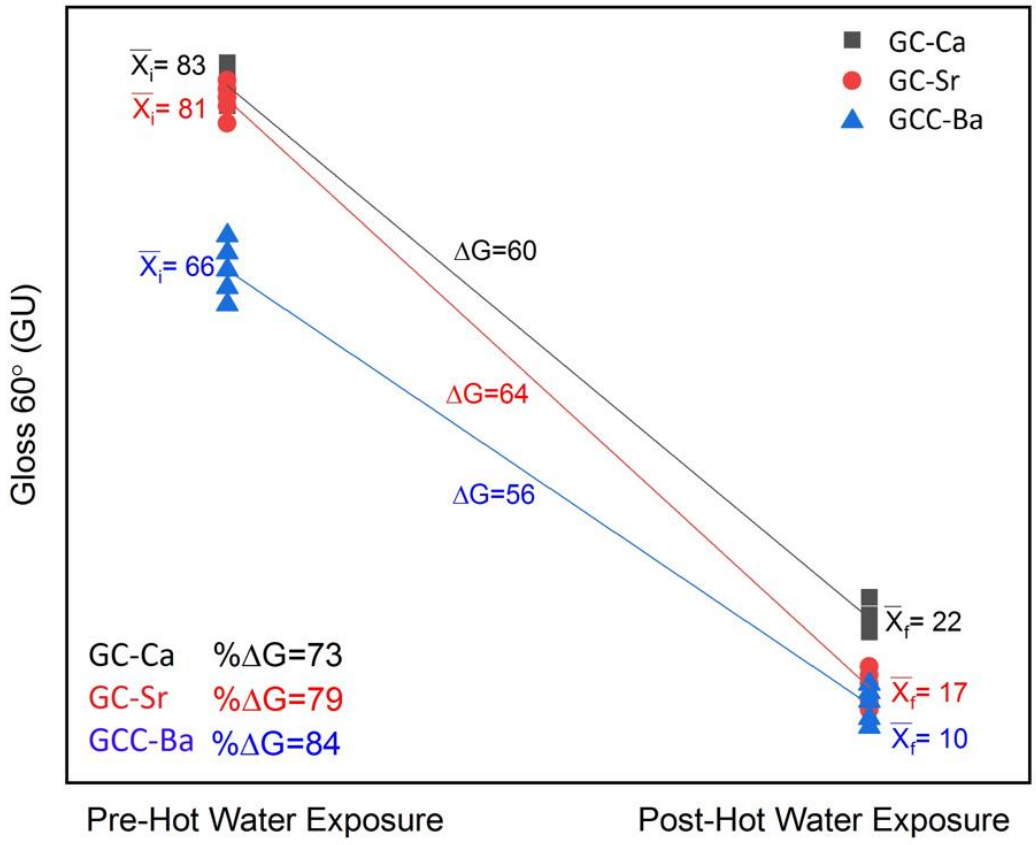


Figure 7.9 The studied GC-Ca, GC-Sr, and GCC-Ba coatings' average values before corrosion and after corrosion in terms of gloss change.

7.2.5 SEM Analysis

The investigation of sample morphology using Scanning Electron Microscopy (SEM) was done with the goal of better understanding corrosion damage on coatings. This method made it easier to observe the coating's cross-section as well as its surface. Figure 7.10 shows the coating's surface morphology both before and after it was exposed to hot water. The findings demonstrate that, for top imaging, very few surface defects are apparent on samples following corrosion for all samples, with the exception of GCC-Ba, which exhibits a surface dimple. This indicates that, except from the previously stated indentation in the GCC-Ba sample upon corrosion, the coatings generally retained their surface integrity well with just minor flaws. Conversely, a closer look at the coating's cross-section reveals corrosion, which seriously damages every sample under investigation. The

influence of hot water corrosion on the internal structure of the coatings is seen in the cross-section SEM pictures, which offer a thorough perspective of the degree of corrosion-induced damage below the surface. In conclusion, SEM research provides important insights into the morphological changes that the coatings undergo after being exposed to hot water, both on the surface and within the cross-section. Understanding the kind and extent of corrosion damage through microscopic analysis is essential for completing a thorough evaluation of the coatings' performance in corrosive environments.

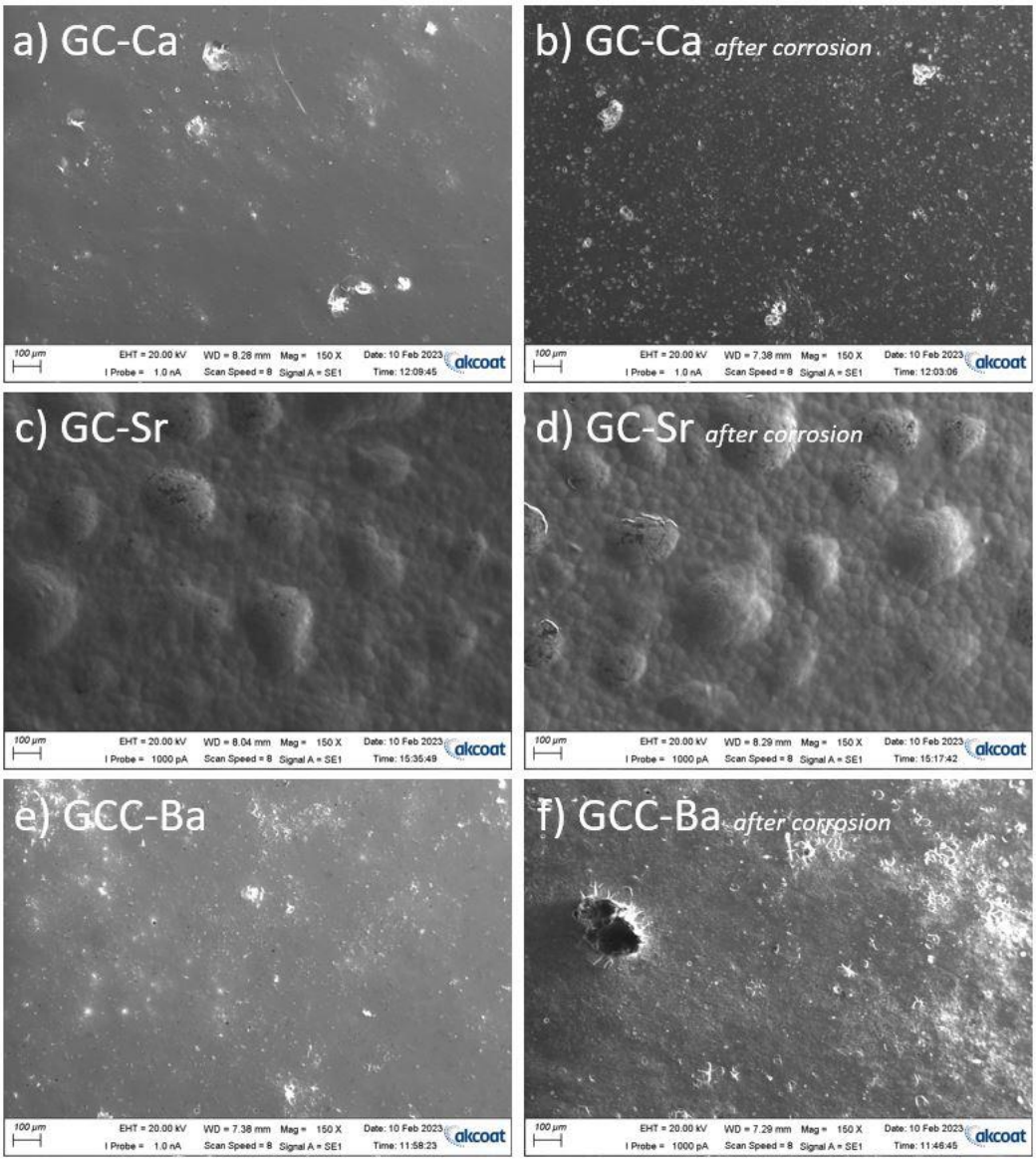


Figure 7.10 SEM analysis surface images with 150x magnification in SEI mode of a) GC-Ca pre-corrosion, b) GC-Ca post-corrosion, c) GC-Sr pre-corrosion, d) GC-Sr post-corrosion e) GC-Ba pre-corrosion f) GCC-Ba post-corrosion

SEM analysis was used to examine the cross-section of the corroded coating surface, and the results were rather insightful into the surface flaws brought on by exposure to hot water. The SEM cross-section pictures shown in Figure 7.11 clearly illustrate the coatings' pre- and post-corrosion conditions. Interestingly, as explained in reference [135], the bubbles in the coatings are caused by gas released from metal structures during the fire process, which further complicates the composition of the coating. Porosity is an intrinsic property of all coatings within their structural frameworks, and there are noticeable differences between them. More specifically, GC-Sr and GCC-Ba show more porosity than GC-Ca does. The coatings exhibit a range of reactions to the corrosive effect of hot water, which can be attributed to this subtle difference in porosity levels. Examining the complex interaction between rising surface flaws, weight reduction, and element releases brought on by hot water reveals an interesting discovery. The surface defect study presents a strong correlation, highlighting the direct proportionality between elevated surface flaws, increased element releases, and amplified weight loss. After 42 days of severe corrosion testing, the prominent surface faults in GC-Ca become more noticeable, offering a clear example of the transformational impacts of exposure to hot water. When it comes to resistance, GC-Ca performs better than GC-Sr, but neither coating can match the effectiveness of GCC-Ba. The element release statistics and weight loss results further support this performance disparity. GC-Ca shows a weight loss of 19.33 g/dm2 and a total element release amount of 619,525 ppb following exposure to hot water. GCC-Ba, on the other hand, exhibits a total element release of 381822 ppb, while GC-Sr records a weight reduction of 39.79 g/dm^2 along with a total element release of 741774 ppb. For both GC-Ca and GC-Sr, the penetrative effect of hot water on the coating structure is transformational, resulting in significant damage to the coating's interior and outside. Delicate roughness change and profilometer investigations help to further clarify this chemical attack on the integrity of the coating. The roughness change for GC-Ca is increased by 60%, whilst the Ra value for GC-Sr is increased by 77%, indicating a significant effect of hot water exposure on surface characteristics. GCC-Ba, on the other hand, stands out as a shining example of resistance to corrosion brought on by hot water. The coating performs well, showing a little 12% inhancing in roughness before and after corrosion. This confirms that GCC-Ba is more resistant than other samples that are being studied, which leads to fewer flaws

being found. The knowledge of protective coating materials in practical applications is greatly enhanced by the detailed investigation of these coatings and their varied reactions to hot water-induced corrosion.

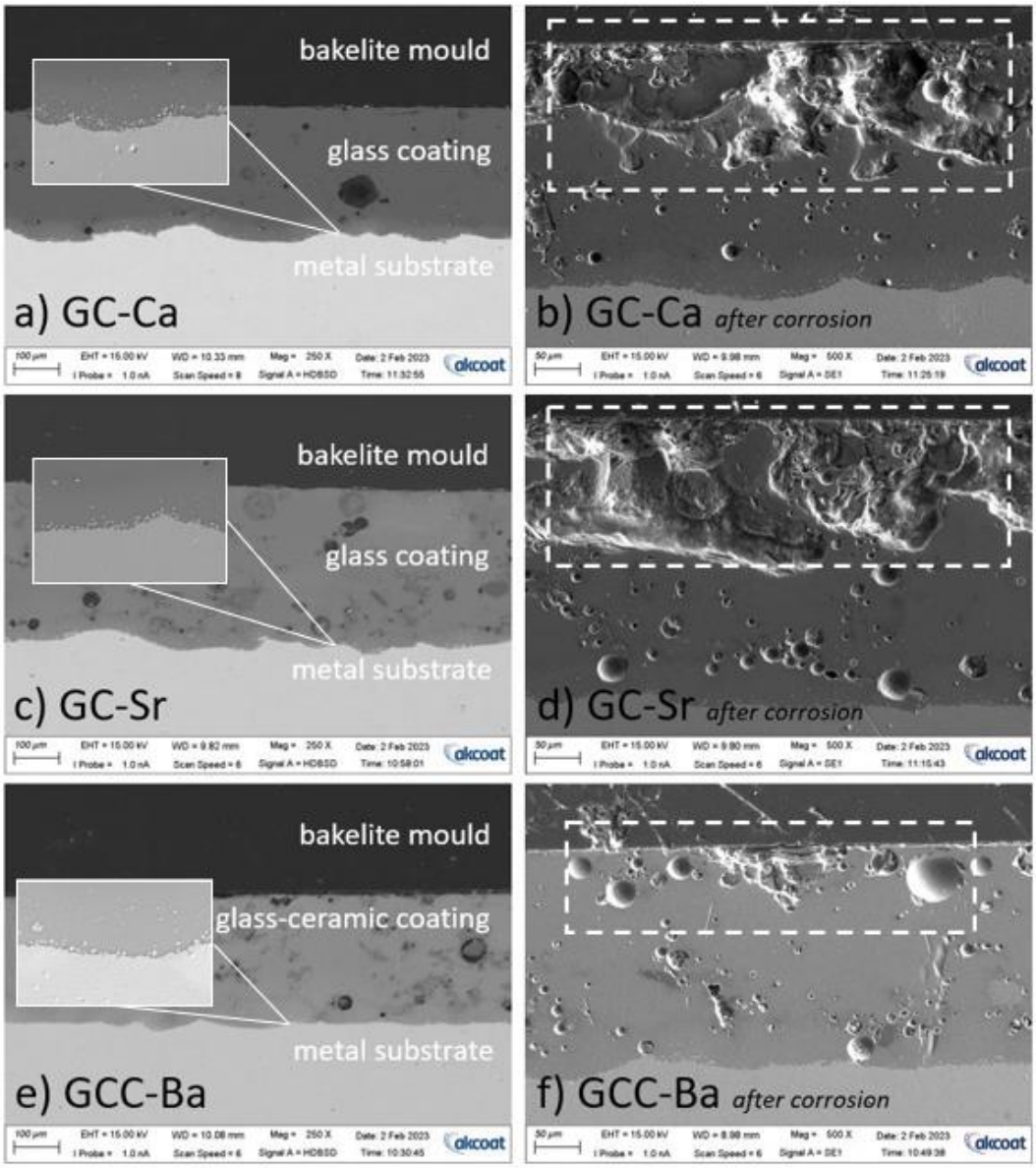


Figure 7.91 SEM analysis cross-section images with 250x magnification in HD BSD mode for pre-corrosion and 500x magnification in SEI mode of a) GC-Ca pre-corrosion, b) GC-Ca post-corrosion, c) GC-Sr pre-corrosion, d) GC-Sr post-corrosion e) GC-Ba pre-corrosion f) GCC-Ba post-corrosion.

8

CONCLUSION

In the investigation involving three earth alkaline oxides, namely CaO, SrO, and BaO, selected as candidates for preliminary studies to comprehend and explore their impact on the glass matrix, the corrosion mechanism of enamels was thoroughly examined. The thermal behavior of these structures plays a pivotal role in regulating the erosion and corrosion mechanisms. Factors such as element diffusion during firing, reaction efficiency, and crystal presence in the matrix significantly influence the corrosion rate.

Upon subjecting the enamel surface to hot water etching, H^+/H_3O^+ ions initiate an attack on the Si matrix, forming a gel-like Si-OH structure on the surface. This structure reduces the diffusion (corrosion) rate on the surface. However, during boiling, the Liquid Droplet and Particulate Erosion mechanisms remove all gel-like structures slowing down the corrosion rate, rendering the corrosion progression unstoppable.

In the hot water attack, following the ion exchange rule, H^+/H_3O^+ ions settle in the structure, while alkali metal ions concentrate and move away from the structure. Regions with low Si density and high alkaline density dissolve away from the structure. Sanbornite ceramic particles exhibit resistance to corrosion in the structure. However, if alkali-intensive regions around the particle dissolve due to hot water attack, and bubbles reduce the bonding density at the crystal-enamel interface, corrosion of the crystals becomes inevitable.

Macro-scale interventions, such as the presence of different earth alkaline oxides in the matrix, result in distinct weight loss values directly proportional to element migration values from the enamel coating to the aqueous solution. CaO presence in sodium borosilicate glass systems provides greater resistance to hot water corrosion than SrO. This is attributed to the fact that the presence of SrO weakens the glass network by increasing the amount of nondirectional ionic connections between cations and borate or silicate anions, leading to a greater weight loss compared to other coatings.

BaO induces the crystallization of sodium borosilicate glass. The existence of a crystal phase throughout the glass matrix enhances corrosion resistance, resulting in the coating having the lowest weight and element release values compared to other coatings. Changes in gloss, surface topography, macro and micro surface images, and the amount of elements released from the coatings complemented each other as reasons for the weight loss of the coating during exposure to hot water in the hot water corrosion test (DIN 4753-3) results. Thus, each earth alkaline oxide's effects on the sodium borosilicate glass system were comprehensively explained through various analyses in this study.

To sum up, this study sought to determine how the 2A alkaline-earth oxides (CaO, SrO, and BaO) affected the changes that were seen in glass or glass-ceramic coatings when they were exposed to hot water. When these oxides were incorporated into sodium-borosilicate glass systems, different compositions were obtained. The results of the Raman and DTA spectroscopy were in line with the XRD study, which showed a significant increase in intensities at 540 and 1080 cm-1. These findings clearly suggest that at 774 °C, BaO catalyzed the nucleation of crystals, resulting in the formation of a crystalline phase rich in Ba-Si components, which was designated as Sanbornite. After the hot water exposure durations of 21 and 42 days, the weight loss data were collected. When compared to the other two glass coatings, the GCC-Ba (16.64 g/dm^2) has the lowest weight loss value. The GC-Ca (19.33 g/dm^2) coating was awarded a lower weight loss value than the GC-Sr (39.78 g/dm^2) coating. The results showed that the glass matrix's crystalline structure produced the lowest weight loss value. In the Raman analysis, the heat-treated BGC-Ba sample had a sharper band, which was linked to the glass-ceramic's sanbornite crystalline phase. Different corrosion resistances were found in water samples after element release studies were conducted. When SrO is present in the glass matrix, GC-Sr demonstrated a lesser resistance (a decrease in Si-O and B-O covalent bonds). This is because there are more nondirectional ionic interactions. The total element release values in water samples are listed below, in order of equivalent mass loss: GC-Ca (619525.7 ppb) > GC-Sr (741775.9 ppb) > GCC-Ba (381821.9 ppb)

Ba^{2+} ions have a higher ionic radius than Ca^{2+} and Sr^{2+} ions, which limits ion exchange and diffusion of alkali oxides at high temperatures. This limitation

reduces extraction and increases resilience to corrosion, stabilizing coatings that contain BaO. This increased stability might be attributed to the sanbornite crystal phase's facilitation of an improved resistance to hot water corrosion. This idea is corroborated by the studies that were performed, which included ICP-MS, weight loss, gloss modification, roughness variation, surface profilometry, and SEM analysis of glass coating samples that were compared, namely GC-Ca, GC-Sr, and glass-ceramic coating GCC-Ba. Analysis of the gloss, roughness, and surface topography of the coatings revealed significant differences between them. For the roughness change values (%ΔRa and %ΔRz), there is a similar process in mass loss and element release as follows: > GCC-Ba (%ΔRa:12, %ΔRz:25) > GC-Sr (%ΔRa:77, %ΔRz:127) > GC-Ca (%ΔRa:60, %ΔRz:62). The gloss change from pre-to-post coating was calculated using the following formulas: GC-Ca (Δ60), GC-Sr (Δ64), and GCC-Ba (Δ56). After post-corrosion investigation using a scanning electron microscope, the surfaces of GCC-Ba coatings showed less deterioration as a result of exposure to hot water. This indicates that these coatings are more resistant to hot water corrosion and had fewer faults than GC-Ca and GC-Sr coatings.

The combined results highlight how important 2A alkaline-earth oxides are for determining how glass and glass-ceramic coatings behave in terms of corrosion and structural stability when exposed to hot water.

REFERENCES

[1] Grambow, B. (2011). Corrosion of glass. Uhlig's corrosion handbook, 51, 399.

[2] Fernández–Navarro, J. M., & Villegas, M. Á. (2013). What is glass?: An introduction to the physics and chemistry of silicate glasses. Modern methods for analysing archaeological and historical glass, 1, 1-22.

[3] Rossi, S., & Scrinzi, E. (2013). Evaluation of the abrasion resistance of enamel coatings. Chemical Engineering and Processing: Process Intensification, 68, 74-80. https://doi.org/10.1016/j.cep.2012.10.009

[4] Rossi, S., Russo, F., & Calovi, M. (2021). Durability of vitreous enamel coatings and their resistance to abrasion, chemicals, and corrosion: a review. *Journal of Coatings Technology and Research*, *18*, 39-52. https://doi.org/10.1007/s11998-020-00415-3

[5] Kassem, A. S., Mostafa, M. Z., Abadir, M. F., & Sherbiny, S. E. (2010). Hot water acid-resistant enamels for sheet steel. Materials and corrosion, 61(1), 58-63. https://doi.org/10.1002/maco.200805230

[6] Clark, D. E., & Zoitos, B. K. (1992). Corrosion of glass, ceramics and ceramic superconductors: principles, testing, characterization and applications.

[7] Gin, S., Delaye, J. M., Angeli, F., & Schuller, S. (2021). Aqueous alteration of silicate glass: state of knowledge and perspectives. *npj Materials Degradation*, *5*(1), 1-20.

[8] Arena, H., Godon, N., Rébiscoul, D., Podor, R., Garcès, E., Cabie, M., & Mestre, J. P. (2016). Impact of Zn, Mg, Ni and Co elements on glass alteration: additive effects. Journal of Nuclear Materials, 470, 55-67.

[9] Lenting, C., Plümper, O., Kilburn, M., Guagliardo, P., Klinkenberg, M., & Geisler, T. (2018). Towards a unifying mechanistic model for silicate glass corrosion. npj Materials degradation, 2(1), 1-10.

[10] Galusková, D., Hnatko, M., Kraxner, J., Galusek, D., & Šajgalík, P. (2012). Influence of Calcium Addition on the Chemical Durability of the Model Alumino-Silicate Glass in Aqueous Solutions. In Key Engineering Materials (Vol. 512, pp. 1009-1014). Trans Tech Publications Ltd.

[11] Bergeron, B., Galoisy, L., Jollivet, P., Angeli, F., Charpentier, T., Calas, G., & Gin, S. (2010). First investigations of the influence of IVB elements (Ti, Zr, and Hf) on the chemical durability of soda-lime borosilicate glass. Journal of non-crystalline solids, 356(44-49), 2315-2322.

[12] Gin, S., Beaudoux, X., Angéli, F., Jégou, C., & Godon, N. (2012). Effect of composition on the short-term and long-term dissolution rates of ten borosilicate glass of increasing complexity from 3 to 30 oxides. Journal of Non-Crystalline Solids, 358(18-19), 2559-2570

[13] Shelby, J. E. (2020). *Introduction to glass science and technology*. Royal society of chemistry.

[14] Freiman, W. S. (1980). Elasticity and Strength in Glasses. Glass; Science and Technology, 5, 63-65.

[15] Varshneya, A. K. (2013). *Fundamentals of inorganic glasses*. Elsevier.

[16] S. D. Stookey, “History of the Development of Pyroceram,” Research Management, vol. 1, no. 3, pp. 155–163, Sep. 1958, doi: 10.1080/00345334.1958.11755484.

[17] F. A. Hummel, “Thermal Expansion Properties of Some Synthetic Lithia Minerals,” 1951.

[18] W. Holland and G. H. Beall, Glass-Ceramic Technology, 3rd Edition, vol. 3rd Edition. New Jersey: Wiley - American Ceramic Society, 2020.

[19] S. Rossi, F. Deflorian, L. Fontanari, A. Cambruzzi, and P. L. Bonora, “Electrochemical measurements to evaluate the damage due to abrasion on organic protective system,” in Progress in Organic Coatings, Apr. 2005, vol. 52, no. 4, pp. 288–297. doi: 10.1016/j.porgcoat.2004.09.005.

[20] V. Günay and Ş. Yılmaz, Glass Ceramics: Science and Technology (Cam Seramikler: Bilim ve Teknolojisi). Kocaeli: Tübitak Marmara Araştırma Merkezi, 2010.

[21] J. Deubener, M. Allix, M. J. Davis, A. Duran, T. Höche, T. Honma, T. Komatsu, S. Krüger, I. Mitra, R. Müller, S. Nakane, M. J. Pascual, W. P. Schmelzer, E. D. Zanotto and S. Zhou, "Updated definition of glass-ceramics," Journal of NonCrystalline Solids, vol. 501, pp. 3-10, 2018.

[22] S. Fujita and S. Tanabe, "Fabrication, microstructure and optical properties of Er3+:YAG glass–ceramics," Optical Materials, vol. 32, no. 9, pp. 886-890, 2010.

[23] S. W. Freiman and L. L. Hench, "Effect of Crystallization on the Mechanical Properties of Li2O-SiO2 Glass-Ceramics," Journal of the American Ceramic Society, vol. 55, no. 2, pp. 86-90, 1972.

[24] G. Partridge, “An overview of glass ceramics. I: Development and principal bulk applications,” Glas. Technol., vol. 35, no. 3, pp. 116–127, 1994.

[25] C. Lee, I.-S. Kim, and B. Lee, “Slow crack growth in a cordierite-based glass– ceramic missile radome due to stress corrosion,” Eng. Fail. Anal., vol. 93, pp. 76–86, Nov. 2018, doi: 10.1016/j.engfailanal.2018.04.007.

[26] G. H. Beall, “Design and Properties Of Glass-Ceramics,” Annu. Rev. Mater. Sci, vol. 22, no. 1, pp. 91–119, Aug. 1992, doi: 10.1146/annurev.ms.22.080192.000515.

[27] H. S. Maiti, “Transparent and Machinable Glass-Ceramics,” in Handbook of Advanced Ceramics and Composites, Springer International Publishing, 2020, pp. 461–493. doi: 10.1007/978-3-030-16347-1_13.

[28] W. Ostertag, G. R. Fischer, and J. P. Williams, “Thermal Expansion of Synthetic **β**-Spodumene and **β**-Spodumene-Silica Solid Solutions,” J. Am. Ceram. Soc., vol. 51, no. 11, pp. 651–654, 1968, doi: 10.1111/j.1151-2916.1968.tb12638.x.

[29] L. Kang, T. Liu, Z. Su, and Y. Kong, “Research on glass ceramics with negative coefficient of thermal expansion used as fiber Bragg grating

substrate," in Materials, Active Devices, and Optical Amplifiers, May 2004, vol. 5280, p. 638. doi: 10.1117/12.520427

[30] E. El-Meliegy and R. van Noort, Glasses and glass ceramics for medical applications, vol. 9781461412281. Springer New York, 2012. doi: 10.1007/978- 1-4614-1228-1.

[31] A. Herczog, "Application of Glass-Ceramics for Electronic Components and Circuits," IEEE Trans. Parts, Hybrids, Packag, vol. 9, no. 4, pp. 247–255, 1973, doi: 10.1109/TPHP.1973.1136735.

[32] A. Sakamoto and S. Yamamoto, "Glass-Ceramics: Engineering Principles and Applications," Int. J. Appl. Glas. Sci., vol. 1, no. 3, pp. 237–247, Sep. 2010, doi: 10.1111/j.2041-1294.2010.00027.x.

[33] H. Wang, J. Liu, J. Zhai, and B. Shen, "Ultra High Energy-Storage Density in the Barium Potassium Niobate-Based Glass-Ceramics for Energy-Storage 93 Applications," Journal of the American Ceramic Society, vol. 99, no. 9, pp. 2909–2912, 2016, doi: 10.1111/jace.14446.

[34] L. Samiee, H. Sarpoolaky, and A. Mirhabibi, "Microstructure and adherence of cobalt containing and cobalt free enamels to low carbon steel," Mater. Sci. Eng. A, 2007, doi: 10.1016/j.msea.2006.12.108.

[35] X. Fu, C. H. Zhang, C. Q. Li, K. J. Li, and Y. B. Zuo, "Design and processing of temperature resistant enamel coating materials," 2014, doi: 10.4028/www.scientific.net/AMM.457-458.168.

[36] N. Çöpoğlu, "DEVELOPMENT OF NANO PARTICLE REINFORCED ABRASION RESISTANT GLASS-CERAMICS," Yıldız Technical University, 2020.

[37] E. Yılmaz, "Taban Malzemeye Emaye Arayüz İlişkilerinin Emaye Kalitesine Etkisi," İstanbul Teknik Üniversitesi, 2014.

[38] I. A. Shimanskiy, V. G. Babkin, V. K. Frizorger, E. S. Goloskin, and A. B. Nabiulin, "Influence of Initial Components Mechanical Activation on the Properties of Protective Enamel Coating on the Cast-Iron Surface," 2012.

[39] E. Güngör, "Termik Santrallerin Döner Tip Hava Isıtıcılarında Kullanılan Isı Değiştirici Plakalar İçin Emaye Kaplama Optimizasyonu," İstanbul Teknik Üniversitesi, 2015.

[40] F. Russo, S. Rossi, and A. M. Compagnoni, "Porcelain Enamel Coatings," Encyclopedia, 2021, doi: 10.3390/encyclopedia1020032. [62] B. Karasu, İ. Saçkan, and M. C. Tapli, "Enamel from past to present time," El-Cezeri J. Sci. Eng., 2020, doi: 10.31202/ecjse.660254.

[41] W. D. Andrews, Andrew Irving and Pagliuca, Silvano and Faust, Porcelain (vitreous) Enamels and Industrial Enamelling Processes: The Preparation, Application and Properties of Enamels. Tipografia commerciale Mantova, Italy, 2011.

[42] W. D. Faust, "Porcelain (Vitreous) Enamels and Industrial Enamelling Processes," Ohio, 2012.

[43] K. Karaman, Y. Bozkurt Yılmaz, T. Cengiz, B. Çiçek, S. Yazar, and C. Author, "Examination of Enamel Different CaO-P2O5 Sources-Karaman at

al. SERAMİK Examination of Vitreous Enamel Coating Properties Prepared from Different CaO-P2O5 Raw Material Sources," Seramik-Journal Turkish Ceram. Soc., vol. 1, no. 3, pp. 19–25, 2021, Accessed: Jan. 30, 2023. [Online]. Available: https://orcid.org/0000-0001-8195- 4153.

[44] R. A. Eppler and D. Eppler, Glazes and glass coatings. Ohio: The American Ceramic Society, 2000.

[45] A. I. Andrews, S. Pagliuca, and W. D. Faust, Porcelain (Vitreous) Enamels - Industrial Enamelling Processes. Mantova: International Enamellers Institue, 2011.

[46] İ. Ceylan, "Sustainable Waste Utilization in Glass-Ceramic Coating Production," Yıldız Technical University, 2022.

[47] N. Çöpoğlu, "Development of Nano Particle Reinforced Abrasion Resistant Glass-Ceramics," Yıldız Technical University, 2020.

[48] S. Daloğlu, "Design, Synthesis And Characterization Of Functional Glass-Ceramic Coatings For Anti-Fouling Surface Applications," Yıldız Technical University, 2023.

[49] A. A. Andrews, S. Pagliuce, and W. D. Faust, "Raw Materials for Enamels," in Porcelain Enamels: The Preparation, Application and Properties of Enamels. Mantova: Tipografia Commerciale, 2011.

[50] K. Benzesik, M. İ. Terzioğlu, F. Sahin, and O. Yucel, "Optimizing the Migration Behavior of Enamel Coatings Used as Food Contact Materials," Oct. 2018. [Online]. Available: https://www.researchgate.net/publication/329327438

[51] A. P. Tomsia and A. Pask, "Chemical reactions and adherence at glass/metal interfaces: an analysis," 1986.

[52] Ellingham, H. J. (1944). Reducibility of oxides and sulphides in metallurgical processes. J. Soc. Chem. Ind, 63(5), 125-160.

[53] B. Karasu, İ. Saçkan, and M. C. Tapli, "Enamel from past to present time," El-Cezeri Journal of Science and Engineering, vol. 7, no. 2, pp. 923–939, 2020, doi: 10.31202/ecjse.660254.

[54] ASTM C385-58, "Standard Test Method for Thermal Shock Resistance of Porcelain-Enameled Utensils," Pennsylvania, 2018.

[55] M. Garcia-Valles et al., "Calculation of viscosity-temperature curves for glass obtained from four wastewater treatment plants in Egypt," Journal of Thermal Analysis and Calorimetry, vol. 111, no. 1, pp. 107–114, Jan. 2013, doi: 10.1007/s10973-012-2232-7.

[56] Deng, L., Miyatani, K., Suehara, M., Amma, S. I., Ono, M., Urata, S., & Du, J. (2021). Ion-exchange mechanisms and interfacial reaction kinetics during aqueous corrosion of sodium silicate glass. npj Materials Degradation, 5(1), 1-13.

[57] A. A. Andrews, S. Pagliuce, and W. D. Faust, "Porcelain Enamels: The Preparation, Application and Properties of Enamels," no. Raw Materials for Enamels, 2011.

[58] A. I. Andrews, P. S., and W. D. Faust, Fundamentals and Cosiderations, Porcelain (Vitreous) Enamels and Industrial Enamelling Processes The Preparation, Application and Properties of Enamels. Mantova, 2011.

[59] M. Shu, H. Yin, Q. Zhong, X. Shi, And H. Han, "Effect Of Glass Powder On Acid Resistance Of Enamel Coating," Surf. Rev. Lett., Vol. 24, No. 03, P. 1750036, Apr. 2017, Doi:10.1142/S0218625x17500366.

[60] S. G. Schäfer and V. E. Annamalai, "Degradation of Glass Linings and Coatings," in Reference Module in Materials Science and Materials Engineering, Elsevier, 2016.

[61] A. I. Andrews, S. Pagliuca, and W. D. Faust, "Chemical and Electrical Properties," in Porcelain (Vitreous) Enamels and Industrial Enamelling Processes The Preparation, Application and Properties of Enamels, Montava, 2011.

[62] P. W. McMillan, Crystallization of a Glass-Ceramic by Epitaxial Growth. London: Academic Press, 1979.

[63] E. Scrinzi and S. Rossi, "The aesthetic and functional properties of enamel coatings on steel," Mater. Des., 2010, doi: 10.1016/j.matdes.2010.04.030.

[64] S. Baycık, "Granüle Yüksek Fırın Cüruflarının Karo Sektöründe Kullanılabilirliğinin Araştırılması," İstanbul Technical University, 2003

[65] Enamelled Steel: A traditional material for modern living, Arcelor Mittal, 2015. Available: https://industry.arcelormittal.com/flipbook/fce/Brochures/Enamelledsteel_brochure_E N/#page/4

[66] A. Davran, "Enamelling Applications On Metal From Past to Future," İzmir University, 2011

[67] L. Besra and M. Liu, "A review on fundamentals and applications of electrophoretic deposition (EPD)," Progress in Materials Science. 2007, doi: 10.1016/j.pmatsci.2006.07.001.

[68] Boccaccini, A. R., Keim, S., Ma, R., Li, Y., & Zhitomirsky, I. (2010). Electrophoretic deposition of biomaterials. Journal of the Royal Society Interface, 7(suppl_5), S581-S613.

[69] M. R. Dorfman, "Thermal spray coatings," in Handbook of Environmental Degradation Of Materials: Third Edition, Elsevier Inc., 2018, pp. 469–488. doi: 10.1016/B978-0-323-52472-8.00023-X.

[70] P. Fauchais and A. Vardelle, "Thermal Sprayed Coatings Used Against Corrosion and Corrosive Wear," Advanced Plasma Spray Applications, InTech, 2012, doi: 10.5772/34448.

[71] T. Zhang, Y. Bao, and D. T. Gawne, "Process model of plasma enamelling," pp. 1019–1026, 2003, [Online]. Available: www.elsevier.com/locate/jeurceramsoc

[72] O. V. Shalygina, L. L. Bragina, G. I. Mironova, and A. P. Odintsova, "Single-Frit NickelFree Glass-Enamel Coatings Obtained by the Poesta Technology," Glas. Ceram. (English Transl. Steklo i Keramika), 2014, doi: 10.1007/s10717-014-9656-4.

[73] Grob, K. (2017). The European system for the control of the safety of food-contact materials needs restructuring: a review and outlook for discussion. Food Additives & Contaminants: Part A, 34(9), 1643-1659.

[74] European Chemicals Agency (ECHA)

[75] Occupational Safety and Health Administration (OSHA)

[76] Hellmann, R. (2021). Mechanisms of Glass Corrosion by Aqueous Solutions. Encyclopedia of Glass Science, Technology, History, and Culture, 1, 647-662.

[77] Frankel, G. S., Vienna, J. D., Lian, J., Scully, J. R., Gin, S., Ryan, J. V., ... & Du, J. (2018). A comparative review of the aqueous corrosion of glass, crystalline ceramics, and metals. npj Materials Degradation, 2(1), 1-17.

[78] Snellings, R. (2015). Surface chemistry of calcium aluminosilicate glass. Journal of the American Ceramic Society, 98(1), 303-314.

[79] Ngo, D., Liu, H., Sheth, N., Lopez-Hallman, R., Podraza, N. J., Collin, M., ... & Kim, S. H. (2018). Spectroscopic ellipsometry study of thickness and porosity of the alteration layer formed on international simple glass surface in aqueous corrosion conditions. npj Materials Degradation, 2(1), 1-9.

[80] Tribet, M., Mir, A. H., Gillet, C., Jegou, C., Mougnaud, S., Hinks, J. A., ... & Peuget, S. (2020). New insights about the importance of the alteration layer/glass interface. The Journal of Physical Chemistry C, 124(18), 10032-10044.

[81] Kaspar, T. C., Reiser, J. T., Ryan, J. V., & Wall, N. A. (2018). Non-destructive characterization of corroded glass surfaces by spectroscopic ellipsometry. Journal of Non-Crystalline Solids, 481, 260-266.

[82] Bunker, B. C. (1994). Molecular mechanisms for corrosion of silica and silicate glass. Journal of Non-Crystalline Solids, 179, 300-308.

[83] Alloteau, F., Majérus, O., Valbi, V., Biron, I., Lehuédé, P., Caurant, D., ... & Seyeux, A. (2020). Evidence for different behaviors of atmospheric glass alteration as a function of glass composition. npj Materials Degradation, 4(1), 1-11.

[84] Rébiscoul, D., Bruguier, F., Magnin, V., & Gin, S. (2012). Impact of soda-lime borosilicate glass composition on water penetration and water structure at the first time of alteration. Journal of non-crystalline solids, 358(22), 2951-2960.

[85] Topateş, G., Tarhan, B., & Tarhan, M. (2017). Chemical durability of zircon containing glass-ceramic glazes. Ceramics International, 43(15), 12333-12337.

[86] Fröberg, L., Hupa, L., & Hupa, M. (2009). Corrosion of the crystalline phases of matte glazes in aqueous solutions. Journal of the European Ceramic Society, 29(1), 7-14.

[87] Ngo, D., Liu, H., Kaya, H., Chen, Z., & Kim, S. H. (2019). Dissolution of silica component of glass network at early stage of corrosion in initially silica-saturated solution. *Journal of the American Ceramic Society*, *102*(11), 6649-6657.

[88] Zanini, R., Franceschin, G., Cattaruzza, E., Prato, M., Barozzi, M., & Traviglia, A. (2023). Compositional changes by SIMS and XPS analyses on fresh and aged Roman-like glass. *Journal of Non-Crystalline Solids*, *612*, 122356.

[89] Antropova, T. V. (2004). Kinetics of corrosion of the alkali borosilicate glass in acid solutions. Journal of non-crystalline solids, 345, 270-275.

[90] Backhouse, D. J., Fisher, A. J., Neeway, J. J., Corkhill, C. L., Hyatt, N. C., & Hand, R. J. (2018). Corrosion of the International Simple Glass under acidic to hyperalkaline conditions. npj Materials Degradation, 2(1), 1-10.

[91] Dathe, M., & Roggendorf, H. (2018). Dissolution of sodium silicate glass for the production of water glass–Part II: Dependence of corrosion process on pH in basic aqueous media. Physics and Chemistry of Glass-European Journal of Glass Science and Technology Part B, 59(6), 301-310.

[92] Geisler, T., Janssen, A., Scheiter, D., Stephan, T., Berndt, J., & Putnis, A. (2010). Aqueous corrosion of borosilicate glass under acidic conditions: a new corrosion mechanism. Journal of Non-Crystalline Solids, 356(28-30), 1458-1465.

[93] Ghosh, S., & Datta, S. (2014). Surface Degradation Behaviour of MgO-Al2O3-TiO2-SiO2 based Glass-Ceramics. Transactions of the Indian Ceramic Society, 73(3), 216-220.

[94] Gin, S., Guo, X., Delaye, J. M., Angeli, F., Damodaran, K., Testud, V., ... & Kim, S. H. (2020). Insights into the mechanisms controlling the residual corrosion rate of borosilicate glass. npj Materials Degradation, 4(1), 1-9.

[95] Lenting, C., & Geisler, T. (2021). Corrosion of ternary borosilicate glass in acidic solution studied in operando by fluid-cell Raman spectroscopy. npj Materials Degradation, 5(1), 1-9.

[96] Park, Y. J., & Heo, J. (2004). Corrosion behavior of glass and glass-ceramics made of municipal solid waste incinerator fly ash. Waste Management, 24(8), 825-830.

[97] Ludmila, R., & Iva, K. (1996). Corrosion of silica glass by aqueous solutions of organic compounds. Ceramics-Silikáty, 40(3), 94-98.

[98] Vilarigues, M., & Da Silva, R. C. (2006). Characterization of potash-glass corrosion in aqueous solution by ion beam and IR spectroscopy. Journal of non-crystalline solids, 352(50-51), 5368-5375.

[99] Kaya, H., Ngo, D., Smith, N. J., Gin, S., & Kim, S. H. (2021). Network structure in alteration layer of boroaluminosilicate glass formed by aqueous corrosion. Journal of Non-Crystalline Solids, 553, 120494.

[100] Collin, M., Fournier, M., Charpentier, T., Moskura, M., & Gin, S. (2018). Impact of alkali on the passivation of silicate glass. npj Materials

[101] Mellott, N. P., & Pantano, C. G. (2013). A mechanism of corrosion-induced roughening of glass surfaces. *International Journal of Applied Glass Science*, *4*(3), 274-279.

[102] Ngo, D., Liu, H., Chen, Z., Kaya, H., Zimudzi, T. J., Gin, S., ... & Kim, S. H. (2020). Hydrogen bonding interactions of H2O and SiOH on a

boroaluminosilicate glass corroded in aqueous solution. *npj Materials Degradation*, *4*(1), 1.

[103] Surendranathan, A. O. (2014). *An introduction to ceramics and refractories*. CRC Press.

[104] V. A. Borgman, V. K. Leko, and V. K. Markargan, The Structure of Glass, Vol. 8, Trans. Russian, Consultants Bureau, New York, 1973, pp. 66–68.

[105] D. M. Sanders and L. L. Hench, Mechanisms of glass corrosion, J. Am. Ceram. Soc., 56(7): 373–377, 1973.

[106] D. M. Sanders, W. B. Person, and L. L. Hench, Quantitative analysis of glass structure with use of infrared reflection spectra, Appl. Spectrosc., 28: 247–255, 1974.

[107] Brazeau, R. H., & Edwards, M. A. (2011). A review of the sustainability of residential hot water infrastructure: Public health, environmental impacts, and consumer drivers. College Publishing, 6(4), 77-95.

[108] Rayaprolu, K. (2009). Boilers for power and process. CRC press.

[109] https://www.solimpeks.com.tr/sicak-su-tanki-nedir/ 20.12.2023

[110] https://www.tesisat.org/boyler-hakkinda-teknik-bilgiler.html 20.12.2023

[111] Liebau, F. (2012). Structural chemistry of silicates: structure, bonding, and classification. Springer Science & Business Media.

[112] Ojovan, M. I., Lee, W. E., & Kalmykov, S. N. (2019). An introduction to nuclear waste immobilisation. Elsevier.

[113] Ceylan, İ., & Çiçek, B. (2022). Temperature-driven phase transformation of Ca-rich boron waste into CaB2O4: Investigation of microstructure, crystallinity and thermal characteristics. *Materials Chemistry and Physics*, *287*, 126278. https://doi.org/10.1016/j.matchemphys.2022.126278

[114] Tomé-Torquemada, S., Glaser, B., & Sichen, D. "Experimental study of the phase relationships in the SrO-SiO2 system." J. Eur. Ceram. Soc., 38.9 (2018): 3354-3360. https://doi.org/10.1016/j.jeurceramsoc.2018.03.030

[115] Huntelaar, M. E., Cordfunke, E. H. P., & Scheele, A. "Phase relations in the SrO-SiO2-ZrO2 system I. The system SrO-SiO2." J. Alloys Compd., 191.1 (1993): 87-90. https://doi.org/10.1016/0925-8388(93)90276-S

[116] White, J. F., Lee, J., Hessling, O., & Glaser, B. (2017). Reactions between liquid CaO-SiO 2 slags and graphite substrates. *Metallurgical and materials transactions B*, *48*, 506-515.

[117] Takahashi, Y., Masai, H., & Fujiwara, T. (2009). Nucleation tendency and crystallizing phase in silicate glasses: A structural aspect. Applied Physics Letters, 95(7), 071904

[118] Araujo, M. C., Botta, W. J., Kaufmann, M. J., Angelica, R. S., Mercury, J. M., & Cabral, A. A. (2015). Residual glass and crystalline phases in a barium disilicate glass–ceramic. Materials Characterization, 110, 192-196.

[119] Aboud, T. K., Stoch, L., & Środa, M. (2005). Quartz crystallization in soda-lime-silica glass. Optica Applicata, 35(4).

[120] Kolobov, A. Y., & Sycheva, G. A. (2020). Features of crystallization and characteristics of quartz glass obtained on oao dinur plasma torches from the quartz sand of the Ramenskii deposit. *Glass Physics and Chemistry*, *46*, 249-255.

[121] Rezazadeh, L., Baghshahi, S., Golikand, A. N., & Hamnabard, Z. (2014). Structure, phase formation, and wetting behavior of BaO–SiO 2–B 2 O 3 based glass–ceramics as sealants for solid oxide fuel cells. Ionics, 20, 55-64.

[122] Takahashi, Y., Osada, M., Masai, H., & Fujiwara, T. (2010). Transmission electron microscopy and in situ Raman studies of glassy sanbornite: An insight into nucleation trend and its relation to structural variation. Journal of Applied Physics, 108(6).

[123] Yadav, A. K., & Singh, P. (2015). A review of the structures of oxide glasses by Raman spectroscopy. RSC advances, 5(83), 67583-67609.

[124] Takahashi, Y., Ihara, R., Fujiwara, T., & Osada, M. (2011). Crystallization and morphology of glassy sanbornite. Key Engineering Materials, 485, 301-304.

[125] Gomes, E. O., Moulton, B. J., Cunha, T. R., Gracia, L., Pizani, P. S., & Andres, J. (2021). Identifying and explaining vibrational modes of sanbornite (low-BaSi2O5) and Ba5Si8O21: A joint experimental and theoretical study. Spectrochimica Acta Part A: Molecular and Biomolecular Spectroscopy, 248, 119130.

[126] Arena, H., Rebiscoul, D., Garcès, E., & Godon, N. (2019). Comparative effect of alkaline elements and calcium on alteration of International Simple Glass. *npj Materials Degradation*, *3*(1), 10. https://doi.org/10.1038/s41529-019-0072-7

[127] Surendranathan, A. O. (2014). An introduction to ceramics and refractories. CRC Press.

[128] Abou Neel, E. A., Chrzanowski, W., Pickup, D. M., O'Dell, L. A., Mordan, N. J., Newport, R. J., ... & Knowles, J. C. (2009). Structure and properties of strontium-doped phosphate-based glasses. Journal of the Royal Society Interface, 6(34), 435-446.

[129] Stolyar, S. V., & Tyurnina, N. G. (2009). Thermal expansion of glasses in the SrO-B 2 O 3-SiO 2 system. Glass Physics and Chemistry, 35, 149-152.

[130] Li, S., Liu, H., Wu, F., Chang, Z., & Yue, Y. (2016). Effects of alkaline-earth metal oxides on structure and properties of iron phosphate glasses. Journal of Non-Crystalline Solids, 434, 108-114.

[131] Paul, A., & Paul, A. (1982). Chemical durability of glass. Chemistry of glasses, 108-147.

[132] Rossi, S., Russo, F., Gasparre, N., & Fontanari, V. (2020). Influence of graphene addition on the mechanical and surface properties of vitreous enamel coatings. *Surface and Coatings Technology*, *398*, 126071.

[133] Rossi, S., Calovi, M., Velez, D., & Munoz, J. (2019). Influence of addition of hard particles on the mechanical and chemical behavior of vitreous enamel. *Surface and Coatings Technology*, *357*, 69-77.

[134] Tyukanko, V. Y., Dyuryagina, A. N., & Ostrovnoi, K. A. (2019). Effect of Adding Phosphorus-Containing Surfactants on the Properties of Organosilicon Compositions. Glass Physics and Chemistry, 45, 79-81.

[135] Rossi, S., Zanella, C., & Sommerhuber, R. (2014). Influence of mill additives on vitreous enamel properties. *Materials & Design*, *55*, 880-887. *Degradation*, *2*(1), 1-10.

PUBLICATIONS FROM THE THESIS

Conference Papers

1. "High-Temperature Aqueous Corrosion Behaviour of Alkaline Earth-Sodium Borosilicate-Based Glass/Glass Ceramic Coatings on Metallic Substrate" Ötken Ö. F., Çiçek B., 1. Uluslararası Mühendislik ve Fen Bilimleri Kongresi, İstanbul, Turkey, 18 - 19 March 2023, pp.302.

2. "High-Temperature Alkaline Corrosıon Behaviour of [CaO, SrO, BaO]–Na2O–B2O3–SiO2 Enamel Coatings On Metallic Substrates" Ötken Ö. F., Cengiz T., Karaahmet O., Çiçek B., 15th ECerS Conference for Young Scientists in Ceramics, Novi-Sad, Serbia, 11 - 14 November 2023, pp.123.